

65-3-4

ASD-TDR-62-165
Volume II

CATALOGED BY AD 11A 403507

AD 11A 403507

403 507

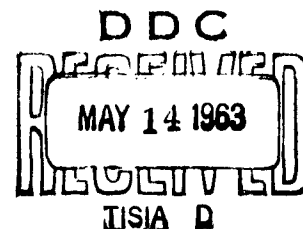
STUDY OF A RESPONSE LOAD RECORDER

TECHNICAL DOCUMENTARY REPORT ASD-TDR-62-165
VOLUME II
MARCH 1963

Flight Dynamics Laboratory
Aeronautical Systems Division
Air Force Systems Command
Wright-Patterson Air Force Base, Ohio

Project No. 1370, Task No. 137005

(Prepared under Contract No. AF 33(616)-7789
by Bolt Beranek and Newman Inc.,
Cambridge 38, Massachusetts
P. W. Smith, Jr., E. A. Starr, C. W. Dietrich, D. U. Noiseux)



NOTICES

When Government drawings, specifications, or other data are used for any purpose other than in connection with a definitely related Government procurement operation, the United States Government thereby incurs no responsibility nor any obligation whatsoever; and the fact that the Government may have formulated, furnished, or in any way supplied the said drawings, specifications, or other data, is not to be regarded by implication or otherwise as in any manner licensing the holder or any other person or corporation, or conveying any rights or permission to manufacture, use, or sell any patented invention that may in any way be related thereto.

Qualified requesters may obtain copies of this report from the Armed Services Technical Information Agency, (ASTIA), Arlington Hall Station, Arlington 12, Virginia.

This report has been released to the Office of Technical Services, U.S. Department of Commerce, Washington 25, D.C., in stock quantities for sale to the general public.

Copies of this report should not be returned to the Aeronautical Systems Division unless return is required by security considerations, contractual obligations, or notice on a specific document.

ASD-TDR-62-165
Volume II

FOREWORD

The research work reported herein was conducted by Bolt, Beranek and Newman Inc., Cambridge, Massachusetts. The work was administered by the Flight Dynamics Laboratory, Directorate of Aeromechanics, Deputy for Technology, Aeronautical Systems Division, Wright-Patterson Air Force Base, Ohio, under Contract No. AF 33(616)-7789. This research is part of a continuing effort to obtain pertinent data in usable form to enable a better estimation of sonic loads encountered by an operational aircraft for more precise noise prediction and fatigue analysis which is a part of the Air Force Systems Command's Applied Research Program 750A, "Mechanics of Flight". The work was conducted under Project No. 1370, "Dynamic Problems in Flight Vehicles", Task No. 137005, "Methods of Noise Prediction, Control and Measurement". Mr. Smith and later Mr. Hermes of the Flight Dynamics Laboratory were the Project Engineers. The research effort was conducted from January to August 1962.

This is Volume II of two volumes which describes the design of an instrument to monitor the response of aircraft panels. Volume I describes an instrument to monitor the sonic excitation at the panel.

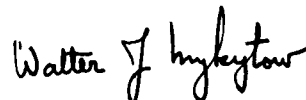
ABSTRACT

A compact instrument to measure the strain history of a point on a resonant structure of a flight vehicle is considered. The output data from the instrument is designed to aid in the estimation of acoustic fatigue damage. The ability of a strain gage to perform under fatigue conditions is examined. The design of circuitry to modify the sonic recorder discussed in Volume I to a response recorder are discussed. Performance data of the breadboarded response recorder, tested with a resonant structure, are given.

PUBLICATION REVIEW

This report has been reviewed and is approved.

FOR THE COMMANDER



WALTER J. MYKYTOW
Chief, Dynamics Branch
Flight Dynamics Laboratory

TABLE OF CONTENTS

<u>Section</u>	<u>Page</u>
I INTRODUCTION.....	1
II GENERAL PERFORMANCE REQUIREMENTS.....	3
A. THE INPUT VARIABLE.....	4
B. FREQUENCY-TIME ANALYSIS.....	4
C. LOW-FREQUENCY DATA.....	5
D. RANGE OF RMS STRAIN LEVELS.....	6
E. PEAK STRAINS.....	10
III STRAIN TRANSDUCERS FOR THE RESPONSE RECORDER....	13
A. EFFECTS OF TEMPERATURE VARIATIONS ON GAGE MEASUREMENTS.....	13
B. FREQUENCY DEPENDENCE OF GAGE RESPONSE.....	15
C. SELF-GENERATING EFFECTS.....	17
D. GAGE FAILURE.....	18
E. CONCLUSION.....	19
IV CIRCUITRY.....	20
A. INPUT CIRCUIT.....	21
1. <u>Strain Gage Circuit</u>	21
a) <u>Strain Sensitivity</u>	21
b) <u>Sensitivity Variation</u>	22
2. <u>Balanced Circuit</u>	23
3. <u>Strain Gage Voltage Supply</u>	25
4. <u>Input Amplifier</u>	26

ASD-TDR-62-165
Volume II

<u>Section</u>	<u>Page</u>
B. DATA FILTERS.....	27
1. <u>Narrow Band Filters</u>	27
2. <u>Over-All Filter</u>	28
C. DETECTOR.....	28
D. MODIFICATION OF THE AMPLITUDE DISTRIBUTOR..	29
1. <u>Expanded Range</u>	30
2. <u>Overflow Window</u>	31
3. <u>Window Variation</u>	31
E. COMPATIBILITY OF RESPONSE RECORDER AND SONIC RECORDER.....	32
V SYSTEM PERFORMANCE.....	34
A. EXPERIMENTAL EVALUATION.....	34
1. <u>Data Acquisition</u>	34
a) <u>Measurements with Insert Voltages</u>	34
b) <u>Measurements of Strain</u>	35
2. <u>Complete System</u>	36
B. ERROR ANALYSIS.....	36
1. <u>Systematic Errors</u>	36
2. <u>Short Term Errors</u>	38
3. <u>Accumulated Error</u>	39
VI CONCLUSIONS.....	40
LIST OF REFERENCES.....	41
APPENDIX A. DATA ANALYSIS TECHNIQUES.....	62
A. INVESTIGATION PLAN.....	62

ASD-TDR-62-165
Volume II

<u>Section</u>	<u>Page</u>
B. RESPONSE DISTRIBUTIONS AND FATIGUE CURVE.....	63
C. DAMAGE ESTIMATES.....	64
D. DISCUSSION.....	67
E. CONCLUSIONS.....	68
APPENDIX B. DEPENDENCE OF SOUND PRESSURE LEVEL ON AMBIENT TEMPERATURE FOR PRATT AND WHITNEY J-57 ENGINE.....	76
A. INTRODUCTION.....	76
B. FUNDAMENTAL RELATIONS.....	76
C. CALCULATIONS FOR J-57 ENGINE.....	78
APPENDIX C. STRAIN GAGE FATIGUE MEASUREMENTS.	81
A. INTRODUCTION.....	81
B. TEST BAR.....	81
C. EXPERIMENTAL SETUP.....	83
D. EXPERIMENTAL PROCEDURE.....	85
E. RESULTS.....	86
F. CONCLUSIONS.....	87
APPENDIX D. REVIEW OF DATA FOR B-52 AND KC-135	95
APPENDIX E. OPERATIONAL RECOMMENDATIONS FOR THE RESPONSE RECORDER.....	99
A. SET UP PROCEDURE.....	99
B. CHECKOUT AND CALIBRATION.....	99
1. <u>Calibration Equipment Required...</u>	99
2. <u>Controls and Adjustments.....</u>	100

ASD-TDR-62-165
Volume II

<u>Section</u>	<u>Page</u>
3. <u>Initial Checkout Procedures</u>	101
4. <u>Field Calibration Procedure</u>	104
C. DETAILED CIRCUIT.....	104

LIST OF FIGURES

<u>Figure</u>		<u>Page</u>
1	Range of Values of Panel Span and Thickness Having Fundamental Resonance Frequencies as Shown	43
2	Typical Cumulative Distributions of Fatigue Damage (From Figures 1, 3, 4 of Appendix A)	44
3	Cumulative Distribution of Fatigue Damage for B-52 and KC-135 Aircraft (Based on Response Data in Appendix D)	45
4	The Return Period for Strain Peaks on RB-47 Aircraft Operated Typically (See Text). The Return Period is the Average Total Number of Strain Cycles for One Strain Peak Exceeding the Indicated Value	46
5	The Return Period for Steady State Operation at Constant RMS Level	47
6	Variation of Gage Factor with Temperature for Some Strain Gage Materials	48
7	Normalized Magnitude of $(\sin x)/x$ Versus x	49
8	Change of B-H Curve for Nickel with Applied Tension σ (After Bozorth)	50
9	Experimental Strain-Life Curve for Constantan Foil Strain Gage (BLH FAB-50-12) Under Random Excitation	51
10	Block Diagram of Response Recorder	52
11	Variation of Strain Sensitivity (S_e) with R_A/R_G	53
12	Single-Ended Strain Gage Application (Resistance, R_G , Balance Gage and Specimen Indicated)	54
13	Balanced Strain Gage Application	55
14	Balanced Strain Gage Input Circuit	56

ASD-TDR-62-165
Volume II

<u>Figure</u>		<u>Page</u>
15	Response of Overall Filter	57
16	Block Diagram of Two-Input History Recorder	58
17	Measurements of Input to Detector Output Transfer Function for Sine Wave Insert Voltage	59
18	Measurements of Strain Input to Detector Input for Sine Wave and Narrow Band Noise	60
19	Bar Chart of Counts Accumulated with Random Data for Various Lengths of Operation T	61

LIST OF FIGURES FOR APPENDIXES

<u>Figure</u>		<u>Page</u>
A-1	Response Distribution I and Corresponding Distribution of Damage	69
A-2	Random Fatigue Curve (Adapted from Schjeldrup Ref. A-1)	70
A-3	Response Distribution II and Corresponding Cumulative Distribution of Damage	71
A-4	Response Distribution III and Corresponding Cumulative Distribution of Damage	72
A-5	Readout Case 13, Derived from Distribution I Using 3 db Windows Starting at -3 db	73
A-6	Readout Case 11, Derived from Distribution I Using 2 db Windows Starting at -5 db	74
A-7	Cumulative Response Distribution for Readout Case 11	75
C-1	Fatigue Test Bars	90
C-2	Driver Circuit for Random Noise Excitation	91
C-3	Strain Gage Output Recording System	92
C-4	Typical Strain Gage Graphic Record	93
C-5	Experimental Strain-Life Curve for Constantan Foil Strain Gage (BLH FAB-50-12) Under Random Excitation	94
D-1	RMS Distribution for Ground Operations for 600-1200 CPS Band	98

LIST OF TABLES

<u>Table</u>		<u>Page</u>
I	RMS STRAIN LEVELS FOR FATIGUE OF RESONANT STRUCTURES IN RANDOM RESPONSE.....	7
II	RANGE OF RESPONSE LEVELS PRINCIPALLY RESPONSIBLE FOR FATIGUE DAMAGE.....	9
III	IDEAL FILTER EDGES FOR 14 DB RANGE.....	31
IV	WINDOWS FOR VARIOUS BIAS VOLTAGES USING FILTERS OF TABLE III.....	32
V	DATA FROM RESPONSE RECORDER DURING STRAIN EVALUATION TESTS.....	37

ASD-TDR-62-165
Volume II

LIST OF TABLES FOR THE APPENDIXES

<u>Table</u>		<u>Page</u>
A-I	THE VARIOUS READOUT CASES AND THEIR ERRORS IN ASSESSMENTS OF DAMAGE.....	66
C-I	FATIGUE DATA FOR RANDOM NARROW BAND EXCITATION OF FAB-50-12 STRAIN GAGE FOUR SAMPLES TESTED CONCURRENTLY AT EACH EXCITATION LEVEL.....	89
D-I	ENGINE GROUND TIME IN HOURS/1000 HOURS OF FLIGHT.....	96

LIST OF SYMBOLS

(Listed in Section where introduced)

Section II

db	decibels
ϵ	strain .
f	frequency
n	number of exceedances per unit time
p	probability
rms	root mean square
σ	standard deviation, or rms level
w	weighting factor

Section III

c	wave velocity
E	Young's Modulus
GF	gage factor
h	plate thickness
k	$2\pi/\lambda$
l	gage length
λ	wavelength
μ	10^{-6}
R	resistance in ohms
ρ	density
x	spatial variable

ASD-TDR-62-165
Volume II

Section IV

B	bandwidth
C	capacitance
cps	cycles per second
dbv	decibels relative to one volt
e	AC voltage
E	supply voltage
KC	kilocycles
K Ω	1000 ohms
L	inductance
m	mean value
ma	milliamperes
Ω	ohms
Q	selectivity
S	sensitivity
T	averaging time
VCO	voltage-controlled oscillator

SECTION I
INTRODUCTION

This study investigates the requirements and accomplishes a design for an instrument to provide information on the long term amplitude statistics of the root mean square response of a point on an aircraft structure to sonic excitation. This instrument, the response recorder, is designed to be airborne and to operate unattended for periods of three months.

The functions performed by the response recorder are the following: 1) the instantaneous strain signal from a structure is amplified by a balanced system and the response modes are separated by filters, 2) the filtered signals are quasi-rms detected, 3) the detected signal is applied to an amplitude distributor which quantizes the rms level into six logarithmic windows covering a fourteen db range, and 4) the time spent by the rms level in each amplitude window is accumulated. Each of these functions has been examined in light of the goal of retaining the information essential for sonic fatigue while keeping the size of the final package to a minimum.

The present report is Volume II of a two-volume report. Volume I discussed the requirements and design of a sonic recorder for accumulating the long term rms amplitude statistics of the sonic excitation. The design allows a basic recorder to be converted to either a response recorder or a sonic recorder by interchanging plug-in modules. In addition, it is possible to simultaneously accumulate rms amplitude information for sound pressure level and for strain, by employing two inputs to the basic recorder, with very little additional equipment.

The general requirements to be fulfilled by the response recorder are discussed in Section II. This section is supported by Appendix A, which considers some data analysis techniques for the response recorder data and the resulting errors, and Appendix B, which considers the sound pressure level variation with ambient temperature for a contemporary jet engine.

Manuscript released by the authors, January, 1963, for publication as an ASD Technical Documentary Report.

ASD-TDR-62-165
Volume II

Characteristics of the strain gage which are important for the dynamic measurements of the response recorder are discussed in Section III. In particular, temperature effects, frequency dependence, magnetostrictive effects, and gage failures are considered. Appendix C describes experiments relating to the failure of gages under random excitation by a cumulative fatigue process.

Section IV describes the design of the circuitry of the response recorder and its relation to the sonic recorder described in Volume I. The breadboard circuit of the response recorder has been evaluated experimentally with narrow band random strain inputs. This data and the long term errors anticipated are discussed in Section V.

SECTION II

GENERAL PERFORMANCE REQUIREMENTS

In this section we consider the general requirements that a response recorder should satisfy.

The purpose of a life-history recorder is to gather statistical data (numbers) which can be combined with analytical schemes (criteria). A completely deterministic design of a recorder, then, can be found only by examination of a pre-existing analytical criterion. In the area of structural fatigue analysis and test, no completely satisfactory criterion presently exists.

For certain limited classes of structures, simple criteria have been postulated and, to some extent, proved (see summary in Ref. 1). One such class includes structures in which the motion is particularly simple, having one predominant mode (in space and frequency), and being not too greatly nonlinear. For structures of this class, the criterion could be expressed equally well in terms of the value of any one of a great variety of variables: strains, accelerations, displacements, sound pressures, etc. However, the more complicated the motion of the structure, the less firm is the formulation of criteria.

In many physical situations there are structures for which no good criteria exist, but to which a good engineer can profitably apply his intuition. These cases are most numerous, and it is therefore very important that the response recorder yield data which the experienced engineer can interpret using his intuition and his previous experience. Indeed, until much more sonic fatigue research has been completed, the use of data from a response recorder will probably depend upon this intuitive sort of interpretation. The possibility of such use of the data is a strong argument in favor of a response recorder.

The requirements discussed below have been determined with these considerations in mind. They are designed to yield information valuable to the experienced engineer, for fatigue analysis, design, and testing. The information gathered on any one structural element should be sufficient to allow an experienced engineer either (1) to make a reasonable assessment of the possibilities of fatigue damage, or (2) to conclude that the loading of this structural element represents a special case, for whose understanding more detailed research measurements are required.

ASD-TDR-62-165
Volume II

A. THE INPUT VARIABLE

When the response of a structure is predominantly motion in a single mode with a determined spatial pattern and a narrow-band spectrum, either measurements of strain or of acceleration are potentially useful for fatigue analysis and test purposes. In such situations, measuring acceleration has the advantage of simplifying some instrumentation problems.

Choice of a position for an acceleration transducer would be based on somewhat different considerations than a position for a strain transducer. The basic problem, brought about by a non-uniform distribution of the variable over the surface of the structure, does not appear to be any more difficult with one or the other transducer. However, it is significant that the problems of placing and orienting a strain transducer have been investigated and a basis of experience and judgment exists. This experience would have to be acquired anew with acceleration transducers.

When we consider structures whose motion is not as simple as in the one-mode case, a very strong argument can be made for using a strain transducer. In such structures there is no simple one-to-one relation between acceleration measured at one point and strain measured at another. Here, the whole body of engineering experience and intuition is based on strain measurements. Therefore use of an acceleration transducer in the response recorder would make application of this knowledge and intuition more difficult. Further, interpretation of the measured data would be made much more difficult and the utility of the recorder correspondingly severely limited.

Acquisition of acceleration data and its comparison with strain and fatigue life data might be considered a useful research project; however a data-gathering recorder must, it appears, use rms strain as the input variable.

B. FREQUENCY-TIME ANALYSIS

The recorder should gather long-time statistics on the rms strain in each of several frequency bands. Suitable bands are

- (1) and (2): moderately narrow-bands (about third- or half-octave), which can be positioned at will in the range 50 to 750 cps;
- (3): an overall band, covering the range 50 to 750 cps or higher.

If the signal is dominated by one or a separated pair of narrow-band modes, the rms strain in these modes must be measured; standard engineering criteria are available for assessing the resulting data (see Refs. 2,3,4,5). If there are two dominant modes, but they are closer than one-third of an octave, the significance of separate data is so doubtful that there seems little reason to acquire it, and a single filter should be used to measure the rms strain of both modes together.

If there are more than two dominant modes, no procedures are available for assessing the separate data, and the overall level should be measured.* The overall level should be processed in any case for several reasons: (a) as a check on the other readings; (b) as a possible indicator of unexpected developments; (c) as general information.

The available reports indicate that the frequency range from 50 to 750 cps is quite adequate for present structures, (Refs. 2-5). Figure 1 shows another way of evaluating the coverage of this frequency range: the panel thickness-span relations which will lead to resonant frequencies in this frequency range are plotted. (We assume resonance in a fundamental mode of a simple uniform plate in bending.) The coverage appears adequate in view of current procedures for design of the skin of an aircraft.

C. LOW-FREQUENCY DATA

In this section we consider the importance of data on low-frequency or static loads which may be superimposed on the sound-induced vibration.

Essentially static loads may arise from gravitational forces, when the aircraft is moving very slowly, and from air pressure when the aircraft is in flight. However,

* Note that a recent study of 24 strain records showed that, even in multimode cases, the range of strain from peak to adjacent trough was very nearly distributed on a Rayleigh curve with an rms within a few percent of the overall rms. If this method of analysis is proved in the future to have predictive value, then this overall reading will be most important. [See Ref. 2.]

the flight load occurs only when the sonic load has been greatly diminished by the reduced value of relative velocity of jet and ambient air (see Fig. 3 of Vol. I of this report). Therefore, data about flight loads do not appear to be important for a sonic response recorder. Instrumentation to determine static loads of gravitational origin (for example, the drooping of wings) would be extremely difficult; the gravitational load would have to be removed (e.g., the wing jacked up) while the gages were being applied. The problems involved would critically and adversely affect the utility of the response recorder. A preferable procedure would use calculations from aircraft design data to determine such static loads.

Low-frequency loading of structures occurs from irregularity of runways used in taxiing and takeoff and from flight through turbulence. Again, most of these loads do not occur at the same time as do the important sonic loads, that is, during maximum power operation with small forward speed. If a recorder were to gather data on such low-frequency loads, the recordings would have to distinguish between cases when sonic and low-frequency loads were simultaneous and cases when they were not. In other words, the data on rms low-frequency loads and data on rms high-frequency loads would have to be correlated. Such correlation would require a much more complicated recorder and analysis system.

However, even if correlated data of this sort were available, there is no accepted criterion by which it could be evaluated. Although use of a modified Goodman Diagram has been proposed for the assessment of combined high and low-frequency random loads (Ref. 6), such a procedure has not been tried experimentally and so is still speculative.

D. RANGE OF RMS STRAIN LEVELS

The available information about surveys of flight vehicles performed by the aircraft manufacturing companies gives only a rough idea of the rms strains that would be presented to the transducer. One paper gives results for investigations, stimulated by existing fatigue problems, on the RB-66 aircraft (Ref. 5). Reported values of rms strain levels range from about 35 db to 45 db re 10^{-6} .^{*} Most other published information does not give absolute strain levels.

* If the strain is ϵ (in./in.), then the strain level in decibels (db) re 10^{-6} (1 microstrain) is $20 \log_{10}(\epsilon/10^{-6})$.

It is possible to estimate rms strains from calculated random fatigue curves and estimated strain concentration factors. This procedure determines an upper limit to the expected rms levels. For example, the rms strains at the point of fatigue for fatigue lives of 10^6 cycles (a short life) and of 10^9 cycles (a long life) have been calculated by various authors as shown in Table I.

TABLE I
RMS STRAIN LEVELS FOR FATIGUE OF RESONANT STRUCTURE
IN RANDOM RESPONSE

Material	Reference	RMS Strain Level (db re 10^{-6})	
		at 10^6 cycles:	at 10^9 cycles:
2024 Al, bare	Ref. 1, Fig. 8	63	--
2024 Al, clad	Ref. 1, Fig. 21	59	--
2024 Al, clad	Ref. 3, Fig. 15	60	53
7075-T6 Al	Ref. 5, Fig. 1	60	52

The rms strain level at the strain gage will be lower than the value at the point of fatigue by the amount of the fatigue concentration factor. The concentration factor depends intimately upon the panel design. Some typical experimental values for 2024 aluminum are:

for a hole, subject to bending, (Ref. 1, p. 36):	3 to 4 db;
for a rivet line, subject to bending, (Ref. 7, p. 96):	3 to 5 db;
for a hole in a bead of a beaded panel, excited by noise, (Ref. 1, p. 66):	8 db.

ASD-TDR-62-165
Volume II

Thus, for typical long-lived structures (10^9 cycles), measured rms strain levels might be expected to range from about 44 to 50 db.

The maximum range of rms strain levels to which a response recorder must respond depends intimately upon the operational characteristics of the aircraft upon which it is mounted. In the course of many flights, an aircraft is operated at many power settings, and the duration of any one power setting varies greatly. In addition the ambient air temperature varies from flight to flight, so that sound levels and strain levels vary at any one power setting.

Because of the combination of these two effects, the response strain at a particular point on a particular aircraft will have a broad distribution of rms values. The relative importance of different rms strain values can be evaluated by (1) estimating the distribution curve for rms strain, and (2) computing a fatigue-damage distribution curve, based on some reasonable fatigue theory. Such a procedure has been carried out using actual operational data for a variety of aircraft. We summarize the results here.

One starts with operational data on power settings, ambient temperature, and acceleration during takeoff. From these the relative durations of various sound pressure levels are predicted; this phase of the analysis was illustrated in Volume I of this report, using data for RB-47 aircraft. (Details of calculations for the change in sound pressure level with temperature are reported in Appendix B, hereto, with sample calculations for J-57 jet engines.) Under the assumption that the response is linear, these data form a probability distribution curve for relative response level.

The response distribution curve is then combined with a fatigue curve, in a manner described in Appendix A, to yield a cumulative distribution curve for fatigue damage. Three such cumulative distributions are shown in Fig. 2. The ordinate in these graphs is the percentage of total damage that is attributable to response levels at or below the abscissa value. The top curve (Distribution I) pertains to the measured data for RB-47 aircraft. The zero level of relative response is the response to military rated power on a standard day (59 deg F). The other two curves in Fig. 2 (Distributions II and III) have been modified to simulate engines which have thrust augmentation devices.

It was assumed that thrust augmentation results in a response level 4 db above that for military power. In these two cases, zero db is the response level to military power with thrust augmentation on a standard day. (Details of calculation are reported in Appendix A.)

Similar cumulative distributions of fatigue damage have been calculated from operational data for B-52 and KC-135 aircraft (Appendix D). These are shown in Fig. 3. In both graphs, the reference value for response (zero db point) is response on a standard day to military rated power without thrust augmentation.

It is apparent from these graphs that significant contributions to fatigue damage are contained in a very restricted range of response level. The ranges which contain 80 percent of all fatigue damage (from the 10 percent level to the 90 percent level) are listed in the following table. In considering the data, it must be remembered that a measurement or calibration error of 0.3 db also results in 20 percent errors in assessing fatigue damage.

TABLE II
RANGE OF RESPONSE LEVELS PRINCIPALLY
RESPONSIBLE FOR FATIGUE DAMAGE

<u>Response Distribution</u>	<u>Response Range Containing 80% of Fatigue Damage</u>
Distribution I(RB-47)	3 db
Distribution II	4.5
Distribution III	6
B-52	4
KC-135	4.5

It appears from these analyses of operations typical of military aircraft that a response range of 6 db is quite adequate for the purposes of the response recorder. However, wider ranges may make the recorder easier to use and may protect against individual cases in which wider distributions occur.

E. PEAK STRAINS

Information concerning the largest probable instantaneous strain is desirable in order to determine that the strain gage is rugged enough. However in random response, no absolute maximum can be set on the expected values of strain. Instead, we must speak of the probability of a selected value being exceeded in a given length of time.

Consider a one-mode, linear, resonant structure which is excited by a random force. The average number of times per cycle of response that the strain can be expected to exceed a value ϵ is called the probability of exceedances.^{*} Its value is given by the formula

$$p(\epsilon) = \exp [-\epsilon^2/2\sigma^2] \text{ exceedances per cycle,} \quad (2-1)$$

where σ is the rms strain.

Equation (2-1) is based on the assumption of a stationary process. If instead, the structure is exposed for different lengths of time to a sequence of quasi-steady states having different rms values, we must combine the probabilities evaluated for each rms level, weighting each probability according to the duration of its rms level. Analytically we state, for the ensemble of different rms levels σ_n , the total probability of exceedances of strain ϵ is

$$p_{\text{tot}}(\epsilon) = \sum_n w_n(\sigma_n) p(\epsilon; \sigma_n) \text{ exceedances per cycle,} \quad (2-2)$$

where $p(\epsilon; \sigma_n)$ is given by Eq. (2-1), and $w_n(\sigma_n)$ is the proportion of the total time that the rms level σ_n exists. For example, $w(\sigma_n)$ may be expressed as "hours per flight hour."

The number of exceedances per unit time is

$$n(\epsilon) = f_r p_{\text{tot}}(\epsilon) \text{ exceedances per flight hour,} \quad (2-3)$$

* Reference 1, Section II-A; especially, footnote on p. 6.

where f_r , the resonance frequency, must be in cycles per hour in order to keep the units straight.

In view of the form of $p(\epsilon)$ given in Eq. (2-1), Eq. (2-2) can be rewritten in a more convenient form

$$p_{\text{tot}}(\epsilon) = w_0 p(\epsilon; \sigma_0) \sum_n \frac{w_n}{w_0} [p(\epsilon; \sigma_0)]^{(\sigma_0^2/\sigma_n^2)-1} \quad (2-4)$$

where σ_0 is any one particular rms value, say the largest one.

Values for the ratios w_n/w_0 and σ_0/σ_n can be evaluated from the data given in Fig. 5 of Volume I of this report. (It is assumed that response is proportional to sound pressure level.) These data pertain to RB-47E aircraft with J-47 engines (no afterburner) and include all ground operations.

Figure 4 is plotted from Eq. (2-4) using the weighting factors obtained from Fig. 5 of Volume I. In Fig. 4 the "return period" [the reciprocal of $p_{\text{tot}}(\epsilon)$ of Eq. (2-4)] is plotted against $20 \log \epsilon/\sigma_0$ where σ_0 is the largest rms level observed. The return period is essentially the average number of cycles between exceedances of the magnitude ϵ . From the data of Fig. 5 of Volume I of this report, the maximum rms strain level σ_0 corresponds to a sound pressure level of 140 db. The value of w_{137}/w_{140} ratio, for example, is found to be 1.075 hours/1000 flight hours vs. 0.025 hours/1000 flight hours, or a ratio of 43. This type of data is used in Eq. (2-4) to obtain Fig. 4. [It must be remembered that the largest sound pressure level (140 db) in the RB-47 aircraft data was 3 db higher than that observed at the "standard-day" temperature, 59°F, (see Volume I).]

To illustrate the use of Fig. 4, consider a structure that resonates at 150 cps. A flight hour would correspond to 0.54×10^6 strain cycles. Then a strain peak exceeding the highest observed rms level by 9.5 db or more would be expected, on the average once per flight hour.

A chart of the same type is given in Fig. 5. This is a plot, from Eq. (2-1) of the "return period" $[1/p(\epsilon)]$ against $20 \log (\epsilon/\sigma)$ for a single rms level. Figure 5 is a special case of Fig. 4, in two particulars. First it pertains to operation at only a single level; for this reason, the shape of the curve is different, especially at lower levels.

ASD-TDR-62-165
Volume II

Secondly, the abscissa in Fig. 5 is based on operating time at the given rms level, while the abscissa in Fig. 4 is based on total flight time, including climb, cruise, etc.

Figure 5 would be applicable to a case, such as afterburner operation, where the highest sound pressure level is so large that its contributions to the highest peaks dominates any other. Figure 5 indicates, for example, that a strain peak exceeding the rms level by 14 db or more is expected once per hour of operating time at that rms level, if the resonance frequency is 150 cps.

The preceding analysis is based on the assumption of a Rayleigh distribution of peak values. The assumption probably leads to conservative predictions in the case of a nonlinear structure. Experimental data indicates that the assumption is quite good, (Refs. 1, 3).

The additional data required to convert the information in Fig. 4 and 5 into calendar time is the average operating time accumulated in the three-month period. The results in Volume I indicated an expected average of 80 hours operation in a three-month period for the RB-47E. For a 150 cps resonant panel, the peak strain level that would be expected to occur, on the average, once in this period, is 11.5 db above rms (see Fig. 4). For a year's operation, this value is increased by 0.5 db.

For an aircraft operating with afterburner, Fig. 4 is applicable, as discussed above. Some rough estimations of the effects of afterburner operation can be made by working backwards from possible fatigue life. If an aircraft withstands only 5 hours of afterburner operation before fatigue damage occurs on a panel with a resonant mode of 150 cps, the fatigue life is about 2.5×10^6 cycles. By extrapolation from Fig. 21 of Ref. 1 for Alclad 2024, as rms strain level of about 58 db is indicated. With a strain concentration of 3 db, the strain gage would be exposed to rms strain levels of about 55 db re 10^{-6} .

If, in a three-month period, the afterburner is used for a total of 0.5 hours, the number of stress cycles is about 2.5×10^5 . The peak strain level with a return period of 2.5×10^5 cycles is approximately 14 db above the rms value (Fig. 3). (For a year's operation, 2.0 hours with afterburner, this increases to 14.5 db.) Thus, there is a high probability that single peak levels as high as 69 db re 10^{-6} will be encountered by the gage. There would be one chance in ten that a peak level of 70 db re 10^{-6} would occur in a year.

SECTION III

STRAIN TRANSDUCERS FOR THE RESPONSE RECORDER

The task to be accomplished by the response recorder has been discussed in the previous section. Here we shall discuss some problems relating to the conversion of the instantaneous strain into an electrical signal.

These problems are: * sensitivity of the strain gage to temperature variations, frequency dependence of the gage response, and self-generation of signals. These problems affect static and dynamic measurements differently. Since, in the response recorder, we are interested only in dynamic measurements, we will evaluate these problems for dynamic measurements only.

Section A considers the effect of temperature on dynamic gage measurements. This problem is indeed critical to static measurements. It is also quite important to dynamic measurements as will be shown.

Section B considers the effect of vibration wavelengths on the gage response. Strain gages yield an output which is a spatial average of the strain existing along the gage length. At wavelengths large compared with the length of the gage the strain is uniform. As the wavelength becomes smaller, one must consider what spatial averaging the gage will introduce, or else use a shorter gage.

Section C discusses the importance of magnetostrictive signals generated by the gage even in the absence of supply voltage.

Finally, the important problem of gage failure either by a single peak or cumulative fatigue is discussed in Section D (and also in Appendix C). Conclusions appear in Section E.

A. EFFECTS OF TEMPERATURE VARIATIONS ON GAGE MEASUREMENTS

Temperature variations will affect dynamic strain gage measurements by: 1) changing the gage factor, 2) affecting the bonding cement, or 3) causing apparent strains due to the difference in thermal expansion between the gage and the test surface. These effects are considered separately in the following paragraphs.

The gage factor is the sensitivity of the gage and is defined as:

$$GF = \frac{\Delta R/R}{\epsilon} \quad (3-1)$$

where $\Delta R/R$ is the unit change in resistance of the gage and ϵ is the strain ($\Delta l/l$). Typical gage factors at room temperature for various materials are: Constantan, 2.1; Nichrome V, 2.2; Karma, 2.4; Silicon, 120; and Iso-Elastic, 3.5. Typical plots of gage factor vs. temperature (Ref. 8, 9) for some materials are shown in Fig. 6. Iso-Elastic is not plotted, but its temperature performance is known to be worse than that of Constantan.

Tests of several cements (Ref. 11) indicate that they contribute to a general decrease of effective gage sensitivity by 2 or 3% above 300°F. Strain gage suppliers list over twenty cements to cover temperature ranges between -350°F to +1500°F. The selection of the correct cement is part of the strain gage art. Two cements were used for our laboratory experiments: Eastman 910 and EPY-400. The Eastman 910 is convenient to use in that it can be applied in a matter of minutes after the gage and surface have been adequately prepared. The effective gage sensitivity using Eastman 910 is within about 2% at 200°F. EPY-400 is an epoxy cement which requires several hours at elevated temperatures to cure. The effective gage sensitivity using EPY-400 is within about 2% at 350°F.

Equation (4-2) of Section IV indicates a minor sensitivity variation of the input circuit with "static" changes of the gage resistance. This effect is shown graphically in Fig. 11. The resistance changes with temperature can be indicated by the thermal coefficient of resistance for the gage material, or by a difference in thermal expansion between the gage and the material on which it is mounted, causing a strain between the gage and the mounting material.

Figure 11 shows that a 5% resistance change will vary the AC sensitivity about 0.2%. The thermal coefficient of resistance for Constantan is of the order of 2 parts per million per degree Centigrade. A 100°C temperature change would yield only a 0.02% resistance change which is completely negligible for dynamic measurements.

Another source of "static" resistance variation is the differences in thermal expansion between the gage and the material on which it is mounted. The maximum difference of thermal expansion between Constantan and aluminum or stainless

steel is less than 10 parts per million per degree Centigrade. A 100°C temperature variation would give 60 db re 1 μ strain of static strain between the gage and the specimen. This corresponds to a very small static resistance change and would have a negligible effect on the AC sensitivity.

The addition of a large DC strain could contribute to the failure of the gage, either through a single strain peak or by alteration of the fatigue properties. This is a strain that would not be present in the material under study. To our knowledge no data is available which aids in evaluating the influence of this DC strain on gage fatigue.

Constantan gages are available with different thermal coefficients of expansion designed to approximate those of typical metals. These are designed to keep the apparent strain within ± 52 db re 1 μ strain over temperatures from -20°F to +400°F.

For the majority of applications, Constantan has the advantage of a gage factor that is more stable with temperature; further, it is commercially available with several coefficients of thermal expansion. Constantan is limited to temperatures below 500°F, but in this lower range it is more stable than the other materials. Although silicon has a much higher gage factor, its limited temperature range and larger temperature variations make it less desirable for the response recorder where the strains to be measured are large.

B. FREQUENCY DEPENDENCE OF GAGE RESPONSE

High frequency measurements with strain gages are limited by the ratio of the wavelength λ in the specimen to the length l of the gage. As the wavelength λ becomes comparable to the gage length, the strain under the gage is not uniform; the gage then measures some spatial average of the strain in the area of its location.

Consider a plane wave propagating in a specimen along the major axis* of the strain gage of length l , creating a local strain along the gage equal to:

* Ideally the gage is sensitive only along one axis. Results for waves propagating from other directions would be modified by the appropriate trigonometric function, and, the apparent wavelength would be longer. Thus the case analyzed here is the worst and the most important.

$$\epsilon = A \cos kx , \quad (3-2)$$

where $k = 2\pi/\lambda$ and x is the distance along the gage. The local strain ϵ_0 at its mid-point x_0 is

$$\epsilon_0 = A \cos kx_0 .$$

The gage indicates the mean strain $\bar{\epsilon}$ along its total length l :

$$\bar{\epsilon} = \frac{1}{l} \int_{x_0 - l/2}^{x_0 + l/2} \epsilon \, dx \quad (3-3)$$

The measured strain $\bar{\epsilon}$ compared to the desired ϵ_0 can then be evaluated as

$$\frac{\bar{\epsilon}}{\epsilon_0} = \frac{\sin(\pi l/\lambda)}{(\pi l/\lambda)} . \quad (3-4)$$

Thus the strains averaged spatially by the gage yield the $(\sin x)/x$ relationship, the magnitude of which is plotted in Fig. 7. For the spatial averaging to yield less than 1% deviation, l/λ must be less than 0.09; for less than 5% deviation, l/λ must be less than 0.18.

The above relationship is applicable for either longitudinal or bending waves in the specimen. It relates a sinusoidal local strain to the averaging over the length l for given wavelength λ . In order to convert the values of λ to frequencies, the different wave velocities in the specimen for longitudinal and bending waves must be considered.

The longitudinal wave velocity c_L is: (Ref. 12)

$$c_L = \sqrt{\frac{E}{\rho}} , \quad (3-5)$$

where E is Young's modulus and ρ is the material density. The bending wave velocity c_B is: (Ref. 12)

$$c_B = \sqrt{1.8hf c_L} , \quad (3-6)$$

for a rectangular plate of thickness h . Since $\lambda = c/f$, the two limiting frequencies for a 5% deviation of the strain measured can be determined; i.e.

$$\begin{aligned} f_L &\leq \frac{.18c_L}{l} \\ f_B &\leq \frac{.06hc_L}{l^2} \end{aligned} \quad (3-7)$$

where l is the length of the gage. Applying this situation to an aluminum panel ($c_L = 15,000$ ft/sec, $h = 1/16$ inch) for a gage length of $1/2$ inch we obtain:

$$f_L \leq 65,000 \text{ cps}$$

$$f_B \leq 2,700 \text{ cps*}$$

For aluminum paneling $1/32$ inch thick, the upper frequencies of interest for the response recorder would be approached at 5% deviation. Materials such as stainless steel, titanium, and Inconel X yield frequencies for f_B close to that of aluminum. If necessary, gages shorter than $1/2$ inch could be used since the frequency f_B increases as the square of the gage length.

C. SELF-GENERATING EFFECTS

Some gages exhibit self-generating effects, that is, generation of an output voltage when no excitation voltage is applied. Experimental data has been presented by Vigness (Ref. 13) which demonstrates that 1) nickel and iso-elastic gages exhibit self-generating effects after current has been passed through the gage; and 2) Constantan gages do not exhibit self-generating effects.

* For 1% strain deviation, the corresponding frequencies are for this example:

$$f_L \Big|_{1\%} \leq 32,000 \text{ cps and } f_B \Big|_{1\%} \leq 650 \text{ cps}$$

The mechanism for self-generation in strain gages is related to the change of the magnetic field with applied stress (i.e., magnetostriction). An alternating stress would give rise to a changing magnetic field after sufficient current has been passed through the gage to leave some residual magnetism. This changing magnetic field will induce a voltage into the closely spaced loops of the strain gage pattern.

The hysteresis loop of many materials is altered with applied stress. Figure 8 illustrates this change for nickel (Ref. 14). At $H = 0$ (no current through the gage), Fig. 8 indicates that an alternating B would be generated for an alternating stress applied. At other levels of H , this effect is somewhat reduced, until at near saturation it becomes negligible.

In generating a residual magnetic field the above mechanism depends on the magnetic properties of the gage material. Permeability is not the critical parameter, but hysteresis loops or values of remanence have not been found for most of the materials; hence permeability is given as an indication of the magnetic properties of the material. The permeability of nickel (at low H) is about 500; the permeability of an Ni-Fe-Cr alloy similar to iso-elastic is above 500. The permeability of other strain gage materials is stated by their manufacturer (Ref. 15) as: Nichrome, 1.45; Nichrome V, 1.001; and Karma, 1.007. Since Nichrome V and Karma approach being non-magnetic (as is Constantan), they would not be expected to exhibit strong self-generating effects.

D. GAGE FAILURE

A single instantaneous peak of strain of the order of 85 db re 1 μ strain might break a strain gage. Instantaneous peak strains have been discussed in Section II where it was concluded that the levels of strain peaks having a reasonable probability of occurring in the period of a year are about 70 db re 1 μ strain.

Several sources of strain peaks were not considered in the earlier discussion. These would include strains due to: mechanical contact during aircraft maintenance, a "hard start" of the afterburner, or static structural loads and thermal gradients. It would seem reasonable that an allowance of an extra 4 to 6 db above the 70 db re 1 μ strain would be a more than adequate margin to accommodate these sources of strain. Since gages can withstand single peaks of about 85 db re 1 μ strain, it appears that single peaks will not fracture the gages.

Strain gage failure can also occur after many cycles through some mechanism of cumulative fatigue. Existing information on strain gage fatigue is very sparse. One strain gage manufacturer has reported data (Ref. 16) on the failure of two samples each of several types of gages excited by constant level sinusoidal strains. In view of the limited data available and the importance of this problem to the response recorder, tests of the fatigue of many samples of one gage type were conducted under random excitation. These experiments are reported in Appendix C.

The results of the gage fatigue experiments can be given in the form of a strain-life curve for the gage examined. This is shown in Fig. 9. The rms strain level for a life of 10^6 is approximately 60 db re 1 μ strain rms, and about 50 db at 10^9 cycles (linear extrapolation). It appears from a comparison of these results and the expected strain levels estimated in Table I that failure of a gage of the type tested is not expected prior to failure of the structure. The conclusion is based on the assumptions that the gage: is not at a stress concentration, has been properly mounted, and that the fatigue life is not radically altered at other than room temperature or by superimposed static strain. The validity of the last assumption is not known.

E. CONCLUSION

The dependence of gage output on temperature has been considered. Constantan seems favorable for the response recorder because of its stability, its availability with several different thermal coefficients of expansion, and its non-magnetic properties.

Consideration of the spatial averaging of local strains by a gage 0.5 inches long indicates that this length should be adequate for the frequencies and panels for which the response recorder will be used.

A 1/2 inch Constantan foil gage was selected and used in the fatigue experiments with random excitation. These experiments established part of a strain-life curve for the gage at room temperature without static strain.

SECTION IV CIRCUITRY

The response recorder is required to operate on the incoming signal in much the same manner as the sonic recorder operates on its own incoming signal. There are however some significant differences. The sonic signal is broad band and is derived from a high impedance transducer; the response (strain) signal, on the other hand, is narrow band with a significantly lower level and is derived from a low impedance transducer. The different circuitry necessitated by these factors is the subject of this chapter.

A block diagram of the response recorder is given in Fig. 10. A comparison of Fig. 10 of this report with Fig. 12 of Volume I shows the following modifications: an "input circuit" is added, the aerodynamic noise discriminator is deleted, three data filters are used rather than four, and a seventh window is added to the amplitude distributor.

The input circuit described in Section A below provides the signal conditioning for the strain gage signal and additional amplification. Possible grounding problems suggest the need for a floating circuit. The input circuit replaces the field effect transistor circuit of the sonic recorder.

In the sonic recorder, aerodynamic noise and jet noise signals must be separated, since each influences panel response very differently. This separation is not needed in the response recorder since it is the panel response that is being monitored. Hence the discriminator is unnecessary for the response recorder.

Relatively narrow band filters are required to separate the narrow band modes of the panel response, whereas octave band filters were used for the sonic recorder. Filters for two such modes and for an "over-all" are discussed in Section B. The over-all filter (50-750 cps) would be useful for cases where no strong modal pattern exists and for a general check on performance. The damping factor of the panel can be rather small, resulting in very narrow band signals. Since the envelope of very narrow band signals fluctuates much more slowly than the envelope of broad band signals, the detector time constant should be reconsidered, as discussed in Section C.

Although no change in the amplitude distributor is dictated for the response recorder, some further refinements have been added which provide more flexibility with a minimum of additional components. These are discussed in Section D.

Our goal has been to maintain interchangeability and compatibility between the sonic recorder and the response recorder. The design has been accomplished with the intent of allowing a basic recorder to be converted to either sonic or response functions with plug-in units. This conversion is discussed in Section E.

A. INPUT CIRCUIT

The input circuit of Fig. 10 includes a circuit sensitive to AC changes of resistance, a temperature-compensated voltage source, and an amplifier. Factors influencing the design of this circuitry are discussed in this section.

1. Strain Gage Circuit

A four-arm resistance bridge is normally used to obtain compensation of long term effects in static strain measurements. For dynamic measurements, this long term compensation is not required unless it influences the sensitivity, linearity, etc., of the dynamic measurement. This is considered below.

a) Strain Sensitivity

The strain sensitivity (S_ϵ) of a Wheatstone-bridge circuit with a strain-gage and three fixed resistors is (Ref. 17):

$$S_\epsilon = \frac{dE_o}{d\ell/\ell} = \frac{E(GF)R_A R_G}{(R_A + R_G)^2} \quad (4-1)$$

where:

- R_G = strain gage resistance and fixed resistor value opposite to gage,
- R_A = fixed pair of resistors in bridge,
- E = supply voltage,
- E_o = output voltage across the bridge,
- $d\ell/\ell$ = ϵ = strain,
- GF = gage factor as given in Eq. (3-1).

The above assumes that the output voltage is monitored by a high impedance device. For the special case of $R_G = R_A$ the formula reduces to:

$$S_e = \frac{E(GF)}{4} \quad (4-2)$$

A similar relation can be derived for a single resistor R_A in series with the gage, where R_G is again the gage resistance. The resulting equation is:

$$S_e = \frac{E(GF)R_G R_A}{(R_G + R_A)^2} \quad (4-3)$$

for a high impedance monitoring device. This is identical to (4-1) above; hence both the bridge and potentiometer circuits have the same strain sensitivity under the conditions analyzed.

b) Sensitivity Variation

Since the equations for the two systems are identical, the influence of static changes of R_G and R_A are identical. The percentage change of S_e for various ratios R_A/R_G is shown in Fig. 11.* Note that changes in the dynamic sensitivity can be caused by static resistance changes. If the ratio of R_A/R_G is 1.00 at calibration, and it slowly fluctuates between .95 and 1.05, the strain sensitivity will vary about 0.2% from calibration. To minimize this variation, it is well to choose R_A and R_G nearly equal and thus operate where the slope is near zero. The change in resistance expected from R_G was considered in an earlier section and was found to have a negligible effect on sensitivity.

* Figure 11 also shows that the maximum sensitivity for a given supply voltage E is reached when $R_A = R_G$.

The series resistor R_A can have a very low temperature coefficient of resistance. It might be possible to effect some compensation of the gage factor variation of Constantan with temperature (see Fig. 6), by using a temperature sensitive resistor for R_A . The gage factor's increase with increasing temperature is already small, and this added compensation is not necessary. However, if other gage materials are used it might be desirable to employ this technique.

In summary, the relative sensitivities for bridge and potentiometer circuits have been reviewed. The influence of resistance changes expected from the temperature coefficients of resistance and thermal expansion are expected to have a negligible effect on strain sensitivity. There appears to be no advantage in using the bridge circuit for the dynamic measurements of the response recorder. Since the potentiometer is simpler, it is applied to the response recorder.

2. Balanced Circuit

In measuring low level signals a balanced circuit is desirable; with such a circuit the effects of ground loop currents and of induced signals common to both sides of the circuit can be considerably reduced. Balanced circuits are often analyzed (Ref. 18) in terms of common mode signals and difference mode signals. A measure of how well the circuit is balanced is given by its common mode rejection; this is defined as the ratio of the circuit transfer function where equal signals are applied to the two sides of the input (common mode) to the circuit transfer function when the same signal is applied between the two sides of the input (difference mode).

A simplified situation is shown in Fig. 12. A potential e_N is assumed between the ground of the input amplifier and the specimen to which the transducer with resistance R_G is mounted. The voltage e_N is applied commonly to both ends of R_G (the input terminals) through the resistance to ground, R_1 . The equivalent circuit shown in Fig. 12b can be drawn if the input impedance of the amplifier is large compared to R_G . If the following values are assumed,

$$R_G = 120 \text{ ohms,}$$

$$R_1 = 1,000,000 \text{ ohms,}$$

$$e_N = 1 \text{ volt,}$$

we see that a potential difference of one volt between grounds causes a current of 1 μ amp to flow through R_G , giving a ground loop voltage of 120 μ volts at the input to the amplifier.

If the amplifier input were floating with respect to ground, the unbalanced current could be reduced. This reduction can be accomplished by using a transformer as illustrated in Fig. 13a. The AC equivalent circuit using a high impedance amplifier is shown in Fig. 13b, from which the response to e_N is found to be zero:

$$\frac{e_a}{e_N} = 0. \quad (4-3)$$

This ideally yields infinite common mode rejection. However, the rejection will be limited by the matching (i.e., balancing) of the components used since the noise currents must split equally between the two paths for ideal cancellation.

The response to the desired strain signal can be found by placing a signal source e_s in series with R_G . This response might be considered the gain of the circuit before the input amplifiers and is:

$$\frac{e_a}{e_s} = \frac{R_1}{R_1 + R_G} \approx 1 \quad (4-4)$$

where R_1 is very large compared to R_G .

The response to an unbalanced noise disturbance can be examined by applying e_N to only one side of R_G (setting one of the R_1 's to infinity). The response to e_N is then found to be:

$$\frac{e_a}{e_N} = \frac{3R_G}{4R_1} \quad (4-5)$$

This is approximately the same attenuation that was shown for Fig. 12a. Much can be done to insure that noise disturbances are balanced by employing twisted pair conductors. The resistance between the gage and ground is a distributed impedance across the gage (and hence balanced) if the gage is properly mounted.

The discussion can be extended by considering also a capacity, C , in parallel with R_1 . Above the break frequency ($2\pi f = 1/R_1C$) the capacity reduces the impedance in series with

ASD-TDR-62-165
Volume II

e_N by 6 db per octave, decreasing the attenuation by 6 db per octave. If there is a rather large capacity, 50 picofarads, in parallel with a low value of R_1 , 1 megohm, the break frequency is about 3000 cps. If R_1 were actually 20 megohms instead of 1 megohm, this break frequency would be 300 cps; but an R_1 of 20 megohms will increase the attenuation of e_N by 26 db, making its contribution negligible. Therefore the combination of 50 picofarads and 1 megohm is considered a severe case.

In summary, ground loop problems can be very serious for strain gage systems. It is therefore best to use a balanced circuit to reduce the effects of ground loops. There are many factors which are difficult to consider. For example, the voltage level of e_N and resistances of R_1 change with time and conditions. It is necessary to provide all the attenuation of unwanted signals possible in the design of the input circuitry. Although under most conditions the single-ended circuit might be adequate, we are using a balanced input to provide additional insurance against ground-loop problems.

3. Strain Gage Voltage Supply

The voltage source shown as the battery in Fig. 13a must be very stable. The strain sensitivity is directly proportional to this voltage (see Eq. (4-1)). It would be convenient if the required voltage could be derived from the regulated supplies used for the other circuits.

Zener diodes which are temperature compensated to .01% per degree Centigrade over a range of -55 to +100°C are currently available. The total variation in voltage over the 150°C temperature range is 1.5%. It is necessary to maintain the current through the diode at about 7.5 ma. The diode chosen (1N821) has a Zener potential of 6.3 volts. This is the minimum voltage available for temperature compensated units. The breadboard circuit is shown in Fig. 14. The final values for the resistors from the ± 28 volt supplies would be selected to supply 7.5 ma to the diodes with the desired value of R_A and R_G .

The Constantan foil strain gage can be safely used at 50 ma for dynamic measurements. It is then possible to use two diodes in series as shown in Fig. 14 for a 12.6 volt supply, giving a high sensitivity. If other strain gages or conditions demand lower currents, the supply can be reduced to 6.3 volts (25 ma to a 120 Ω gage) by bypassing one of the diodes.

4. Input Amplifier

Shown in Fig. 14 is an amplifier which is transformer coupled to the strain gage circuit. This amplifier employs silicon transistors of the same type used in the sonic recorder, arranged in a circuit with DC feedback to insure good stability. This amplifier is intended to drive the attenuator in Fig. A-1, Volume I, of the sonic recorder, in place of the input cathode follower circuit.

Measurements have been taken with the circuit as shown in Fig. 14. A floating oscillator was placed between input terminals A and C of the simulated strain gage. The maximum gain from terminals A-C at 200 cps is 37 db; the minimum gain, 24 db. The gain is adjustable with the potentiometer in the feedback path of the amplifier. The frequency response is within ± 0.5 db from 18 cps to 10 KC and is within ± 1 db from 12 cps to 18 KC. The maximum peak-to-peak output voltage is 6 volts at minimum gain and 9 volts at maximum gain. The equivalent input noise floor was measured to be -93 db re 1 volt rms wideband with maximum gain.

Measurements have been made of the common mode rejection with the signal source placed between input terminal B and ground, simulating a balanced disturbance such as that in Fig. 13. For this experiment, R_1 between R_g and ground was 600 ohms rather than the several megohms expected for strain gage installations. Common mode rejection of 68 db was observed for frequencies between 50 cps and 20 KC. As shown in Section A.2 above, there should theoretically be infinite rejection, but small non-equalities in the system which create unbalanced disturbances result in a deviation from theoretical rejection.

Measurements with a strain gage mounted to an aluminum specimen yield a common mode rejection of 107 db. This additional rejection is dependent upon the value of R_1 between the gage and the sample (which was measured as greater than 100 megohms for the test). Under conditions of high humidity, R_1 could be significantly reduced; but even if R_1 were 600 ohms, 68 db of rejection would still remain. Special techniques can be employed to waterproof the gage and insure a high value of R_1 (Ref. 19).

The minimum strain signal that can be measured can be estimated. The strain signal is assumed to be:

$$e_a = \frac{(GF)(12.6)\epsilon}{4} = 6.5 \epsilon \text{ volts,}$$

where ϵ is in μstrain .

ASD-TDR-62-165
Volume II

The noise floor of -93 dbv would allow voltages as low as -83 dbv to be 10 db above the noise floor. The -83 dbv would correspond to a strain of 22 db re 1 μ strain. A common mode signal of less than -95 dbv (corresponding to an e_N of 1 volt and 95 db rejection) would also be several db below the minimum strain signal.

The maximum strain signal which can be handled by the input circuit without clipping is -14 dbv peak, or a strain of about 90 db re 1 μ strain. This is above the strain level which fractures the strain gage with a single peak.

B. DATA FILTERS

Two relatively narrow band filters and one broadband filter are required in place of the octave band filters used in the sonic recorder. It is necessary that the narrow band filters match the resonances of the structures being examined.

1. Narrow Band Filters

The simplest form of bandpass filter is the single parallel-tuned circuit. The center frequency required dictates the L and C of the filter. The bandwidth of the circuit is variable with the equivalent resistance appearing across the tuned circuit (subject to the limitations of the Q of the inductor). This simple form of filters has a "rounded top" and fairly shallow slopes for low Q's. More sophisticated filters have squarer tops and steeper edges.

Many filters need be available to cover the frequencies from 50 cps to 750 cps. Tunable filters have been considered. The single-tuned stage can be made variable by incorporating a variable inductor. However, the insertion loss of the filter and its equivalent bandwidth change with the tuning, particularly if the range of frequencies is large. Also, it could be expected that the variable inductor would be less stable than fixed inductors over long periods of time under severe environments. The stability of the center frequency of the filter is very important for the response recorder. More sophisticated filters could also be made variable, but several components would have to be varied and the filter would be more complex and less stable.

For these reasons, it is preferable to use a fixed filter. Since the narrow band filters required for any single installation will be used for a long period of time, it is practical to acquire these filters for a given application. Several manufacturers are currently marketing compact bandpass filters for

ASD-TDR-62-165
Volume II

telemetry purposes. For interim applications, simple LC filters could be designed quickly and used for panels where the modes are narrow and widely separated.

For more general use, a bandpass filter meeting the following performance specifications should be used:

Center Frequency:	as dictated by panel mode,
Insertion Loss:	not more than 10 db,
Impedance:	10,000 ohms,
Pass Band:	flat within 0.5 db for +5% of center frequency; down at least 10 db at +25% of center frequency.

2. Over-all Filter

The over-all filter requirements can be met with a constant-k filter designed for 10,000 ohms. A typical filter of this type was realized and is shown with its response in Fig. 15.

C. DETECTOR

The detector time constant for the sonic recorder was selected as 2.5 seconds. The dominant concern in selecting this time constant was the ability to follow the changing rms value of the sound pressure level. For random narrow band signals, such as those expected for the response recorder, the variation of the detected output (i.e., envelope of the signal) must also be considered. The narrow band signal is derived from the modal response of the panel.

Rice (Ref. 20) has examined the envelope of a narrow band signal as a random energy fluctuation about a mean value. The standard deviation σ of this energy fluctuation is given approximately for an ideal narrow band filter as:

$$\frac{\sigma}{m} \sim \frac{1}{\sqrt{BT}} \quad (4-6)$$

where m is the mean energy, B the filter bandwidth in cps, and T the averaging time in seconds. This deviation of the mean energy causes an uncertainty in the amplitude window due to the random variation of the detector output. Ideally, a large enough T should be used to reduce σ/m to less than the window width. A BT product of 16 restricts σ/m to about 1 db.

ASD-TDR-62-165
Volume II

A step in excitation can arise from thrust augmentation, which results in a step of roughly 4 db, depending upon conditions. This step is usually expected to last at least twenty seconds.

The time constant of the narrow band panel response to a step is $T_p = 1/\pi B$ where B is the bandwidth in cps and T_p is the time constant of the envelope. This time constant is significantly faster than any allowable detector time constant. It is therefore necessary that the detector time constant be a small part of the total time that the step is to be applied*

A detector time constant of 4 seconds, which is about one-fifth of the expected minimum length of thrust augmentation, is the maximum tolerable. For a BT product of 16, the minimum bandwidth of the panel modes would be 4 cps. The variance of the rms level for panel bandwidth narrower than this would have to be accepted.

This detector time constant can be realized by increasing the two capacitors of the detector in Fig. A-4 of Volume I by a factor of 1.5. The 1.35 K Ω series resistor would then have to be adjusted in accordance with Section E of Appendix B of Volume I.

D. MODIFICATION OF THE AMPLITUDE DISTRIBUTOR

The operation of the amplitude distributor has been previously described in Volume I. Considerations given in Appendix A of the present report indicate that 2 db amplitude windows are adequate for the response recorder as well as for the sonic recorder. Information given in Section II and Appendix A indicates that a total range of 12 db should be adequate. However, since the ease of setting the instrument is dependent upon the total range, two techniques have been considered to effectively expand the range of amplitudes without significantly increasing the equipment required.

* First order cancellation of the error due to the slower detector time constant will occur since, although it does not "turn on" quickly, it also does not "turn off" as quickly as the panel response.

ASD-TDR-62-165
Volume II

First, the lowest window is expanded to 4 db instead of the 2 db used in other windows, increasing the total range to 14 db and reducing possible truncation errors. Secondly, an "overflow window" is considered to indicate if there are any counts at higher strains than the calibration.

The total range of the distributor has been established to yield five 2 db windows and one 4 db window. A unique bias voltage from the reference supply in Fig. 10* is required. The amplitude range is a function of this bias voltage. If non-equal windows can be tolerated, an adjustment of the bias voltage varies the windows. Methods of expanding the range are discussed in the next section.

1. Expanded Range

There are two methods whereby the range can be expanded to 14 db. First, the 0 to 5 volt input voltage to the voltage-controlled oscillator (VCO) can be made to correspond to 14 db rather than 12 db. This change would require a slightly different bias voltage and would compress the bandwidths of the analysis filters following the VCO.

The second method uses the VCO at input voltages higher than the standard 0-5 volts used for telemetry purposes. This is possible since the linearity required for this application is not as stringent as for telemetry. Measurements on the VCO used in the sonic recorder indicate that it is linear within $\pm 1\%$ up to 8 volts input. Inputs above 5 volts could then be used to expand the range to 14 db, retaining the same bias voltage and filters. The maximum input voltage required for 14 db is 6.79 volts. However, this method has the disadvantage of requiring higher output from the quasi-rms detector and amplifier, effectively reducing the peak factor from 10 db to 8 db.

The second method was used in the breadboard of the analyzer and is expected to be slightly more accurate since the filter bandwidths are slightly larger. The effect of the reduced peak factor with random inputs is evaluated and discussed in a later section. The filter edges used are tabulated in Table III.

* See Section III.B. of Volume I of this report.

TABLE III
IDEAL FILTER EDGES FOR 14 DB RANGE

<u>Window No.</u>	<u>db Window</u>	<u>VCO Input Voltages</u>	<u>Frequency Band Edges</u>	<u>Bandwidth (cps)</u>
1	0 - 4	0.0 - 0.97	18,700 - 19,990	1290
2	4 - 6	0.97 - 1.65	19,990 - 20,900	910
3	6 - 8	1.65 - 2.51	20,900 - 22,040	1140
4	8 - 10	2.51 - 3.58	22,040 - 23,480	1440
5	10 - 12	3.58 - 5.00	23,480 - 25,300	1820
6	12 - 14	5.00 - 6.79	25,300 - 27,680	2380

2. Overflow Window

An extra counter, in addition to the six previously used, is included to accumulate the exceedances above the 14 db range, performing essentially as an overflow counter. This counter will give information about the applicability of the range over which the instrument has been calibrated and the general operation of the system. The overflow counter is provided instead of an additional window because: (1) no additional linearity or peak factor requirements are imposed on the VCO or detector, and (2) the output from the strain gage frequently rises as it begins to fatigue as indicated by the gage fatigue experiments (See Appendix C). This signal increase may be above an additional 2 db window and not be noticed.

The overflow position requires another filter and counter following the voltage-controlled oscillator. The filter could be a constant-k 10,000 ohm high-pass filter with the 6 db frequency at 28,000 cps. The rest of the circuitry would be the same as for the other windows.

3. Window Variation

A unique bias voltage (1.66 volts) is required to establish the 14 db range required. The bias voltage supply (shown in Fig. A-6 of Volume I) is variable up to about 2.5 volts. This

allows some flexibility in the window widths, although the resulting windows will not be equally spaced as shown in Fig. 16. The resulting windows for various bias voltages are tabulated in Table IV.

TABLE IV
WINDOWS FOR VARIOUS BIAS VOLTAGES USING FILTERS OF TABLE III

Window No.	Bias Voltages		
	-1.00	-1.66	-2.00
1	5.9	4.0	3.5
2	2.5	2.0	1.7
3	2.5	2.0	1.8
4	2.4	2.0	1.9
5	2.4	2.0	1.9
6	2.3	2.0	2.0
RANGE	17.9	14.0 db	12.9 db

The circuitry has been designed to yield even windows covering 14 db, as shown, for the -1.66 volts bias. However, the other bias values can be used if the variation of window width is accounted for in the data reduction. The total detector range as indicated in Fig. 18 must be considered.

E. COMPATIBILITY OF RESPONSE RECORDER AND SONIC RECORDER

The design has been conducted with the intent of allowing a basic recorder to be converted to sonic or response functions. The basic recorder would be converted by inserting one or the other of the following sets of modules:

	<u>Response Recorder</u>	<u>Sonic Recorder</u>
Input Circuit:	As described in Section A above	Field Effect Circuit (Fig. B-1 of Volume I)
Filters:	2 narrow band 1 over-all	4 octave bands

ASD-TDR-62-165
Volume II

The same detector time constant, sampling arrangement, and amplitude distributor is used for both. As a result one of the sampled channels would not be used for the response recorder and an unused bank of counters would be present. Thus the price of convertibility is slightly increased instrumentation.

A combined two-input recorder as illustrated in Fig. 16 could be considered.* Such a combination could be accomplished by adding a second amplifier and attenuator to the basic recorder and using the strain gage and microphone concurrently.

* This is essentially the Type 4 Recorder discussed in Volume I.

SECTION V

SYSTEM PERFORMANCE

System performance is examined in two ways: 1) experimental data taken in the laboratory and 2) estimated errors expected for long operation in a severe environment.

A series of experiments with the breadboarded response recorder have been conducted. These experiments consist of applying consistently a known strain signal to the response recorder for long periods of time and comparing the resulting accumulation with the expected one. These experiments are discussed in Section A.

Much of the error analysis for the sonic recorder is applicable to the response recorder. Differences will be reflected in the input circuit, calibration, etc. These error contributions for the complete response recorder are considered in Section B.

A. EXPERIMENTAL EVALUATION

The response recorder is designed to acquire the amplitude distribution of the rms of a signal over a long period of time. This operation can be divided into two functions: 1) converting the input signal into a DC voltage proportional to the rms level of the input signal, and 2) examining the amplitude of this DC voltage by quantizing it into levels and accumulating the counts. The evaluation of the circuitry can also be separated into these two functions.

1. Data Acquisition

Measurements have been made with the breadboarded data acquisition equipment. This equipment performs the function of conditioning and detecting the input signal, yielding a DC output proportional to the rms of the input signal.

a) Measurements with Insert Voltages

A floating sinusoidal input signal was applied to the insert voltage connector of the input circuit in Fig. 14. The resulting input voltage to the VCO and the rms level of the insert voltage were monitored. The data is plotted in Fig. 17. The range of detector output which is used in the response recorder is indicated by the brackets. At both ends the detector output becomes

nonlinear, but the total usable range is about 19 db (14 db is required). The nonlinearity at the low end is caused by the detector diodes. The limiting at the high voltages is caused by clipping in the amplifier preceding the detector. The accuracy of the data of Fig. 17 is believed to be within ± 0.2 db.

b) Measurements of Strain

An excitation system similar to that in Fig. C-2 of Appendix C was used to drive a strain gage. The rms of the excitation voltage to the shaker and the rms of the output voltage of the amplifier preceding the detector were monitored.* The resulting data for sinusoidal and random excitation are given in Fig. 18. The frequency was set at the resonance of the bar on which the gage was mounted. The Q of the bar is approximately 30. The random signal was filtered into an octave band before application to the shaker. The strain gage output was a narrow band random signal (corresponding to the resonance of the bar) which served as the input to the response recorder.

The effect of the peak factor of the random signal is shown by the data in Fig. 18. The sine wave output showed visible distortion beginning about 24 dbv. With random noise the limited peak factor affects the output as low as 18 dbv. Since the upper window edge corresponds to 16 dbv, this peak factor is considered adequate.

Note that the slope of the sine and random data is the same, but the random signal required consistently more excitation voltage to the shaker for the same output voltage. This is due to the driver excitation voltage being an octave band (150-300 cps) whereas the bandwidth of the strain gage signal was only 7 cps.

The accuracy of the sine data is expected to be within ± 0.2 db. The random data is difficult to read closer than within ± 0.3 db.

* A Ballantine 320 RMS Meter with a long averaging time was used instead of the detector so that the rms value of the random signals could be more accurately read. The performance of the detector with sine and random excitation was reported in Volume I and has been checked for narrow band random excitation.

The data presented in Fig. 17 and 18 indicate the performance of the data acquisition equipment in the measurement of actual strain for sine and narrow band random signals.

2. Complete System

Evaluation of the complete system required a method of programming the amplitude of the excitation voltage for the shaker. A controlled gain amplifier was used to program the rms level. The DC control voltage is applied to the grid of the tubes. The change of AC gain with the control voltage was not linear over the total range, exhibiting a curvature near both ends which would tend to increase the counts collected at both end windows. This curvature has been measured and is accounted for in the data. Data from a programmed sine wave is given in Table V for a 15 1/2 hour experiment. The resulting error in counts is less than 1.5% for all windows.

Data employing an octave band of random noise to excite the resonant bar is also tabulated in Table V and shown in Fig. 19. The BT product for this experiment was 17.5 ($T = 2.5$ sec and $B = 7$ cps). Resulting errors are less than 2.5% for all windows.

In addition to the above experiments, the response recorder has been operated continuously with strain input signals for more than a week. During all of the experiments conducted on the response recorder, the counter associated with the No. 6 window (the widest) received 147,786 counts. The six counters combined received over 514,000 counts.

B. ERROR ANALYSIS

Errors were classified into three categories in Volume I for the sonic recorder: systematic, short term, and long term. Since much of the sonic recorder is used for the response recorder, some of the error data from Volume I apply. The systematic and short term errors for the response recorder are discussed below. All error figures are assumed as 2σ values.

1. Systematic Errors

Systematic errors are those inherent in the recorder when all external factors are disregarded. Errors from calibration, data acquisition, amplitude distribution, and sampling were discussed for the sonic recorder. Only the calibration and transducer errors will be discussed here; the other errors are expected to be slightly lower than in the sonic recorder since: (1) some of the amplitude distributor window widths are slightly larger, and (2) the activity of the aircraft will probably be greater than assumed in the original estimate, thus reducing the sampling errors.

TABLE V
DATA FROM RESPONSE RECORDER DURING STRAIN EVALUATION TESTS

	Amplitude Window (db)	Sine Wave Excitation		Random Excitation									
		Expected	Actual	Exp.	Act.	Exp.	Act.	Exp.	Act.	Exp.	Act.	Exp.	Act.
Counts	12-14	10350	10302	2000	2022	3080	3102	11300	11497	13300	13517		
	10-12	7650	7719	1510	1508	2320	2336	8550	8418	10000	9825		
	8-10	5460	5539	1060	1013	1630	1566	6000	5874	7050	6912		
	6- 8	4650	4667	900	865	1380	1336	5100	4984	5960	5829		
	4- 6	3550	3578	686	662	1055	1022	3890	3849	4550	4481		
	0- 4db	5920	5987	1160	1228	1790	1891	6580	6821	7700	7895		
Per-Cent Error	12-14		+0.5%		-1.1%		-0.7%		-1.7%		-1.6%		
	10-12		-0.9		0.0		-0.7		+1.5		+1.8		
	8-10		-1.45		+4.4		+3.9		+2.1		+1.9		
	6- 8		-0.4		+3.9		+3.2		+2.5		+2.2		
	4- 6		-0.8		+2.0		+3.1		+1.1		+1.5		
	0- 4		-1.1		-5.8		-5.6		-3.7		-2.5		
Length of Test		15 1/2 hours		2 1/2 hours		4 hours		14 1/2 hours		17 hours			

A satisfactory method of physical strain calibration is not available. Standard practice for static measurements uses shunt resistors to simulate a small resistance change and does not calibrate the transfer function between strain and resistance change (gage factor), although it does calibrate the rest of the system. A technique that yields a similar result for dynamic measurements is an insert voltage, i.e., a voltage from a very low impedance source applied in series with the gage.

The gage factor is quoted from the manufacturer's data. It is usually assumed that this is within 5% of the actual value for a correctly mounted gage and this variation is incorporated here, contributing ± 0.5 db error (2σ).

The voltage calibration of the recorder involves many steps (see Appendix E). Our estimate of a minimum error for a careful calibration is ± 0.3 db.

Total systematic errors are then:

Transducer	± 0.5 db,
Calibration	± 0.3 db,
Data Acquisition	± 0.3 db,
Amplitude Distribution	± 0.1 db,
Sampling	± 0.4 db.

Combination of these independent errors yields a 2σ value of ± 0.77 db.

2. Short Term Errors

The short term errors are those caused by cyclic external factors, the primary source being temperature variations.

Temperature effects on the strain gage have been discussed in this report. The recorder variations with temperatures have been discussed in Volume I and need be slightly modified to reflect circuit changes. The gage factor variation of Constantan is .0008 db per $^{\circ}\text{C}$ (See Fig. 6). A change of $\pm 60^{\circ}\text{C}$ yields about $\pm .05$ db variation. The temperature sensitivity of the voltage supply is .001 db per $^{\circ}\text{C}$, yielding $\pm .06$ db variation.

The other error contribution should be identical to the sonic recorder yielding $+.00003$ db/ $^{\circ}\text{C}$ gain variation and $+0.25$ millivolts/ $^{\circ}\text{C}$ window width shift, and $+0.4$ millivolts/ $^{\circ}\text{C}$ of bias shift from the amplitude distributor.

ASD-TDR-62-165
Volume II

The lowest amplitude window is 4 db and 0.97 volts wide. A ± 0.04 volt variation corresponds to about $\pm 4\%$ of the window, i.e., ± 0.16 db. The narrowest amplitude window is #2 at 0.68 volts, with the $\pm 4\%$ corresponding to ± 0.24 db (the worst case).

To summarize the short term errors for -50°C to $+70^{\circ}\text{C}$:

Strain gage error	± 0.05 db
Recorder error	± 0.28 db

These errors may not be independent.

3. Accumulated Error

The total error is anticipated to be:

$$\begin{aligned}\text{error}_{2\sigma} &= \sqrt{(0.77)^2 + (0.33)^2} \\ &= \pm 0.85 \text{ db}\end{aligned}$$

for ambient temperature of -50°C to $+70^{\circ}\text{C}$. This includes errors from the strain gage, but assumes the desired strain is present at the gage. This error is less than that anticipated for the sonic recorder, primarily because of the lower temperature variation of the gage factor compared to the sensitivity of the microphone.

SECTION VI

CONCLUSIONS

Requirements for a response recorder have been considered. A design to meet these requirements has been made, and a representative system breadboarded and evaluated. This evaluation verifies that the design satisfies the requirements for the response recorder.

Although the response recorder has been designed for application to aircraft, it is, in a general way, a strain exposure meter, just as the sonic recorder is a sonic exposure meter. As such, applications of these types of instruments can vary widely. Specific uses of the recorders as applied to aircraft could include:

- 1) Gathering data of the accumulated exposure of an individual aircraft under operational conditions.
- 2) Gathering an ensemble of data over a population of aircraft under certain conditions, which would allow estimation of the fatigue damage of the whole population of aircraft.
- 3) Using the above ensemble of data to check hypotheses on fatigue damage mechanisms.
- 4) Providing background data for specifications for new vehicles.

It is tempting to consider the use of a combined strain and sonic recorder to gather some indirect data on the relative contribution to fatigue of jet and aerodynamic noise. In principle, this would be possible since the sonic recorder accumulates the long term rms amplitudes of the jet noise excitation only, while the response recorder would accumulate the response to both jet and aerodynamic noise (if the response to aerodynamic noise is great enough). However, more useful data on this subject could be obtained by tape recording the instantaneous pressure and strain amplitudes for a few flights, and then analyzing them more completely. The sonic and response recorders are best applied where the long term statistics are most important.

LIST OF REFERENCES

1. Smith, Jr., P. W., and Malme, C. I., "Sonic Fatigue Life Determination by Siren Testing," ASD TR 61-639 [BBN Report No. 885] December 1961.
2. Schjelderup, H. C., and Galef, A. E., "Aspects of the Response of Structures Subject to Sonic Fatigue," WADD TR 61-187, July 1961, also AD 268260.
3. Eshleman, Jr., A. L., VanDyke, Jr., J., and Belcher, P., "A Procedure for Designing and Testing Aircraft Structure Loaded by Jet Engine Noise," ASME preprint paper 59-AV-48; especially see Fig. 9.
4. Thrall, Jr., E. W., "Acoustically Induced Fatigue -- Cause, Solution, and Design Analysis," SAE preprint paper 164A, SAE National Aeronautic Meeting, April 1960; on the A3D aircraft.
5. Schjelderup, H. C., "Structural Acoustic Proof Testing," Noise Control, 5, 351-360, (1959); on the B-66 aircraft.
6. Schjelderup, H. C., "The Modified Goodman Diagram and Random Vibration," J. Aerospace Sciences, 26, 686, (1959).
7. Dyer, I., Smith, Jr., P. W., Malme, C. I., and Gogas, C. M., "Sonic Fatigue Resistance of Structural Designs," ASD TR 61-262 (BBN Report No. 873) March 1961.
8. Weymouth, L. J., "Present-Day State of the Strain Gage Art," 1960, Baldwin-Lima-Hamilton.
9. Bulletin 4328, Baldwin-Lima-Hamilton, December 1961.
10. Talmo, R. E., "Semiconductor Strain Gages Offer High Sensitivity," Electronics, February 24, 1961.
11. Technical Data, Baldwin-Lima-Hamilton, No. 4310-2, March 1958 and No. 4310-8, May 1959.
12. Beranek, L. L., Noise Reduction, McGraw-Hill, 1960, 284-285.
13. Vigness, I., "Magnetostrictive Effects in Wire Strain Gages," Proc. Soc. Experimental Stress Anal., 14, No. 2, 139-148; and "Magnetostrictive Electricity in Strain Gages," JASA, 27, No. 12, December 1956.

ASD-TDR-62-165
Volume II

14. Bozorth, R. M., Ferromagnetism, Van Nostrand, New York, 1951.
15. Correspondence with Driver-Harris Company, New Jersey.
16. Technical Data, Baldwin-Lima-Hamilton, No. 4310-3, August 1958, No. 4310-7, May 1959, and No. 4310-8, May 1959.
17. Perry, C. C., and Lissner, H. R., Strain Gage Primer, McGraw-Hill, 1955.
18. Valley, Jr., G. E., and Wallman, H., Vacuum Tube Amplifiers, MIT Radiation Laboratory, Vol. 18, McGraw-Hill, 1948, Page 443.
19. Perry, C. C., and Lissner, H. R., Strain Gage Primer, McGraw-Hill, 1955, Chapter 8.
20. Rice, S. O., "Mathematical Analysis of Random Noise," Noise and Stochastic Processes, edited by N. Wax, Dover, 1954.

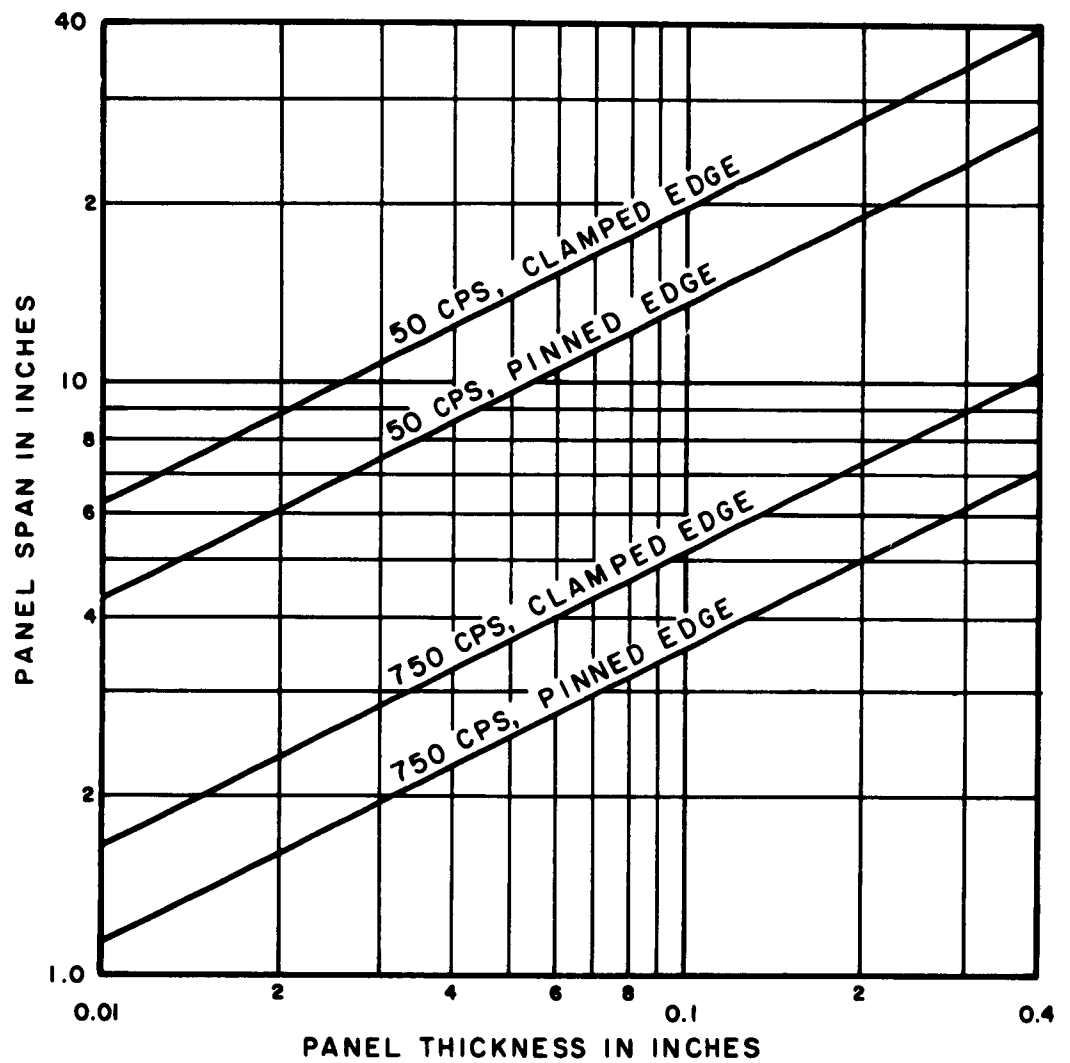


FIG. 1 RANGE OF VALUES OF PANEL SPAN AND THICKNESS HAVING FUNDAMENTAL RESONANCE FREQUENCIES AS SHOWN

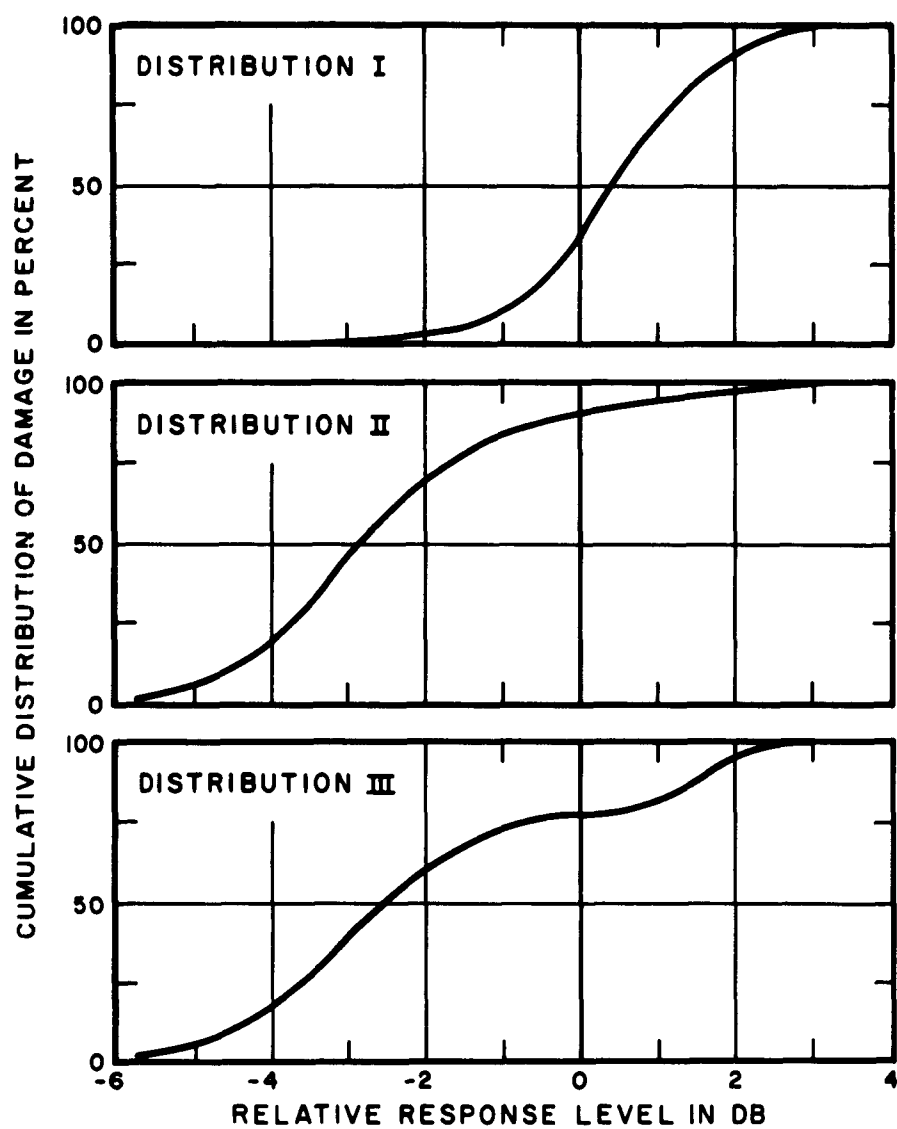


FIG. 2 TYPICAL CUMULATIVE DISTRIBUTIONS
OF FATIGUE DAMAGE (FROM FIGURES
I, 3 AND 4 OF APPENDIX A)

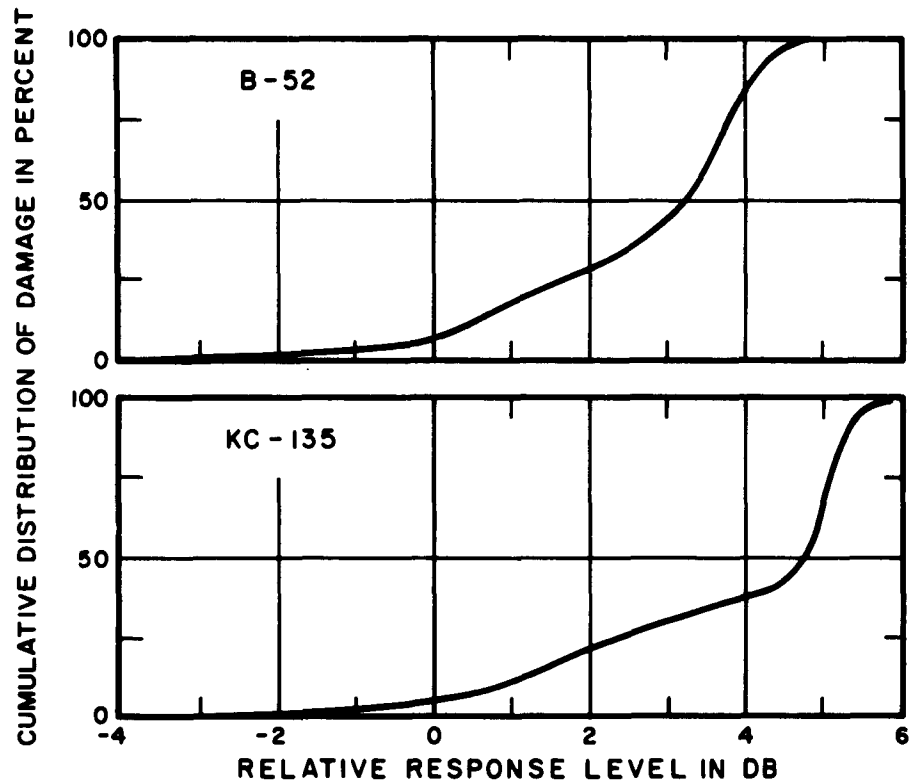


FIG. 3 CUMULATIVE DISTRIBUTION OF FATIGUE
DAMAGE FOR B-52 AND KC-135 AIRCRAFT
(BASED ON RESPONSE DATA IN APPENDIX D)

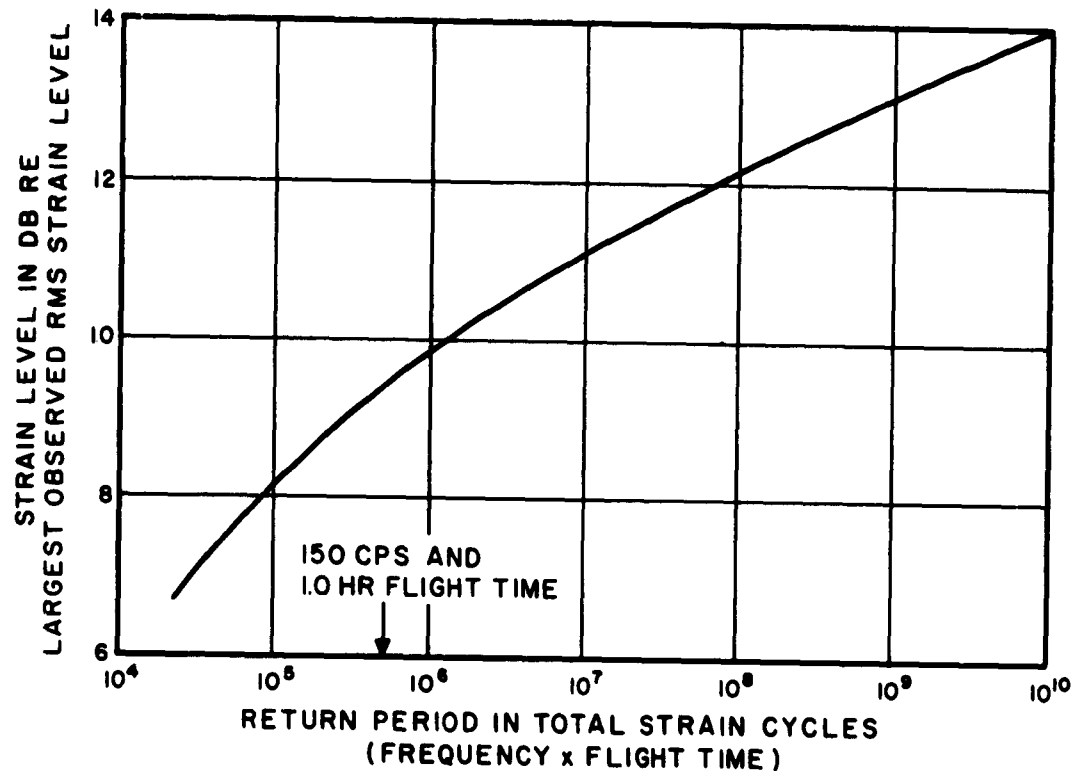


FIG. 4 THE RETURN PERIOD FOR STRAIN PEAKS ON RB-47 AIRCRAFT OPERATED TYPICALLY (SEE TEXT). THE RETURN PERIOD IS THE AVERAGE TOTAL NUMBER OF STRAIN CYCLES FOR ONE STRAIN PEAK EXCEEDING THE INDICATED VALUE.

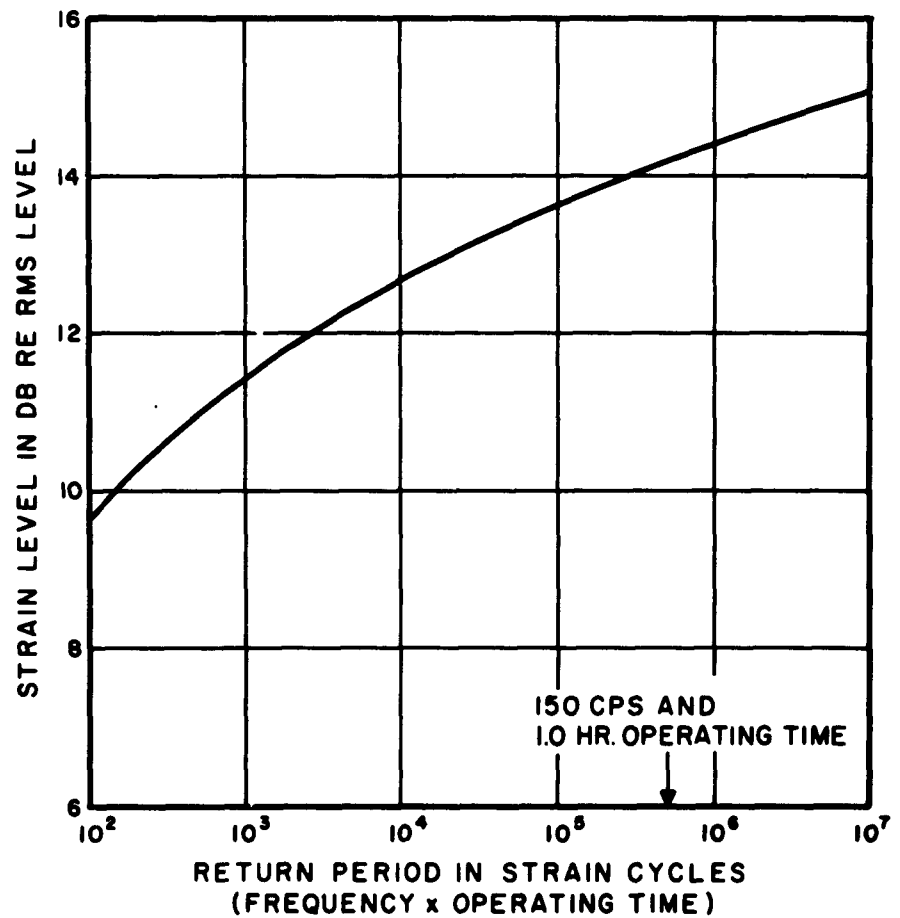


FIG. 5 THE RETURN PERIOD FOR STEADY
STATE OPERATION AT CONSTANT
RMS LEVEL

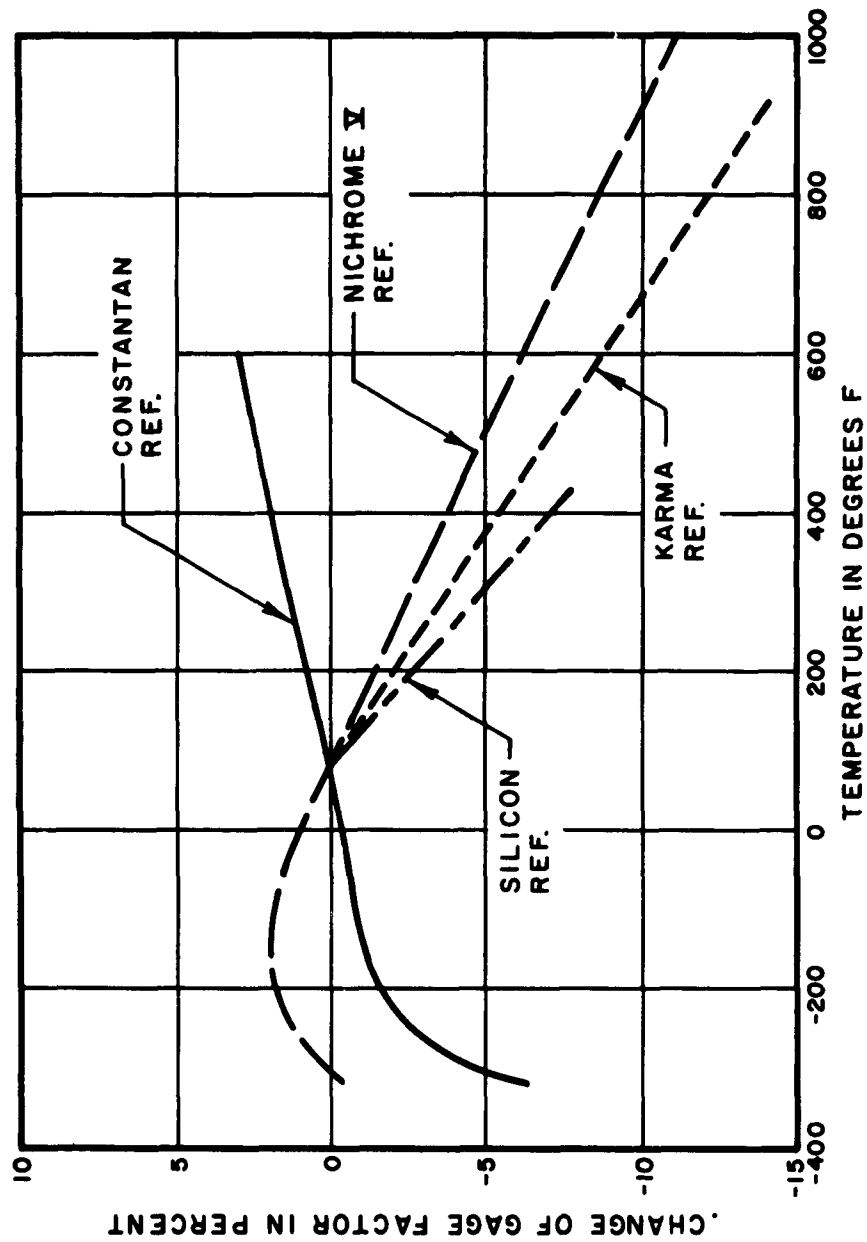


FIG. 6 VARIATION OF GAGE FACTOR WITH TEMPERATURE
FOR SOME STRAIN GAGE MATERIALS

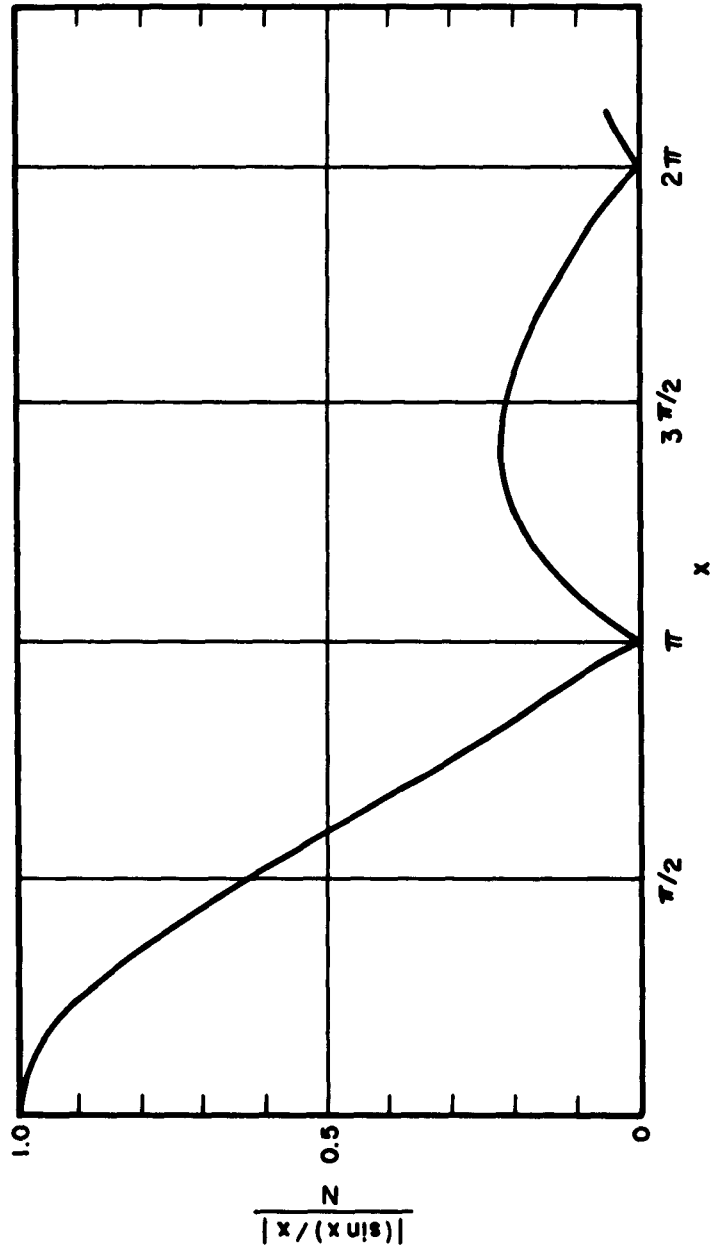


FIG. 7 NORMALIZED MAGNITUDE OF $(\sin x)/x$ VERSUS x

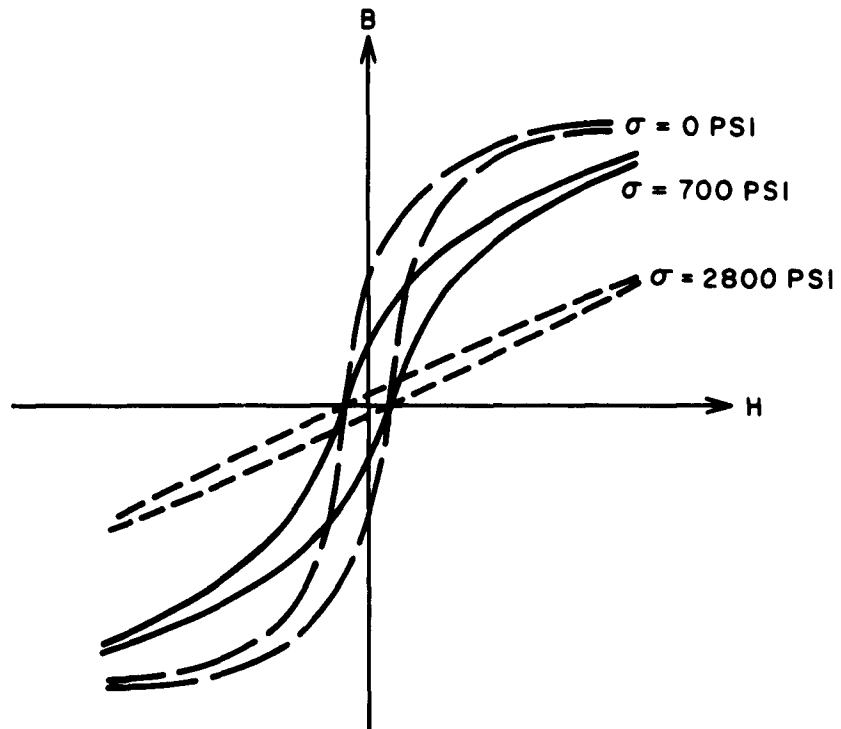


FIG. 8 CHANGE OF B-H CURVE FOR NICKEL
WITH APPLIED TENSION σ
(AFTER BOZORTH)

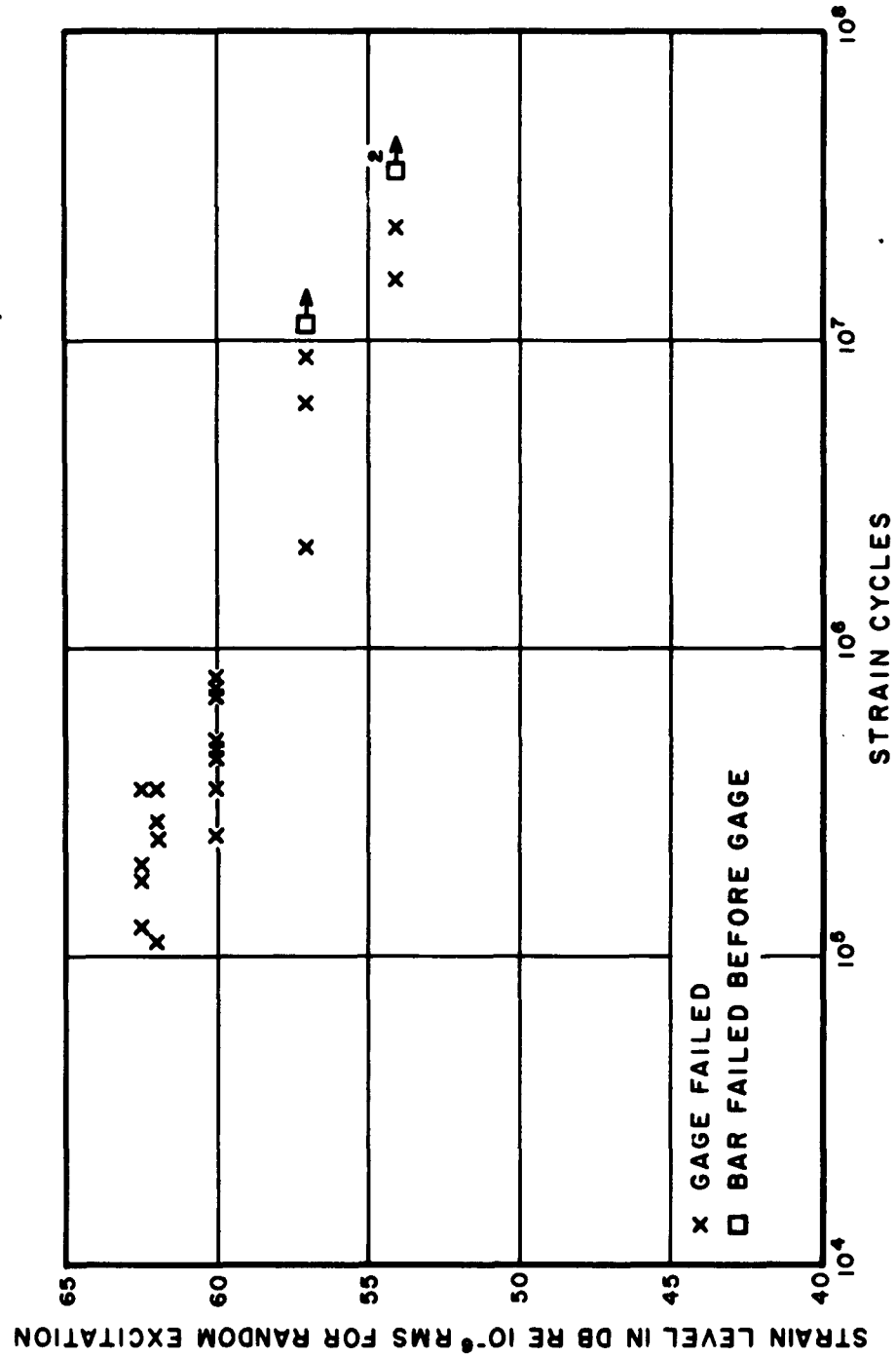


FIG. 9 EXPERIMENTAL STRAIN-LIFE CURVE FOR CONSTANTAN FOIL
STRAIN GAGE (BLH FAB-50-12) UNDER RANDOM EXCITATION

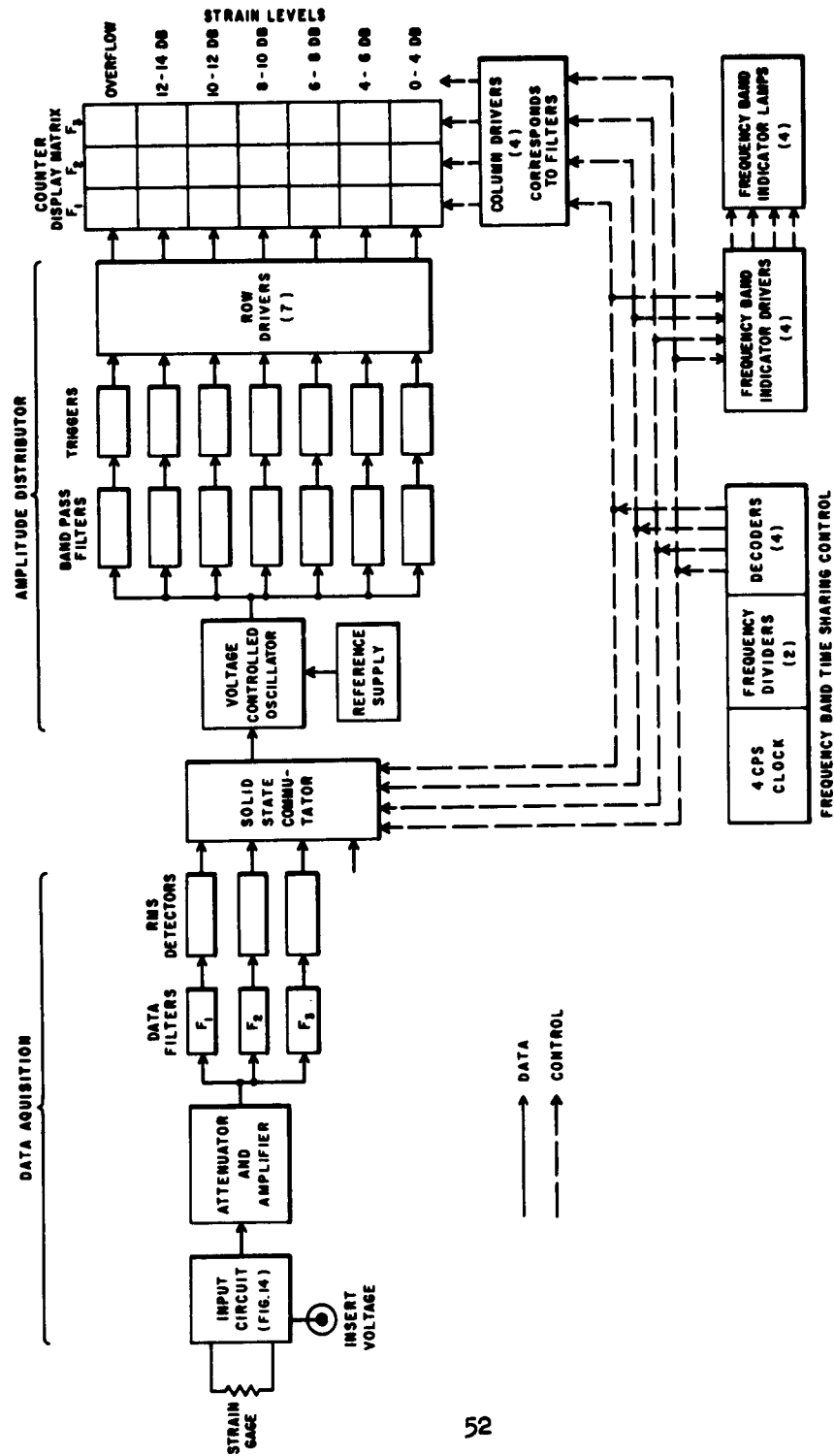


FIG. 10 BLOCK DIAGRAM OF RESPONSE RECORDER

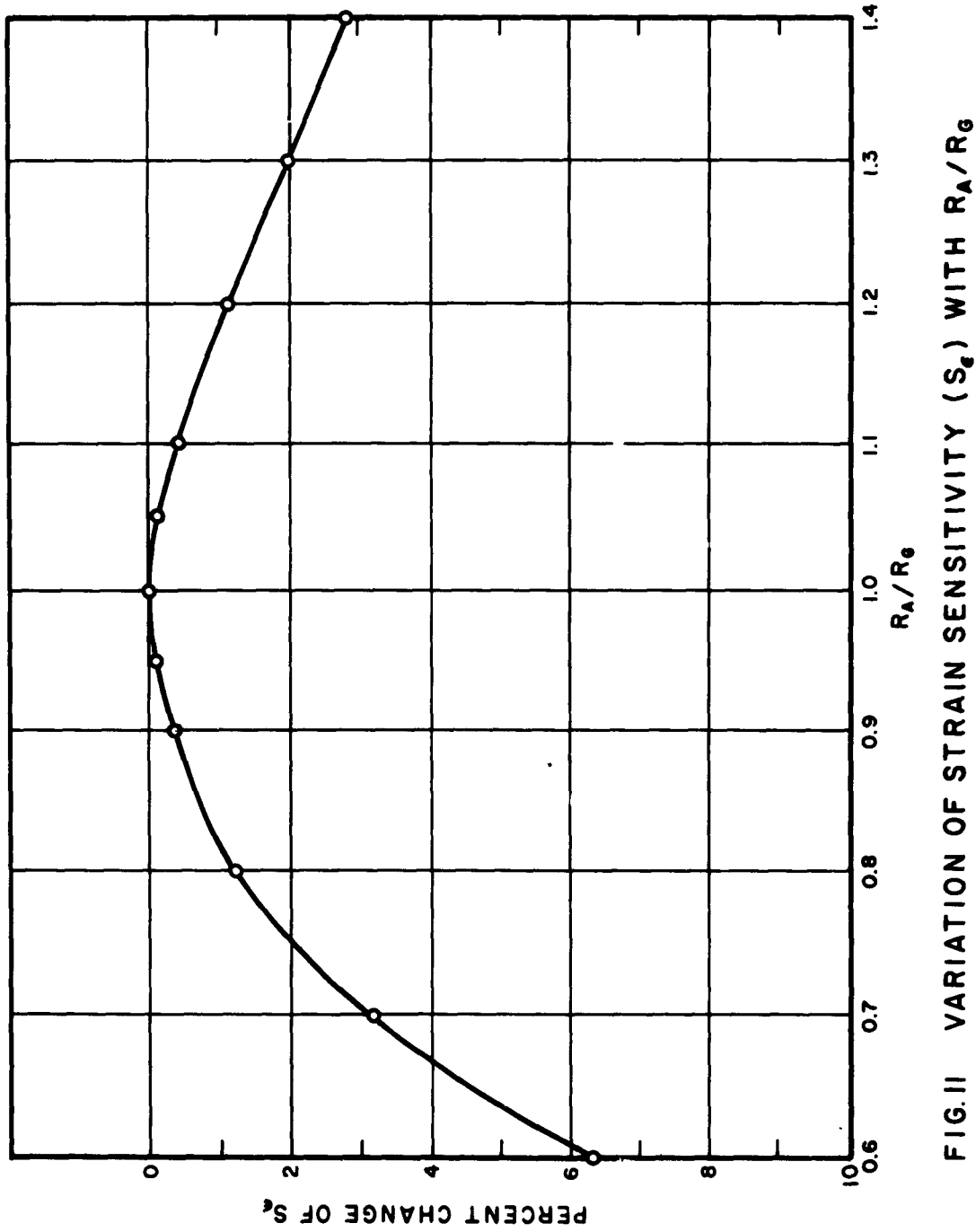
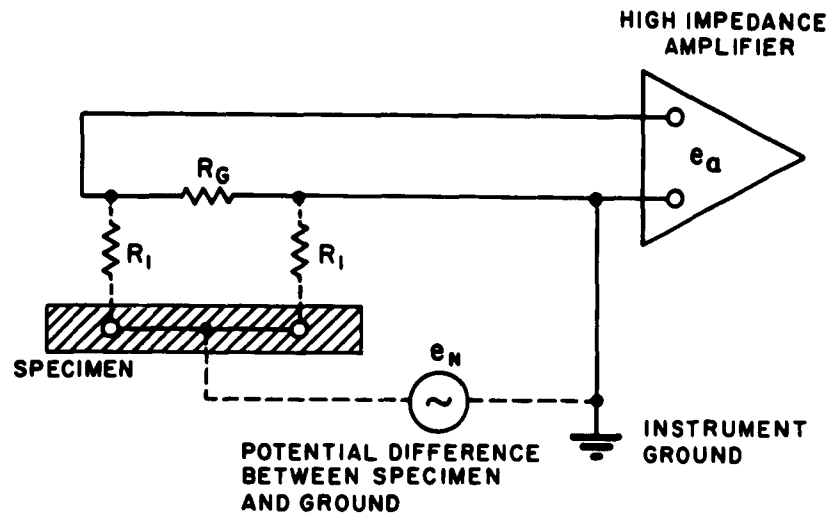
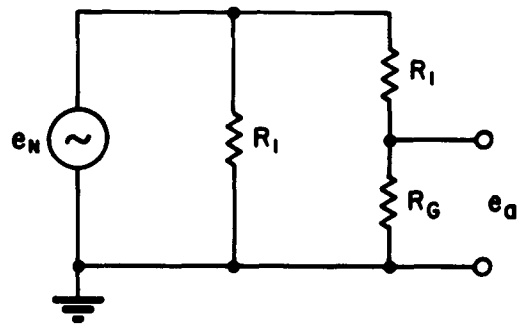


FIG. II VARIATION OF STRAIN SENSITIVITY (S_e) WITH R_A/R_G



a. CIRCUIT



b. EQUIVALENT CIRCUIT

FIG. 12 SINGLE-ENDED STRAIN GAGE APPLICATION
(RESISTANCE, R_1 , BETWEEN GAGE AND
SPECIMEN INDICATED)

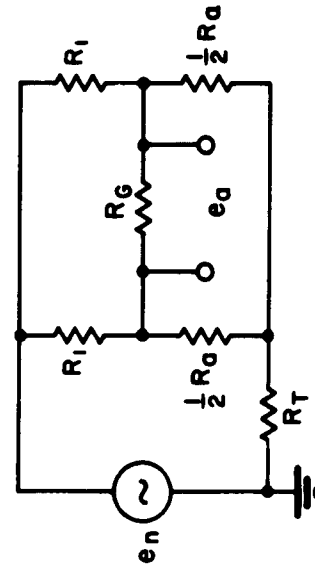
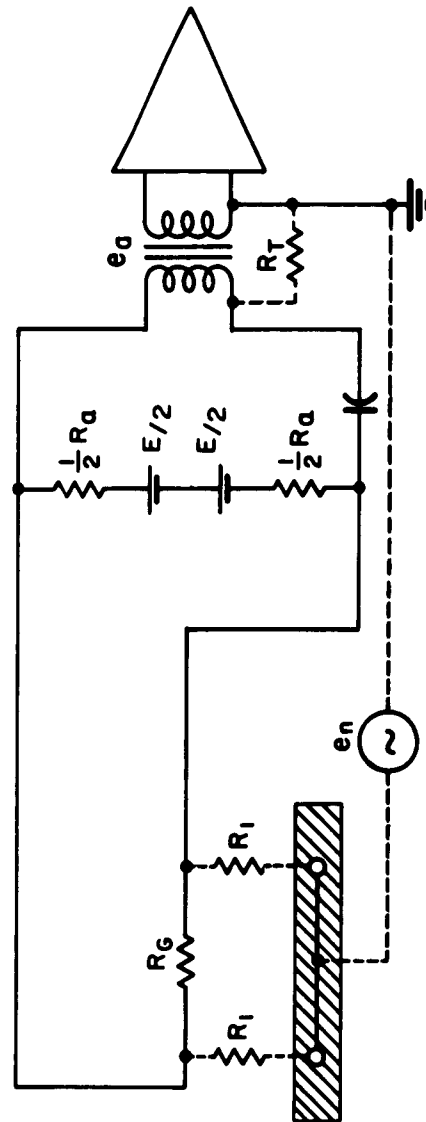


FIG. 13 BALANCED STRAIN GAGE APPLICATION

SIMULATED STRAIN
GAGE FOR EXPERIMENT'S

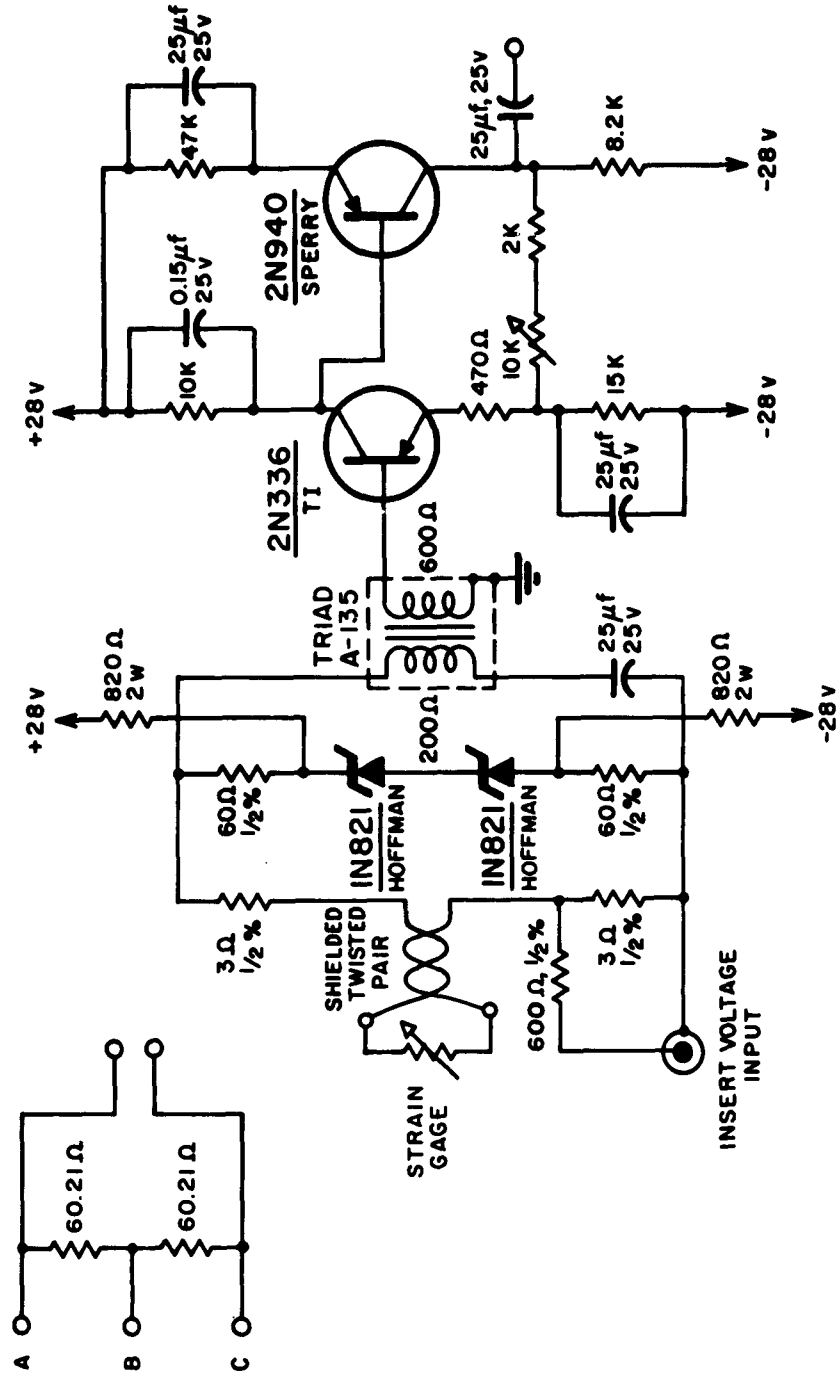


FIG.14 BALANCED STRAIN GAGE INPUT CIRCUIT

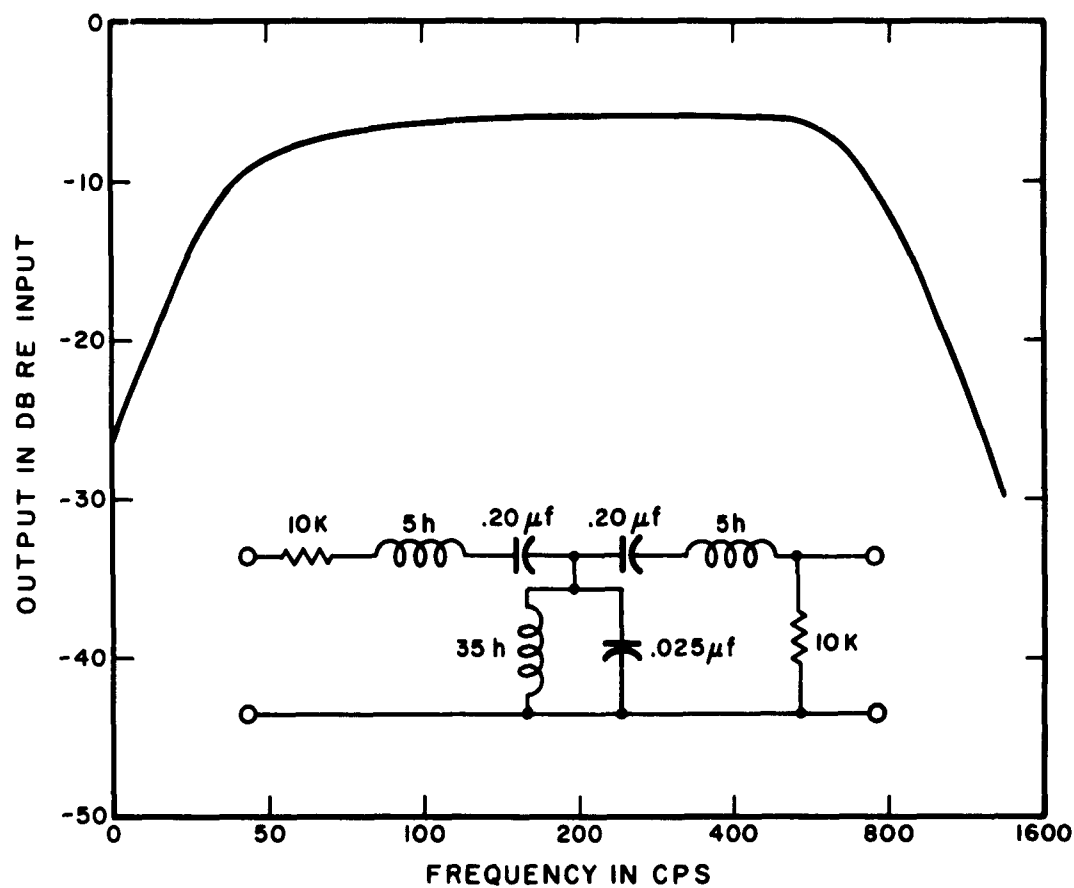


FIG.15 RESPONSE OF OVERALL FILTER

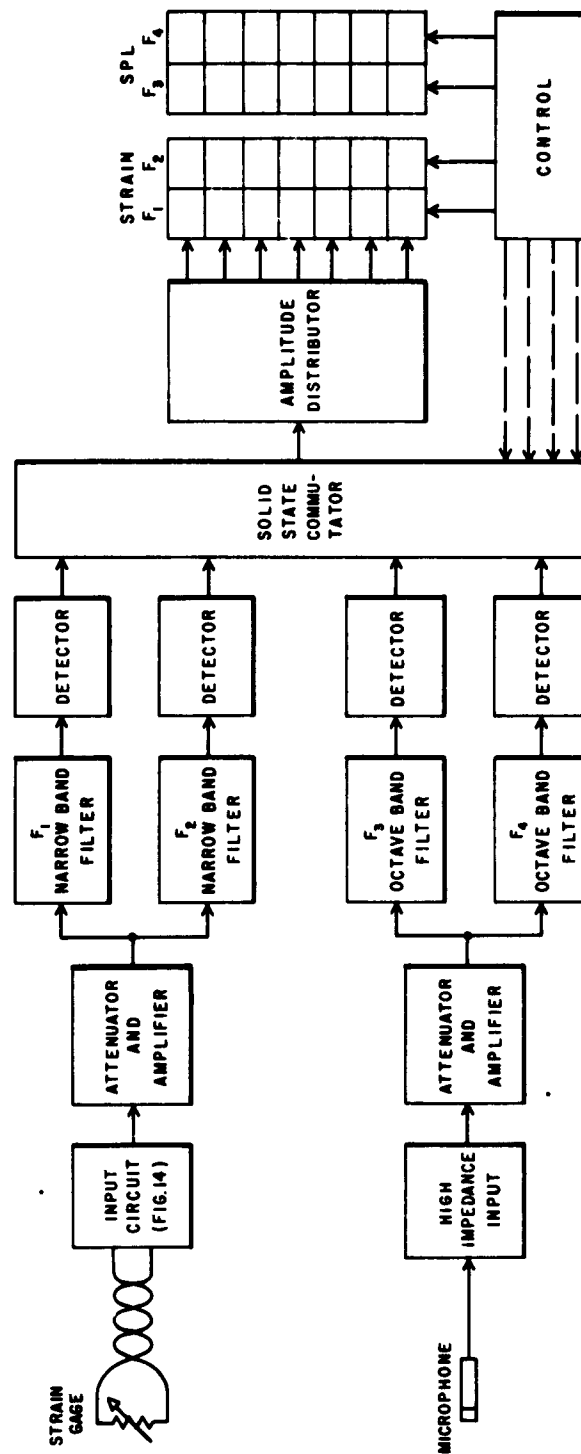


FIG. 16 BLOCK DIAGRAM FOR TWO INPUT HISTORY RECORDER

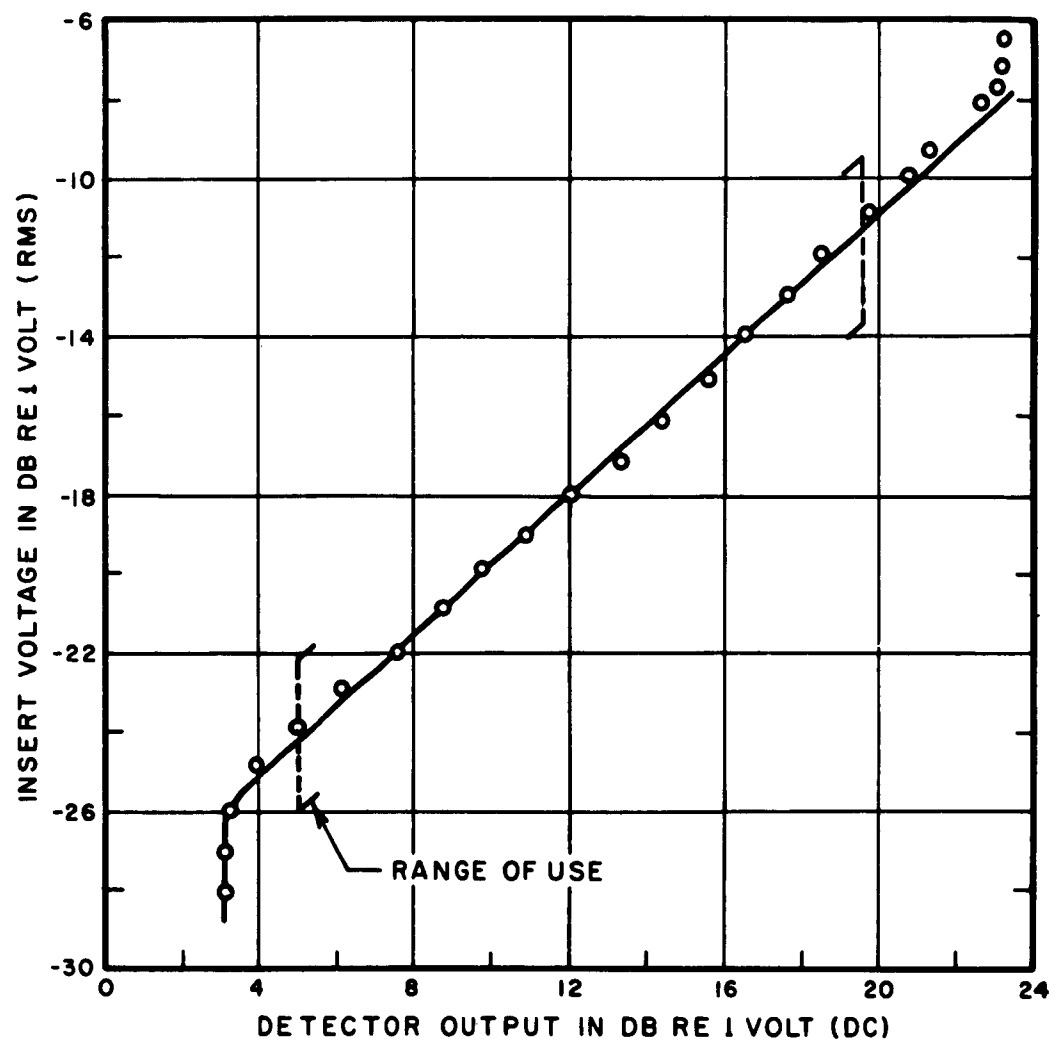


FIG. 17 MEASUREMENTS OF INPUT TO DETECTOR
OUTPUT TRANSFER FUNCTION FOR SINE
WAVE INSERT VOLTAGE

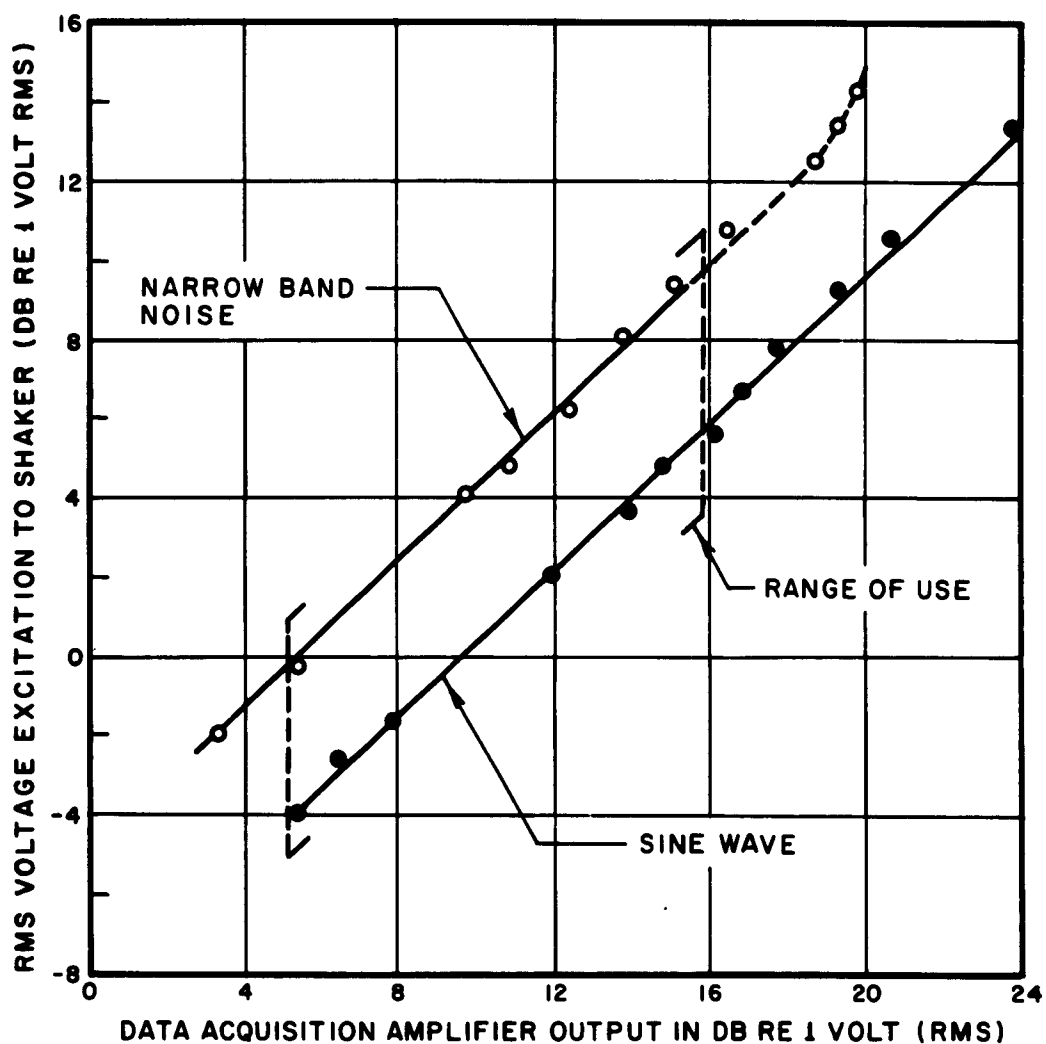


FIG.18 MEASUREMENTS OF STRAIN INPUT TO
DETECTOR INPUT FOR SINE WAVE AND
NARROW BAND NOISE

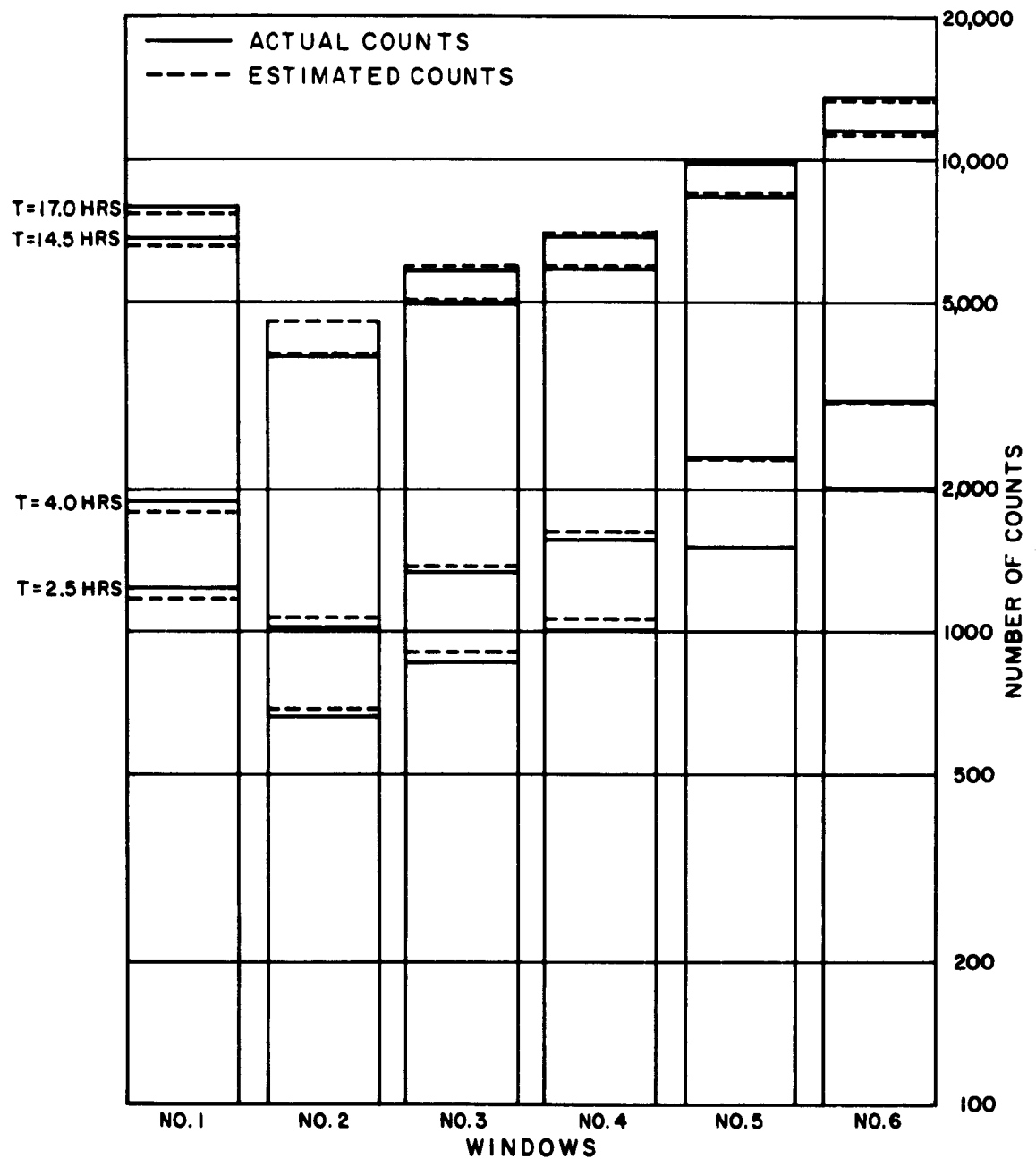


FIG. 19 BAR CHART OF COUNTS ACCUMULATED WITH
RANDOM DATA FOR VARIOUS LENGTHS OF
OPERATION T

APPENDIX A
DATA ANALYSIS TECHNIQUES

We report here the results of an investigation of techniques for processing data typical of the output of a response recorder.

Three different time-histories of structural response were processed by hand to obtain response recorder readouts, for recorders with various window widths and calibration settings. The fatigue damage consequent to each of the three original response distributions was calculated. Estimates of fatigue damage were also made from the recorder readouts using several different techniques. From a comparison of these estimates with the calculations, conclusions are drawn concerning (1) desirable widths for recorder windows, and (2) techniques for processing the readout data of a response recorder.

A. INVESTIGATION PLAN

The starting point of the present study is a distribution "curve" (actually, a bar-chart) giving the average time that the rms strain response dwells in consecutive 0.5 db windows. This distribution is typical of the long-time (one-year) average aircraft operation. A typical random fatigue curve, adapted from the literature, is then used to assess the fatigue damage. In this computation, a simple linear, non-interacting theory of fatigue damage accumulation is used. If the dwell time in the n th window (rms response equal to σ_n) is w_n , and if the fatigue curve indicates a lifetime N_n for steady operation at that response, then the damage D is given by the sum

$$D = \sum w_n / N_n \quad (A-1)$$

over all windows. In this expression D is the average fraction of fatigue damage accumulated. A value of D equal to 1 indicates that failure should be expected.

From the original distribution, we also compute typical readout data for response recorders using different window widths and different values of sensitivity (that is, the smallest response level that is recorded). A large number of readout

cases are constructed. The estimates of the fatigue damage are made from these readout data, using the same random fatigue curve. These estimates are formed in different ways, as discussed below. Conclusions are drawn from a comparison of these estimates of damage and the value computed by Eq. (A-1) from the original distribution.

B. RESPONSE DISTRIBUTIONS AND FATIGUE CURVE

Three different response distributions are used in this study. Distribution I is an adaptation of Fig. 5 of Volume I of this report, which represented the distribution of sound pressure levels for operation of RB-47 aircraft (Fig. A-1, bottom). We assume that the rms response is linearly proportional to the rms sound pressure. (Nonlinearity in the rms response will be much less than the possible nonlinearity at peak amplitudes larger than the rms value; therefore the linear assumption should be sufficiently accurate.) The reference response, corresponding to zero relative response level on the abscissa of Fig. A-1, is chosen as the response to the noise generated at full power (100% rpm) on a standard day (temperature of 59°F).

The random fatigue curve shown in Fig. A-2 is used to assess damage. This curve is an adaptation of one published as pertaining to 7075-T6 aluminum (Ref. A-1). The zero level of response on Fig. A-1 has been arbitrarily set equivalent to an rms strain level of 61 db re 10^{-6} , corresponding to a life of 4.5×10^5 cycles (1 hour at 125 cps) for steady operation at that level.

From the response distribution curve and the fatigue curve, a cumulative distribution curve for damage has been computed (Fig. A-1, top). This cumulative distribution of damage shows the percent of damage attributable to rms response levels less than the abscissa value.

Figure A-3 shows a response distribution (number II) differing slightly from distribution I. The differences are due to an attempt to construct a typical distribution for aircraft using afterburners or water injection.* The use of afterburner,

* Specific assumptions are: (1) increment in response level due to afterburner operation: +4 db; (2) afterburner used on all takeoffs, ignited 20 sec. after brake release; (3) afterburner used for 1 percent of static (ground) operation time.

ASD-TDR-62-165
Volume II

with which the response level is assumed to be 4 db above the level for 100% rpm, leads to a less precipitous fall-off of the bar chart at high levels and to a corresponding prolongation of the cumulative distribution of damage (Fig. A-3, top). The reference response (zero db on the abscissa) is response to afterburner on a standard day.

Distribution III (Fig. A-4) is another distribution thought to be typical for some aircraft operating with afterburner. It differs from distribution II in that a greater proportion of time is spent with response levels between +1 and +3 db (afterburner operation).

Two of the dozen charts of readout data used in this study are given in Figs. A-5 and A-6. Each was generated from distribution I (Fig. A-1). Figure A-5 shows the readout for a recorder with 3-db windows having a truncation point (lowest recorded level) at -3 db. Figure A-6 shows the readout for a recorder with 2-db windows and a truncation at -4.5 db.

C. DAMAGE ESTIMATES

Estimates of fatigue damage were made from the readout data in various ways, all using the same fatigue curve. These estimates were compared with the damage for the original distribution, evaluated by means of Eq. (A-1), and the errors due to data processing determined.

The principal error in some cases is that arising from truncation. The recorder ignores all response with levels below the truncation point; if that point is set too high, really damaging responses will be ignored. We define the truncation error as the ratio of damage due to levels above the truncation point to the damage due to all response levels. (The value of the ratio is converted to a percentage; thus, a ratio of 0.82 is an error of -18%.)

However other errors, called estimation errors, result from the use of wide windows in deriving the readout charts. We define the estimation error as the ratio (converted to a percentage) of the estimated damage to the precise damage due to response above the truncation point. The size of the estimation error varies with the method and care used in estimation.

In our tests the readout data were processed in three different ways. First, and simplest, is a procedure which assumes that all the indicated time that the response was in a given window was spent at the level of the center of the window. Thus,

ASD-TDR-62-165
Volume II

in the case illustrated in Fig. A-5, we assume that the response was at -1.5 db for 3991 time units, at +1.5 db for 2590 units, and at +4.5 db for 10 units of time.

The second processing technique starts from a plot of readout data such as those in Figs. A-5 and A-6. The engineer sketches in a smooth curve, which is his estimate of the actual response distribution. From the smooth curve he reads off relative time values for 0.5 db windows of response level. He verifies that sums of these values check the actual readout data, adjusting values as necessary. In this manner he tries to reconstruct a response distribution bar-chart with 0.5 db windows from the readout data, in which the window width is larger.

The third processing technique plots the readout data as points on a cumulative distribution curve of response, e.g., plotting on the ordinate the total time that response exceeded the abscissa values. Exact values for this curve are known, from the readout data, at the response values marking the edges of windows. Thus in case 11 (Fig. A-6), exactly $824 = 814 + 10$ time units are spent with response level exceeding +1 db. These exact values are plotted and a smooth curve interpolated between them. Such a procedure is illustrated in Fig. A-7, for readout case 11. Estimates of the time spent in 0.5 db windows are read from the curve. For example, on Fig. A-7, we estimate 1190 time units spent in the window from 0 to 0.5 db; the original exact value was 1030 (see Fig. A-1).

The truncation and estimation errors determined from the twelve different cases of readout data are listed in the accompanying table.

TABLE A-1
THE VARIOUS READOUT CASES AND THEIR ERRORS IN ASSESSMENTS OF DAMAGE

Case Number	Distribution Number	Relative Response Level at Truncation Point	Window Width	Truncation Error	Estimation Errors*				
					A	B	C	D	E
		db	db	%	%	%	%	%	%
6	I	-1	1	-8	+4	-2	+2	+2	
2	II	-1	1	-82	+5	-2	0		
11	I	-5	2	0	+10	+4			+5
1	I	-4	2	0	+7	-3	+1		
7	II	-5	2	-3	+14	0	-6	-5	
14	II	-4	2	-13	+17	+1	+2		+1
4	III	-5.5	2	-7	+15	+14	0	0	
10	III	-5	2	-8	+21	+17			+6
8	I	-3.5	3	-1	+22	+15	+10	+12	
13	I	-3.0	3	-1	+29	+6	+7		+10
9	II	-3.5	3	-29	+58	+34	+19	-13	
12	II	-6	3	0	+26	+9			-4

* Different processing techniques identified as follows:

- A = all time lumped at window's center
 B = interpolation on cumulative distribution of response
 C, D, E = estimation of smooth curve for response distribution (different individuals)

D. DISCUSSION

The relatively small size of the errors in damage resulting from any of the processing techniques is quite striking. The shape of the fatigue curve, Fig. A-2, can be represented approximately by

$$\sigma^7 N = \text{constant.} \quad (\text{A-2})$$

From this relation it can be shown that a 50% error in estimation of damage corresponds approximately to a 0.5 db error in response measurement. Thus errors in damage rate of 10 or 20% have quite negligible importance. Those cases with significantly larger error, cases 2 and 9, are characterized by truncation points lying above the response level under 100% rpm, no afterburner, standard day conditions.

Among the various techniques used in processing readout data, that in which all the time in a window is lumped at the window's center (method A, in the table) appears to be most inaccurate. It is also the easiest. With this method, the estimation errors are found not to be excessive (equivalent to 0.2 db or less in response) if the window width does not exceed 2 db.

To some extent, this precision is a reflection of the smoothness of the original response distributions, Figs. A-1, A-3, and A-4. The maximum possible error using this technique is equivalent to one half of a window width, i.e., 1 db with 2 db windows. Situations in which this maximum error might be realized are conceivable but extremely unlikely. To realize the maximum error, all of these conditions must be satisfied:

- (1) nearly all damage results from a single response level;
- (2) fluctuations of level due to temperature and human operator variability are small compared with the window width, in the course of the whole record;
- (3) initial calibration locates the damaging level near, but not on, a window edge.

The other techniques for processing readout data--interpolation on the response cumulative distribution (column B in table) and estimation of a smooth curve for response distribution (columns C, D, E, in table)--each led to smaller errors. Since these techniques require the engineer to draw and estimate "smooth" curves, more or less by eye, the precision depends considerably on the time and care he is willing to take.

ASD-TDR-62-165
Volume II

E. CONCLUSIONS

It appears from these tests that a window width of 2 db yields very satisfactory precision in estimating fatigue damage from the readout data. It also appears that a set of six 2-db windows, or a total range of 12 db, is adequate to acquire all necessary data with a reasonably small truncation error.

REFERENCES

- A-1. Schjelderup, H. C., "Structural Acoustic Proof Testing," Noise Control, 5, 351-360, (1959); on the B-66 aircraft.

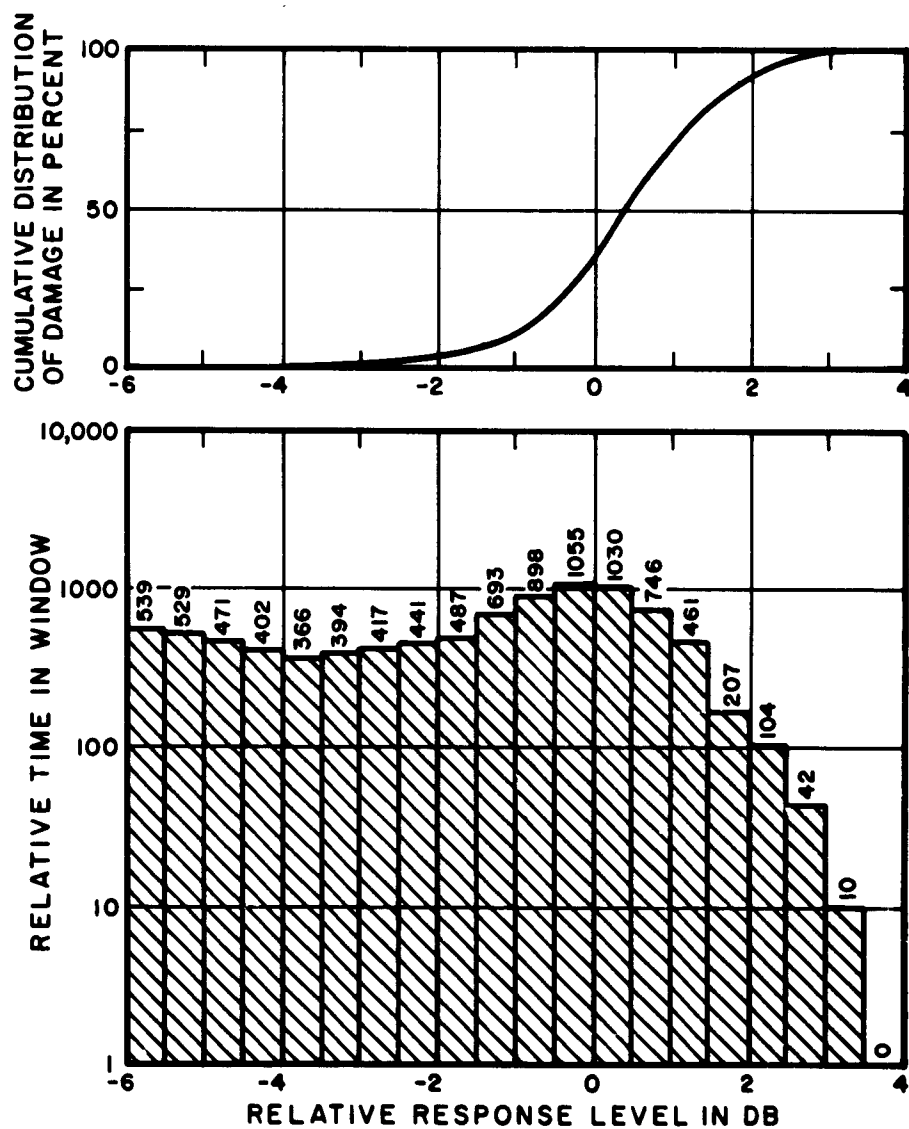


FIG. A-1 RESPONSE DISTRIBUTION I
AND CORRESPONDING CUMULATIVE
DISTRIBUTION OF DAMAGE

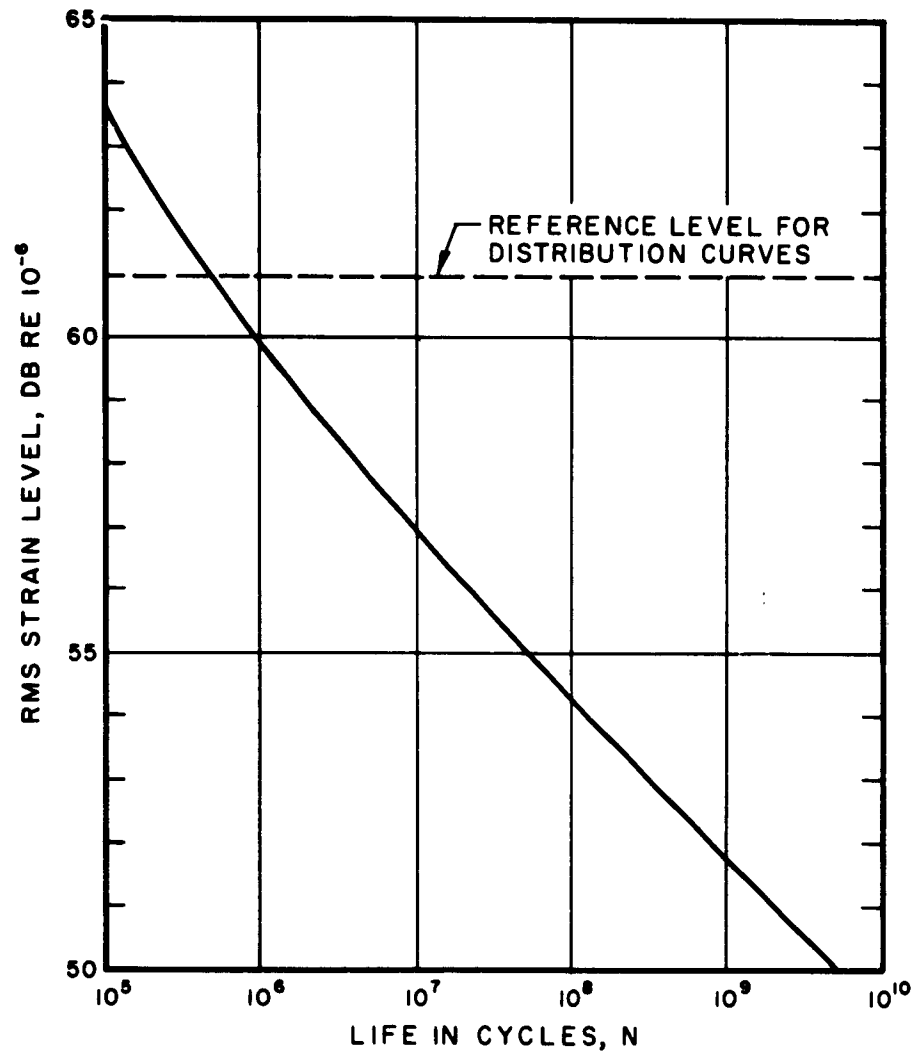


FIG. A-2 RANDOM FATIGUE CURVE
(ADAPTED FROM SCHJELDERUP,
REF. A-1)

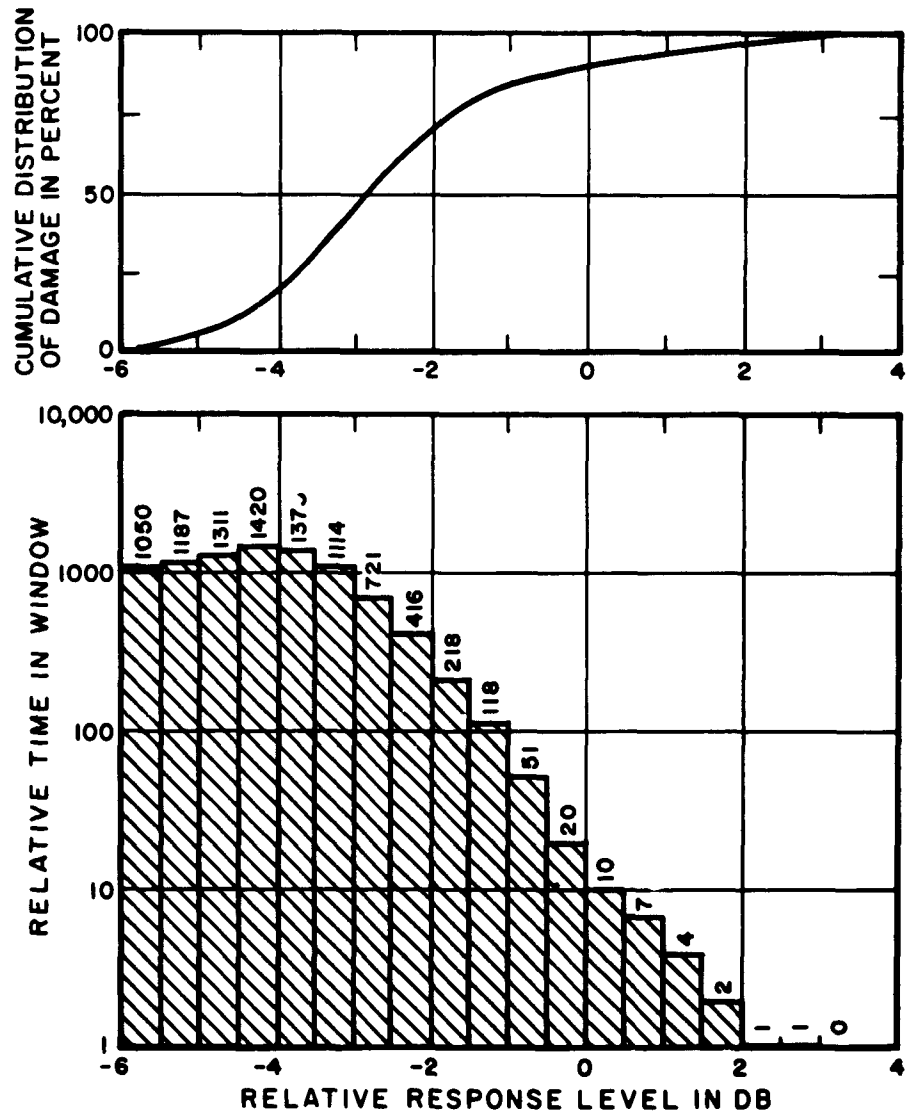


FIG. A-3 RESPONSE DISTRIBUTION II
AND CORRESPONDING CUMULATIVE
DISTRIBUTION OF DAMAGE

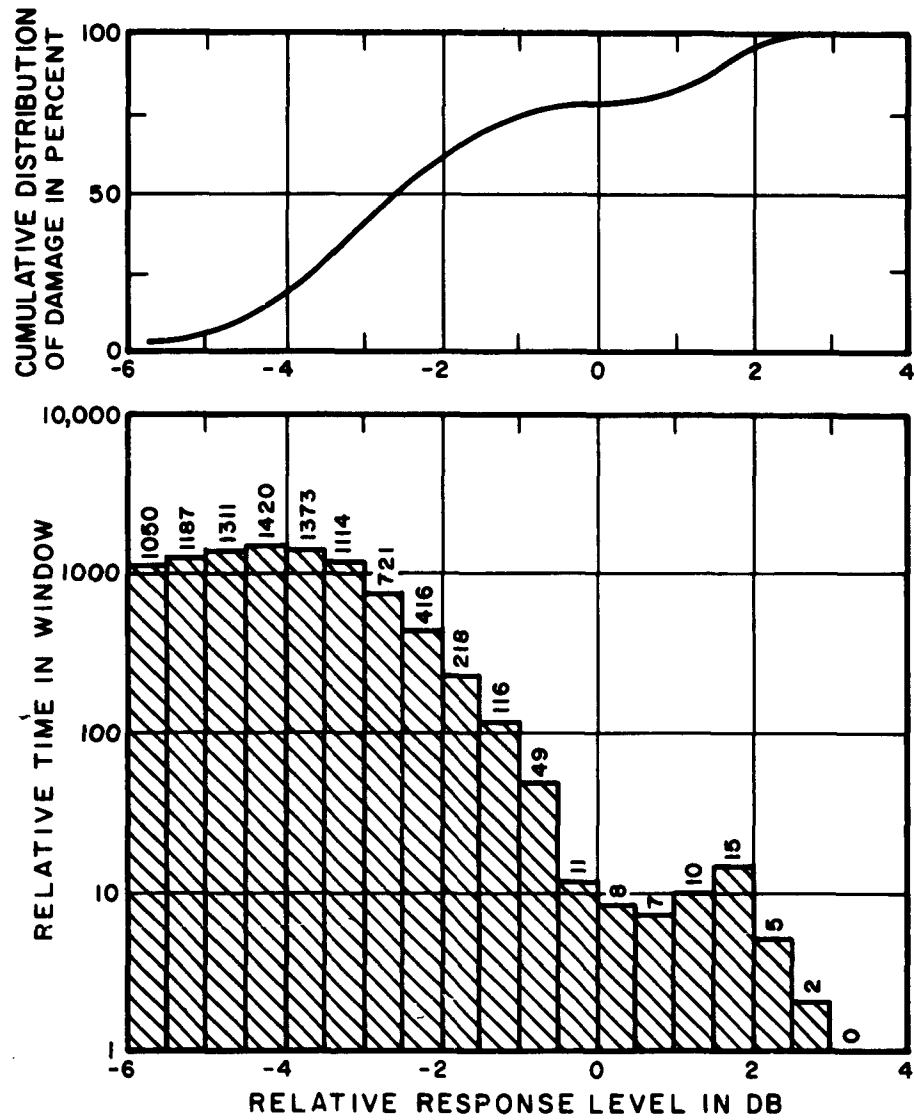


FIG. A-4 RESPONSE DISTRIBUTION III
AND CORRESPONDING CUMULATIVE
DISTRIBUTION OF DAMAGE

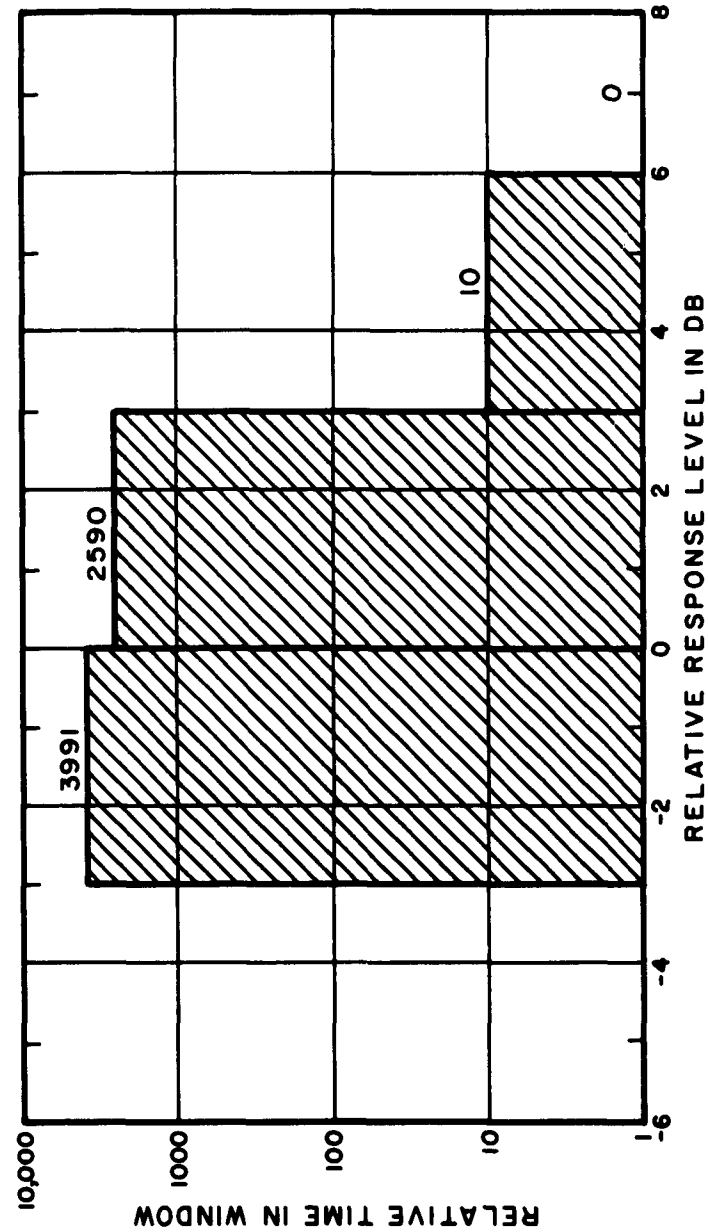


FIG. A-5 READOUT CASE 13, DERIVED FROM DISTRIBUTION I
USING 3 DB WINDOWS STARTING AT -3 DB

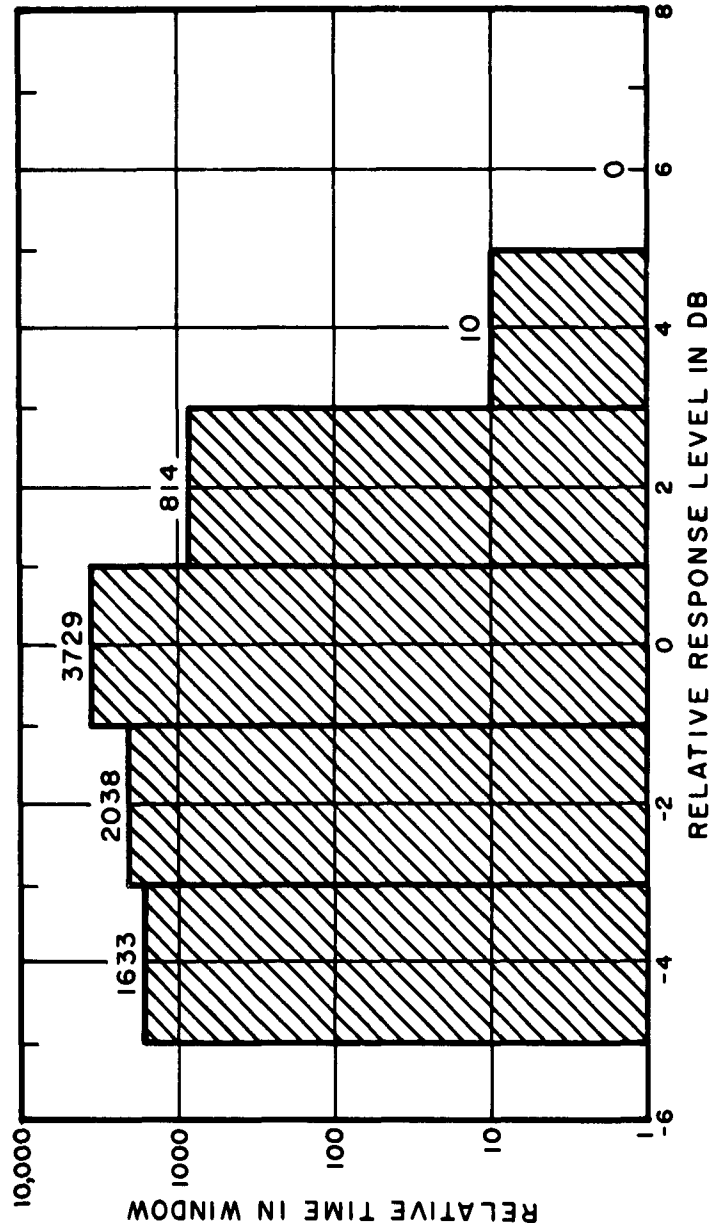


FIG. A-6 READOUT CASE II, DERIVED FROM DISTRIBUTION I
USING 2 DB WINDOWS STARTING AT -5 DB

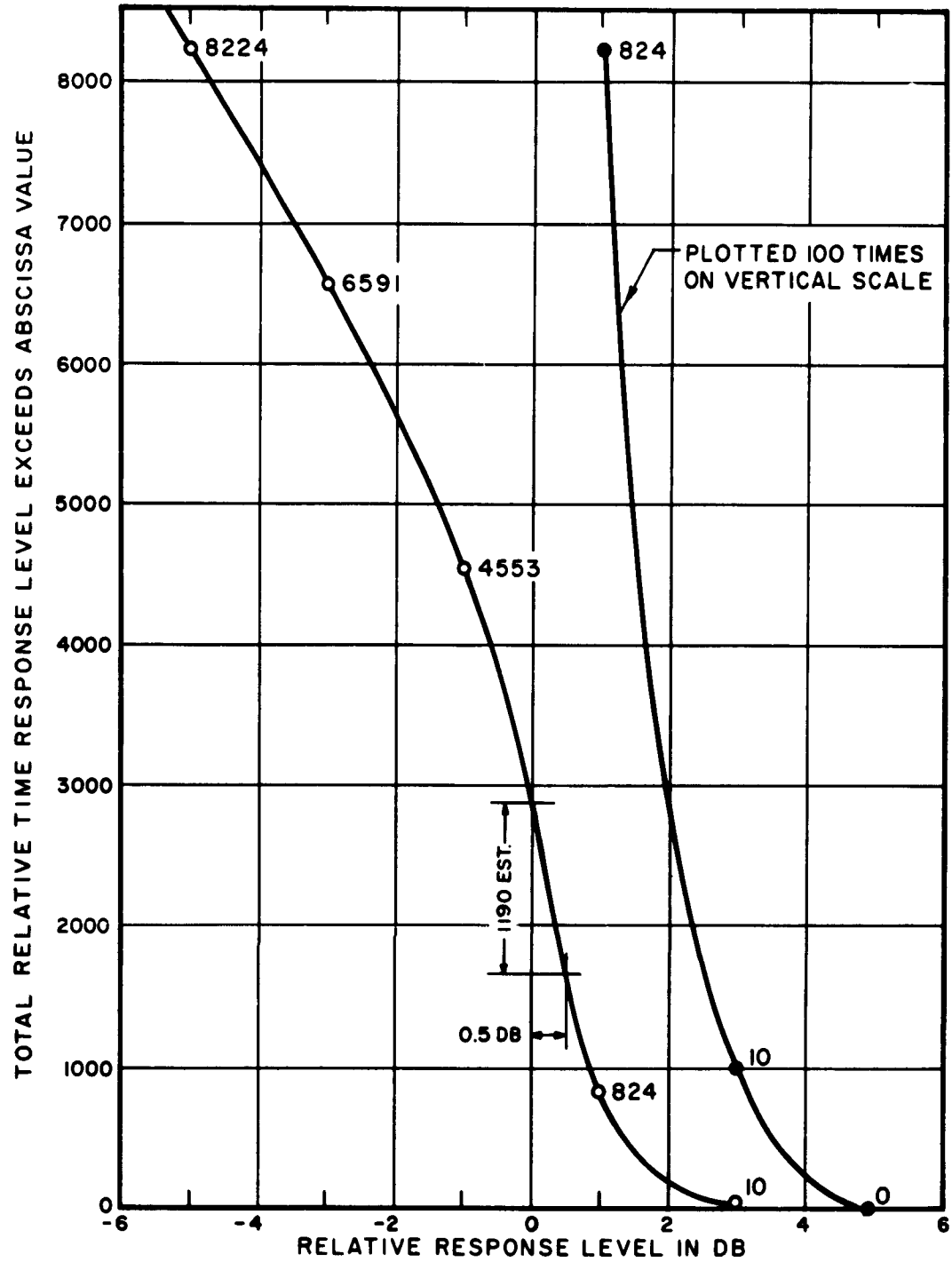


FIG. A-7 CUMULATIVE RESPONSE DISTRIBUTION FOR READOUT CASE II

APPENDIX B

DEPENDENCE OF SOUND PRESSURE LEVEL ON AMBIENT TEMPERATURE
FOR
PRATT AND WHITNEY J-57 ENGINE

NOTATION

A jet nozzle area
 c_o sound speed in ambient air
F thrust force
 L_p sound pressure level
 \dot{m} mass flow in jet
p sound pressure
 T_o absolute temperature (deg Rankine) of ambient air
V jet efflux velocity
W sound power
 $\theta_o = T_o - 518$, change in ambient temperature (deg F) from 59°F
 ρ_j jet density
 ρ_o ambient air density

A. INTRODUCTION

In this appendix we derive an expression in terms of jet engine operating parameters for the change in sound pressure level with ambient temperature. For a fixed throttle setting, both the mass flow (weight flow) and the thrust will change with temperature. Data on these changes are usually available from jet engine model specifications. We use data for the J-57-P43 engine to compute the change in sound pressure level with temperature, for this engine at military rated power with and without thrust augmentation (water injection).

B. FUNDAMENTAL RELATIONS

The jet parameters -- mass flow, velocity, thrust, etc. -- are related by the two equations:

$$\dot{m} = \rho_j AV \quad (B-1)$$

$$F = \dot{m}V \quad (B-2)$$

ASD-TDR-62-165
Volume II

The fundamental acoustical equations, for sound power W and sound pressure p , are (Ref. B-1)

$$W \propto \rho_o A V^8 c_o^{-5},$$

and (B-3)

$$p^2 \propto W \rho_o c_o.$$

The combination of these two equations yields

$$p \propto \rho_o c_o^{-2} A^{1/2} V^4. \quad (B-4)$$

These equations are strictly pertinent only to far field sound pressures; however, they should be good approximations for the pressure at points near the aircraft. The combination of Eqs. (B-2) and (B-4) yields

$$p \propto \rho_o c_o^{-2} F^4 \dot{m}^{-4}, \quad (B-5)$$

if we assume that the jet nozzle area A is constant.

From the definition of sound pressure level, we compute

$$\begin{aligned} \frac{dL_p}{d\theta} &= 20 \log_{10}(e) \frac{d(\log_e p)}{d\theta} \\ &= 8.68 \frac{dp}{p d\theta} \quad \text{db per deg.} \end{aligned} \quad (B-6)$$

The combination of Eqs. (B-5) and (B-6) yields

$$\begin{aligned} \frac{dL_p}{d\theta} &= 8.68 \frac{d(\rho_o c_o^{-2})}{\rho_o c_o^{-2} d\theta} \\ &\quad + 34.72 \left(\frac{dF}{F d\theta} - \frac{d\dot{m}}{\dot{m} d\theta} \right) \end{aligned} \quad (B-7)$$

We shall evaluate all the derivatives in Eq. (B-7) at the standard temperature, $59^\circ\text{F} = 518^\circ\text{Rankine}$. We assume that the fractional change of any variable with ambient temperature (the logarithmic derivative, $dx/xd\theta$) is a constant. This is an excellent first approximation.

ASD-TDR-62-165
Volume II

The variations in ambient air density and sound speed with temperature are given by the proportionalities

$$\begin{aligned}\rho_o &\propto T_o^{-1} , \\ c_o &\propto T_o^{1/2} , \\ \rho_o c_o^{-2} &\propto T_o^{-2} ,\end{aligned}$$

so that

$$\frac{d(\rho_o c_o^{-2})}{\rho_o c_o^{-2} d\theta} = -2/T_{o,std} \quad (B-8)$$

where $T_{o,std}$ is 518 deg Rankine.

The combination of Eqs. (B-7) and (B-8) yields a general expression for static operation of jet engines:

$$\frac{dL_p}{d\theta} = -0.0335 + 34.72 \left(\frac{dF}{F d\theta} - \frac{d\dot{m}}{\dot{m} d\theta} \right) . \quad (B-9)$$

C. CALCULATIONS FOR J-57 ENGINE

We illustrate the use of Eq. (B-9) by calculations for the J-57 engine, used in the B-52 and KC-135 aircraft. Data on variations in thrust and mass flow with temperature are available from model specifications (Ref. B-2). First, assume static operation without water injection, at military rated power. From Sheet 28 of Ref. B-2,

$$\frac{dF}{F d\theta} \approx -0.0040 \text{ per deg F} , \quad (B-10a)$$

in the temperature range from -30°F to +100°F. From Sheet 29 of Ref. B-2,

$$\frac{d\dot{m}}{\dot{m} d\theta} \approx -0.0025 \text{ per deg F} , \quad (B-10b)$$

in an even wider temperature range. Thus, we calculate from Eq. (B-9) the change in sound pressure level is given by

ASD-TDR-62-165
Volume II

$$\frac{dL_p}{d\theta} = - 0.0335 - 0.0520 = - 0.0855$$

$$\dot{=} - 1 \text{ db per } +12 \text{ deg F.} \quad (\text{B-11})$$

Now consider static, military rated power conditions with maximum water injection at 11 lb/sec. Thrust augmentation by water injection does not affect air flow; temperature does not affect water flow. Thus, in place of Eq. (B-10b), we have

$$\frac{d\dot{m}}{d\theta} \approx - 0.0025 \left(\frac{180}{180+11} \right) = - 0.00236, \text{ per deg F, } (\text{B-12a})$$

since air flow is 180 lb/sec (Sheet 45 of Ref. B-2). From Sheet 45 of Ref. B-2 we also estimate

$$\frac{dF}{F d\theta} \approx - 0.00174, \text{ per deg F, } \quad (\text{B-12b})$$

in the temperature range from $+40^\circ\text{F}$ to $+100^\circ\text{F}$.

It follows from Eq. (B-9) that the change in sound pressure level with temperature, for operation with maximum water injection, is

$$\begin{aligned} \frac{dL_p}{d\theta} &= - 0.0335 + 0.0215 = - 0.012 \text{ db per deg F,} \\ &= - 1 \text{ db per } 83 \text{ deg F.} \end{aligned} \quad (\text{B-13})$$

This rate of change is essentially negligible. The answer is applicable to B-52 aircraft.

However, note that standard takeoff operation of KC-135 aircraft with water injection, holds constant the total thrust (strictly, the engine pressure ratio), up to ambient temperatures of 100°F . This operation requires a throttle setting less than maximum, and increasingly less the lower the temperature. The net effect upon sound pressure level due to ambient temperature changes cannot be predicted from available data.

ASD-TDR-62-165
Volume II

REFERENCES

- B-1. Coles, W. D., and Callaghan, E. E., "Investigation of Far Noise Field of Jets. II - Comparison of Air Jets and Jet Engines," NACA Tech. Note 3591, National Aeronautics and Space Administration, Washington, D. C., 1956.
- B-2. Specification No. A-1704-D, Model J-57-P-43W, -43WA, Engines, Pratt and Whitney Aircraft, East Hartford, Connecticut, 1 August 1957.

APPENDIX C

STRAIN GAGE FATIGUE MEASUREMENTS

A. INTRODUCTION

Experiments were conducted to obtain data for application to the response recorder. As such only one type of strain gage was tested with octave band random strain excitation. With this experimental information, we would hope to be able to use a strain gage with confidence that its fatigue life would at least equal or exceed that of the panel on which it was affixed.

In particular, it was hoped to derive enough data to outline a strain-life curve for the gages themselves. In this context, efforts were made to eliminate failures of the wire connections to the gage and of the cements. These efforts represented no more elaborate techniques than would be possible in the field use of the response recorder system.

B. TEST BAR

The experimental arrangement was similar to that used in the random strain metal fatigue experiments of Smith and Malme (Ref. C-1) except that the bar itself was designed to have 1) a much longer fatigue life, and 2) a section of uniform strain for locating the strain gages. Such a test bar is shown in Fig. C-1. (The strain gages are cemented in a symmetrical array about the center line of each arm of the double cantilever bar, room for four being allowed on each face.) This bar, of uniform thickness sheet stock, has a tapered width. A first order approximation shows a constant strain over the first 30% of length (approximately 1") from the clamp.

This shape is derived from the analysis of the dynamic behavior summarized in the work of Bishop and Johnson (Ref. C-2). The characteristic function of a clamped-free (cantilever) beam of uniform cross section is numerically tabulated in their work. The second derivative of the envelope (or peak) of the displacement is proportional to the bending moment, M :

$$M = EI \frac{d^2 y}{dx^2}$$

M is related by the parameters of the bar to the surface strain ϵ :

$$\epsilon = \frac{M}{EI} \frac{h}{2}$$

where h is the thickness. For the first mode, plotting the tabulated value of d^2y/dx^2 as a function of position x on the bar shows that a straight line is a reasonable approximation up to the point $x/l = 0.3$. Making the simplest assumption, that if the moment of inertia (I) is varied along x so that $\frac{1}{I(x)} \frac{d^2y}{dx^2}$ is constant, then the required $I(x)$ results in a 14% width taper. The effect of this variation of $I(x)$ is to make the strain considerably more constant than in a fixed cross section bar throughout the range of interest ($0 < \frac{x}{l} < 0.3$). No exact solution is possible for a constant strain throughout the complete length of a bar of this configuration under dynamic excitation.

This taper of the bar is carried out to the end. This is done to raise the resonant frequency relative to a constant width bar, which allows the completion of more cycles in a given amount of real time. The time saving for the same weight bar and required driving power at the shaker is approximately 20%.

A bar of the same weight as the tapered bar we have selected, but terminating in a constant width section would have higher strain at the root section; however, it would have a lower first resonance. The generalization is that the product of root stress and frequency of resonance is approximately constant for a given driver power available.

In a bar that does not have a hole or other systematic stress concentration, the failure occurs at the clamp. The magnitude of this stress concentration at the clamp has been estimated by Smith and Malme to be no more than 3 db higher than the stress just outside the clamp (a factor of 1.4). It is impossible to place the strain gage so that it is subjected to this maximum stress, since the principle stress vector does not lie on the surface of the bar. Filleting of the bar root is introduced to relieve the stress concentration at the clamp. This modification increases the fatigue life of the bar.

While some modifications of this type can be made, it must be remembered that the design goal is a section of uniform high stress. These changes place a stress gradient near the region where none is desired, since the region of highest stress is the most suitable for

gage placement. This is particularly critical in some phases of the experiment where the strain-life curves for the bar and for the gage may cross, so that the experimenter must choose the gage mounting area of uniform strain at the highest strain possible if a gage failure is to precede bar failure.

To check the distribution in high strain area, several bars were partially fatigued using large values of sinusoidal excitation. A rather wide area near the root showed stress cracks. In addition, variations of placement of gages (in the subsequent experiments) involving distances up to 1/8th of the gage length had no measurable effect on the strain output as read on a meter with 2% accuracy.

A second contribution toward early fatigue failure was taken into account as follows. During test, observation of the clamp and test bar showed signs of surface pitting at the clamping line. Since the clamp was aluminum (to reduce the shaker dynamic mass), it was assumed that local surface welding and breaking had taken place such that the minute break did not occur at the weld point, but below or above in the parent metals. Such pits would of course act much as corrosion pitting in reducing the fatigue life. As a solution, a dry film lubricant was painted on the clamp halves and the bar surfaces under the clamp. Short comparative tests show a marked reduction in the pitting on the bar.

C. EXPERIMENTAL SETUP

The equipment used for excitation of the bar was similar to that used in the previously mentioned metal fatigue experiments (Ref. C-1). Different strain gage circuits, amplifiers, and subsequent read-out equipment were devised for the present work.

The excitation of the bar consisted of an octave band of random noise centered at the first resonance of the bar (140 to 280 cps for the 200 cps bar resonance). The block diagram of the excitation circuit is shown in Fig. C-2. A feedback circuit is provided to hold the amplitude of the random noise band constant. It is shown in dashed lines. Each of the two power amplifiers was tested to show an rms power output of 160 watts continuous, and together in parallel give a peak power output of 530 watts on random occurring peaks.

A diagram of the output data recording system is shown in Fig. C-3. The strain gages are wired in a potentiometer circuit with the series resistor being a variable multi-turn rheostat. In this way the output transfer functions, $\Delta E_{out}/\epsilon$, of each strain gage can

ASD-TDR-62-165
Volume II

be adjusted. The outputs of all the strain gage circuits are carried to a stepping switch (25 pos. 2 pole) where the outputs are time sampled. The stepping switch is pulsed by a clock timer at a 2 minute interval. With four gages on a test bar, all gages would be examined by the recording system every 8 minutes. The second bank or pole of the switch is a break-before-make switch that provides a very short dead space on the recorded output between each strain gage sample. This output is fed into a true rms meter (Ballantine) modified with a very long time averaging constant so that the output is representative of the true rms of the narrow-band gage signal. This output is in turn fed to a B+K graphic level recorder operating with a paper speed of .03 mm/sec, or approximately 4-1/4 inches per hour. The entire apparatus requires very little operator time after setup.

The actual output voltage from the circuit as shown in the left of Fig. C-3 is:

$$\Delta E_{out} = - E \frac{R R_g}{(R+R_g)^2} \cdot GF \cdot \epsilon$$

For the following

$$\begin{aligned}\epsilon &= 1000 \text{ microstrain} \\ E &= 6 \text{ volts} \\ R &= R_g = 120 \text{ ohms} \\ GF &= 2.12\end{aligned}$$

we get

$$\Delta E_{out} = 3.18 \text{ mv}$$

The actual strain gage tested was an etched foil gage, type FAB-50-12, manufactured by Baldwin-Lima-Hamilton (BLH). This gage has an etched Constantan foil with bakelite backing. The gage length is 0.5 inches. Such etched foil gages are recommended (Ref. C-3) for fatigue application. Two cements were used in the experiment. One was the contact-hardening Eastman type 910, and the other was an Emerson + Cummings epoxy sold as BLH EPY-400 and requiring a heat curing cycle at temperatures of 400°.

The tests were all conducted under normal laboratory environment conditions. However, the temperature of the test gages was influenced by the level of excitation. For the higher strain levels the power dissipated in the Goodmans Shaker armature coil as well as the fatigue energy heated the clamp. For a run involving a type (b) bar shape (see Fig. C-1b) and a level of 1000 μ strain rms, the equilibrium temperature of the clamp and bar root (where little fan cooling due to deflection was present) was 130°F. This temperature is not a significant factor in bond failure for either of the cements according to their manufacturers, but it may have an influence on the fatigue life.

D. EXPERIMENTAL PROCEDURE

A typical test was made as follows. The bar was milled from 0.065" thick 2024 aluminum with the grain flow along the bar length and protected from accidental nicks or scratches. It is first cleaned in Chlorathane (R)* solvent. The strain gage application area is outlined on the bar with a soft wax pencil, and the surface oxide accumulation removed with number 400 emery cloth. Because of the possible imbedding of hard abrasive particles, the next step is a very thorough scrubbing of the area with acetone. The edges of the bar are examined at this time under a low power binocular microscope for freedom from cracks or nicks, particularly in the high stress region. Next the strain gages are glued onto the bar. The exact steps reflect the expressed instructions of both the strain gage manufacturer and the glue manufacturer in every detail. After the heat cycle or other wait period, the leads of the gage are cut to 1/2" and bent back toward the center of the bar using a 0.051" diameter mandrel. No. 30 stranded wire is attached with a minimum of solder and flux using as low a soldering temperature as possible. The joint is taped to the bar between 2 layers of 1/2 mil teflon adhesive tape, arranged so the gage lead is fixed securely for 3/8" minimum. In addition, 1/4" of the No. 30 stranded wire is also fixed. The No. 30 wire is taped to the clamp and hangs in a loop to the terminals of the chassis. All connections are soldered. Resistance checks are made before each experimental run and daily during longer runs to insure both good solder joints and absence of fatigue breaks in the No. 30 wire.

* Registered Trademark of Dow Chemical Co., Midland, Michigan

ASD-TDR-62-165
Volume II

The apparatus is then switched on and a 200 cps sine wave applied to the power amplifiers at a level not exceeding -10 db re actual test rms level. The selector switch is manually advanced and the oscillator frequency adjusted to give the maximum readings for each gage on each side of the bar. "Q" measurements are taken for each side and compared to gain assurance about the symmetry of the assembly and clamping force. Only 4 gages were attached to a given bar in order to maintain a high Q. Values of Q were typically in the range 20-35 for either arm of the bar.

E. RESULTS

A sample of the graphic recorder output is shown in Fig. C-4. This is the record of time to failure of a set of four gages subjected to a random narrow band excitation with an rms level of 60 db re 1 μ strain. The sampling of each gage in 2 minute sections can be noted as soon as one gage differs from the others. The failure of each of the gages is marked with an "f" along the bottom of the record. The output level would often rise as the failure first occurred. This was true because the first rupture in the metal foil would close for a considerable part of the cycle, making the output voltage vary between zero and the original dc level at the gage and series resistor junction. As the rupture or break widened, the "closed contact" duty cycle would diminish or go to zero, and the output would do the same. The spread of amplitude is due to the short averaging time constant available in the particular recorder used. This time constant has the advantage of allowing quick recovery from the switching transients of the sampling mechanism.

For the purposes of this work a failure was defined as a change in output of the gage of 1.5 db (or 20%). No evidence was seen that such a failure ever occurred without an actual rupture or discontinuity being created in the foil structure. It did not occur at the leads of the gage, their attaching points, the bonding cement, or the gage backing material. There was no evidence of a failure mechanism involving a continuous change in gage resistance similar in effect to the creep error phenomenon in steady strains.

The data gathered on the FAB-50-12 gages are plotted in the general form of a strain-life curve in Fig. C-5. Thirty-two samples of this gage were examined at different strain levels under narrow band random excitation centered at 200 cps.

The uncertainty in experimental failure time for the sets of gages at 62 and 62.5 db re 1 μ strain (the group with the shortest lives) was negligible since by chance the majority of the gages failed while being examined by the graphic recorder.

The two sets of gages tested at 60 db re 1 μ strain used two different types of cement, Eastman 910 and EPY-400. All other tests were conducted with Eastman 910 because the mounting time is shorter and elevated temperatures for curing is not required. The above duplicate data was taken to indicate the equivalence at these levels of the life of the gages mounted with either Eastman 910 or EPY-400. This was expected since the failures had occurred in the foil of the gage itself rather than the cement or leads.

An attempt was made to identify and inspect the location of failure on the gage. For this purpose, many of the failed gages were subjected to visual inspection both by naked eye and using a binocular microscope up to 90 power. In no instance has the failure been visible. Forsaking non-destructive methods, a successful technique of inspection was the following: the gage lead wires were connected to the output of a GR Variac and the voltage increased until local overheating and subsequent melting and vaporizing of the film conductor. For a new gage, this will generally take place where an etching defect has produced a narrow section in the foil, and at a high current level. For a gage which has failed in fatigue tests, the failure point will generally provide a visible minute arc or an overheating as described above, but at a much reduced current. Before these destructive tests were carried out, the gages were checked for dc resistance. Each failed gage would indicate either an open circuit or a resistance two to five times the normal value. In many cases this resistance could be reduced considerably by bending the test bar so that the gage was put into compression.

F. CONCLUSIONS

The following direct conclusions can be drawn from these tests:

1. Part of the strain-life curve for an FAB-50-12 type strain gage with random narrow band excitation has been experimentally determined. This curve is for normal laboratory environment with sample temperature between 80° and 130°F.
2. The point of failure in each of these tests occurred within the foil of the gage. The cement used and the method of lead attachment in all cases outlasted the foil material.

3. The fatigue life of the gages is adequate for measuring aluminum panel strain history for the response recorder:
 - a) For the high strain levels (60-62 db re 1 μ strain) the gages have at least the same fatigue life as the test bar with stress concentration reported in Smith and Malme. These stress concentrations are typical of those encountered in the construction of flight vehicles.
 - b) At the lower strain levels (50-53 db re 1 μ strain) the data taken in this experiment show that the gages have at least the same fatigue life as the test bar without stress concentration. (See Table C-1).

The results obtained in these tests of necessarily limited scope suggest the need for further work. There are other parameters than those examined such as temperature, gage material, superimposed static strain, etc., which undoubtedly influence the gage life. Of particular interest is the superposition of static strain and alternating strain. This would be a closer approximation to the actual conditions existing in flight vehicles.

REFERENCES

- C-1. Smith, Jr., P. W., and Malme, C., "Sonic Fatigue Life Determination by Siren Testing," ASD Technical Report 61-639.
- C-2. Vibration Analysis Tables, Cambridge University Press, 1956.
- C-3. Nalle, P. H., "Fundamental of Strain Measurement and Recording," Automatic Control, November 1961.

TABLE C-1
FATIGUE DATA FOR RANDOM NARROW BAND EXCITATION OF FAB-50-12 STRAIN GAGE
FOUR SAMPLES TESTED CONCURRENTLY AT EACH EXCITATION LEVEL

Excitation Level (db re 1 μ strain)	Cycles to Failure of Gages	Comments [Eastman 910 Cement Used, Unless Noted]
51	gages not failed	type (a) bar failed at 1.2×10^7 cycles
51.5	gages not failed	type (a) bar; bar arms failed at 8×10^6 and 1.1×10^7 cycles.
54	1.6, 2.4×10^7	type (b) bar; two gages good when bar failed at 3.6×10^7 cycles.
57	3.4, 6.3, 9.0×10^6	type (b) bar; one gage good when bar failed at 1.1×10^7 cycles.
60	3.4, 4.6, 6.7, 7.2×10^5	type (b) bar; EPY-400 cement
60	2.4, 4.8, 5.0, 7.9×10^5	type (b) bar
62	1.2, 2.9, 3.6×10^5	type (b) bar
62.5	1.3, 1.8, 2.0, 3.6×10^5	type (b) bar

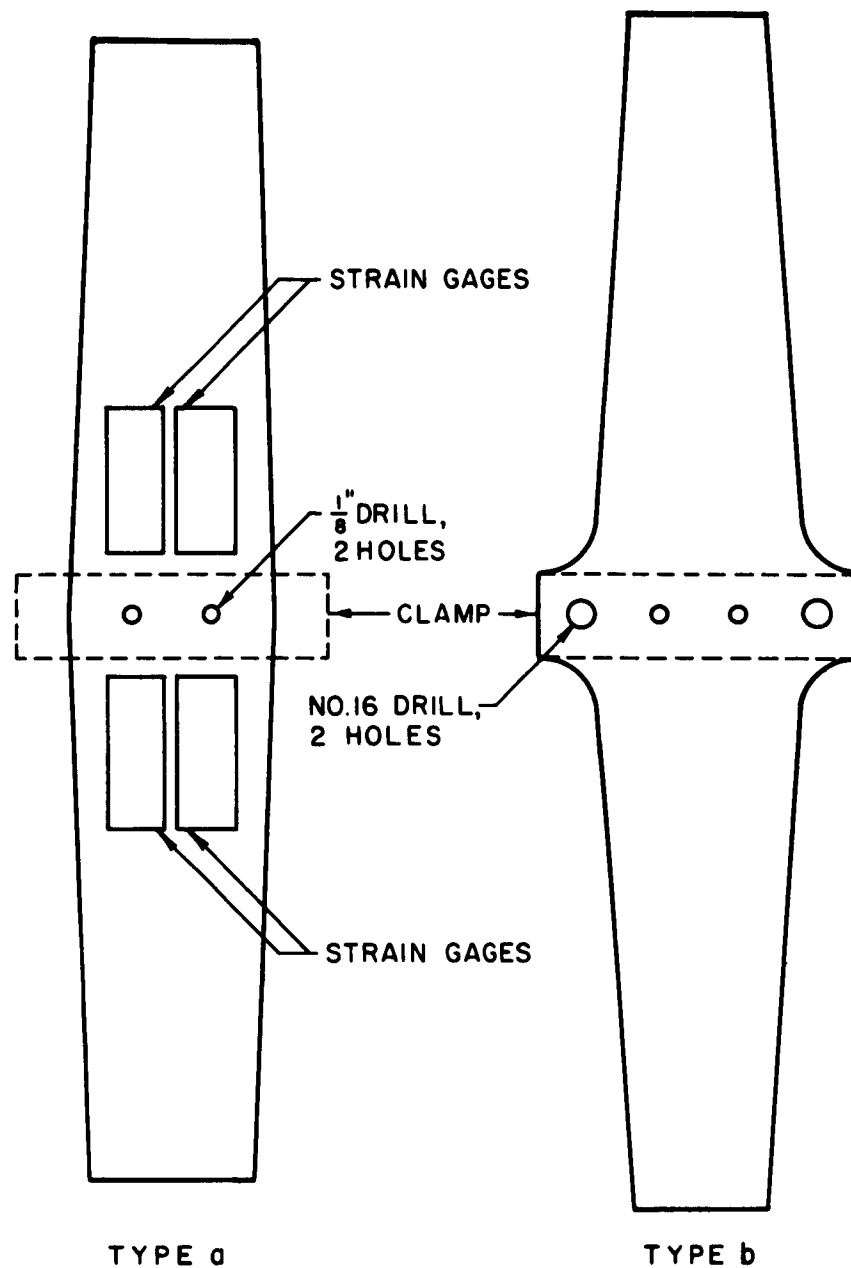


FIG.C-1 FATIGUE TEST BARS

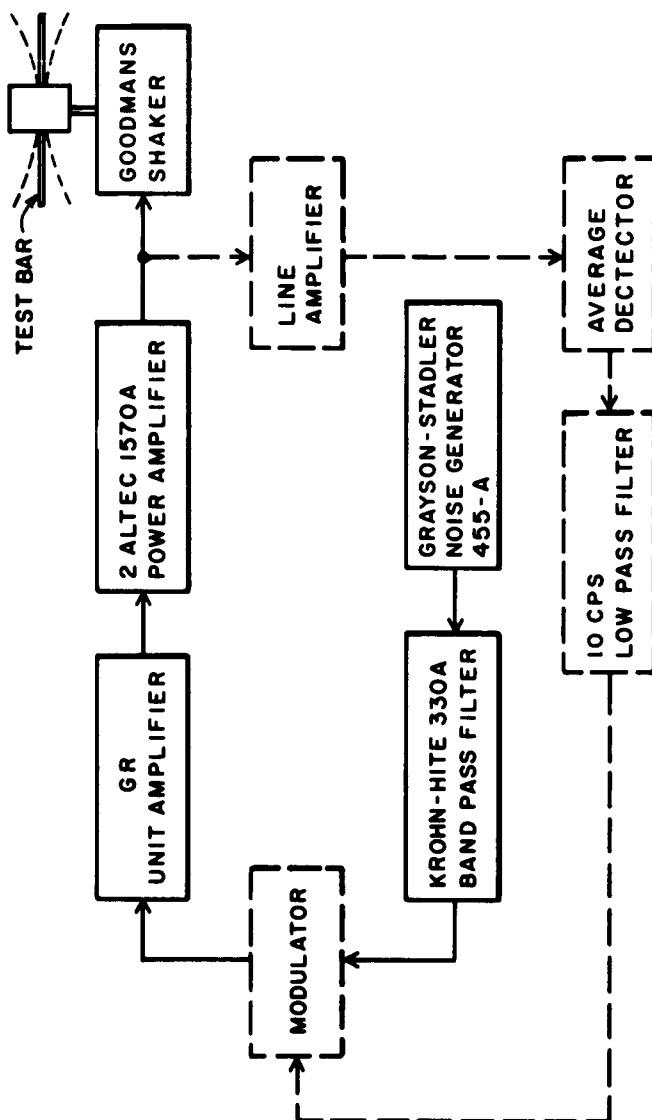


FIG.C-2 DRIVER CIRCUIT FOR RANDOM NOISE EXCITATION

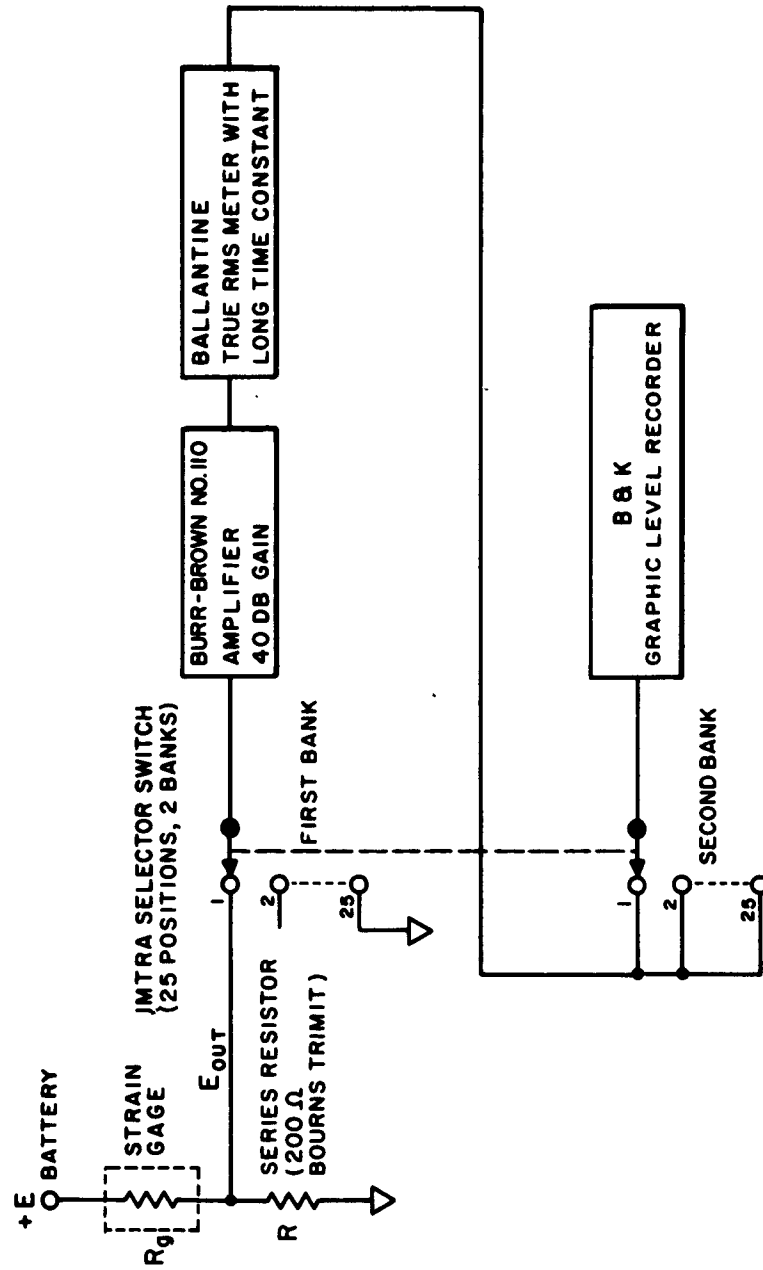


FIG. C-3 STRAIN GAGE OUTPUT RECORDING SYSTEM

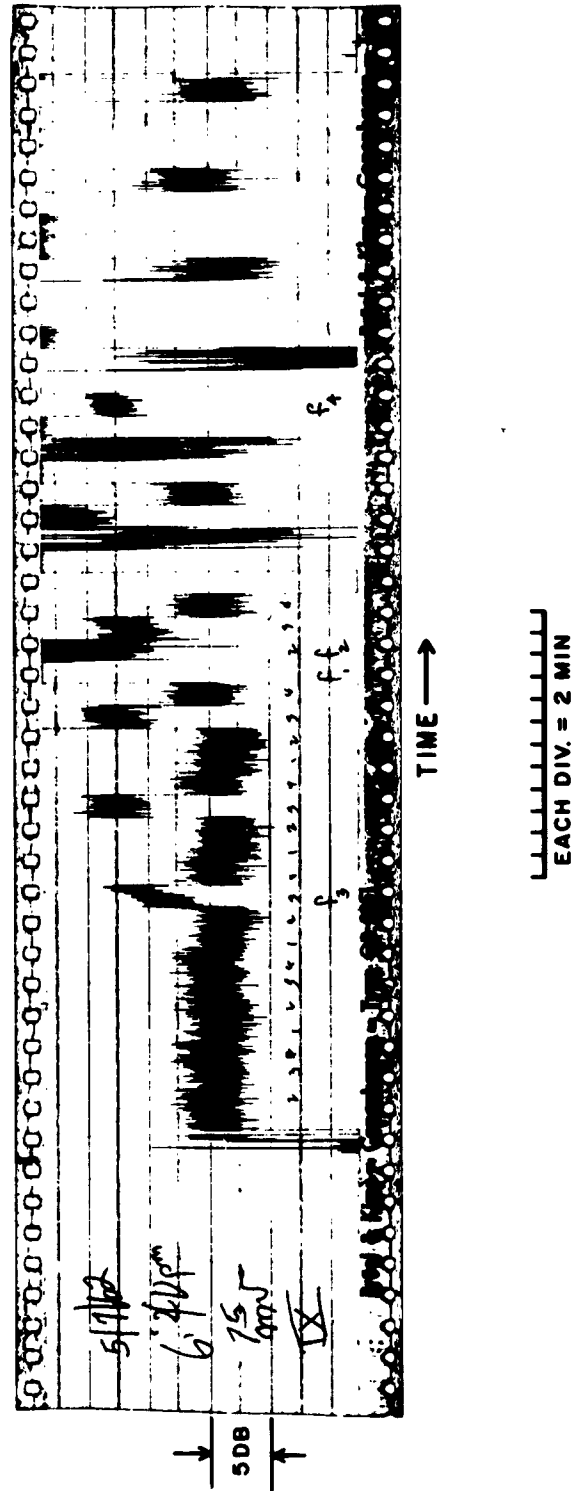


FIG. C-4 TYPICAL STRAIN GAGE GRAPHIC RECORD



APPENDIX D

DATA FOR B-52 AND KC-135

A report prepared by the Battelle Memorial Institute (Ref. D-1) was received from ASD in April 1962. This report contains preliminary data similar to that used for estimates in Volume I of this Technical Report for the RB-47. Battelle's data for the B-52 and KC-135 have been used to estimate the number of counts expected in the analyzer windows in a three month period.

The values of engine ground time per 1000 hours of flight for the most active engines of two B-52 aircraft and two KC-135 aircraft were considered. This ground time must be separated into static operations and takeoff operations, since each contribute differently to the time distribution. The split between takeoff and static operations was estimated by considering the number of flights per 1000 hours of flight* and assuming that 60 seconds of ground roll is required. This yielded 1.3 hours/1000 hours for the B-52 and 3.8 hours/1000 hours for the KC-135. The RB-47 data gave 2.8 hours/1000 hours of flight. Takeoffs were made in both engine categories IV and V; 38% in IV for the B-52 and 29% in IV for the KC-135. The data are tabulated on the following page.

The relative SPL contributed by the J-57 engines was estimated for the 600-1200 cps octave band using engine data from Pratt and Whitney (Ref. D-2) and is presented in Fig. D-1. Category IV was chosen as the reference at 0 db; Category V was +4.0 db, and Category III was -7 db. The takeoff variations of Volume I were used. The temperature data presented by Battelle for the B-52 and KC-135 were employed in conjunction with the computations in Appendix B for the J-57 to estimate the temperature influences.**

* "Touch and go" data is not included as a flight since the noise contribution does not reach a maximum unless the vehicle is stationary. (See Fig. 4 of Volume I.)

** No temperature variation could be established for the KC-135 in Category V in Appendix B. It was assumed that the variation is 20°F per db. Since the Category IV operation is much larger than Category V for the KC-135, the assumption should introduce a very small error in overall damage.

TABLE D-I
ENGINE GROUND TIME IN HOURS/1000 HOURS OF FLIGHT

Engine Category	I 0-80% rpm	II 80-90% rpm	III 90-95% rpm	IV 95-100% rpm	V 95-100% rpm with water injection
B-52, takeoff	0	0	0	0.5	0.7
B-52, static	83.9	7.2	0.6	1.2	0
KC-135, takeoff	0	0	0	1.1	2.8
KC-135, static	275	10.7	6.0	18.9	0
RB-47,* takeoff	0	0	0	2.8	---
RB-47, static	140	2	0.3	2.4	---

The KC-135 is operated with a "taxi spare"; that is, a second KC-135 is taxied to the runway as a backup in case the programmed KC-135 aborts. This would of course increase the ground operation per unit flight time for the KC-135 aircraft. We might expect it to double the average time accumulated for all aircraft in this type of operation. Comparing the takeoff time and static operation in Category IV, we find that the ratio

* From Volume I of this Technical Report.

ASD-TDR-62-165
Volume II

for the B-52 and RB-47 is about 1:1. The KC-135 data is 1:4, which is double again the increase that might be expected because of "taxi spare" operation. It is possible that the two KC-135's examined were used for taxi spare much more frequently than the average of the whole population of KC-135's.

The maximum number of counts anticipated in a counter in a 2 db range has been calculated using the average flight hours in a three-month period. These are tabulated below.

<u>Aircraft</u>	<u>Average Flight Hours In Three Months</u>	<u>Maximum Hours Per 1000 Hours of Flight in a 2 DB Window</u>	<u>Maximum Counts Expected</u>
RB-47	80	1.7	612
B-52	180	0.9	580
KC-135	141	7.1	3600

The radical increase between the RB-47 and KC-135 can be attributed to the large time at Category IV engine operation for the KC-135. Fortunately, a safety factor of twenty was allowed in sizing the counters from the RB-47 data (which can accumulate to 9999). A factor of twenty still remains for the RB-47 and B-52, but the KC-135 factor has been reduced to slightly less than three. As stated in Volume I, ultimately the rate of aircraft utilization will determine how many months the recorder can accumulate. It appears that even an aircraft as active as the KC-135's reported by Battelle can be examined for more than three months.

REFERENCES

- D-1. "Interim Report on Time History of Ground Operation of B-52 and KC-135 Aircraft Engines," Contract AF 33(616)-7066 1 November 1961, Battelle Memorial Institute.
- D-2. Specifications A-1704-D, 1 August 1957, Model J57 P-43W, Pratt and Whitney Aircraft.

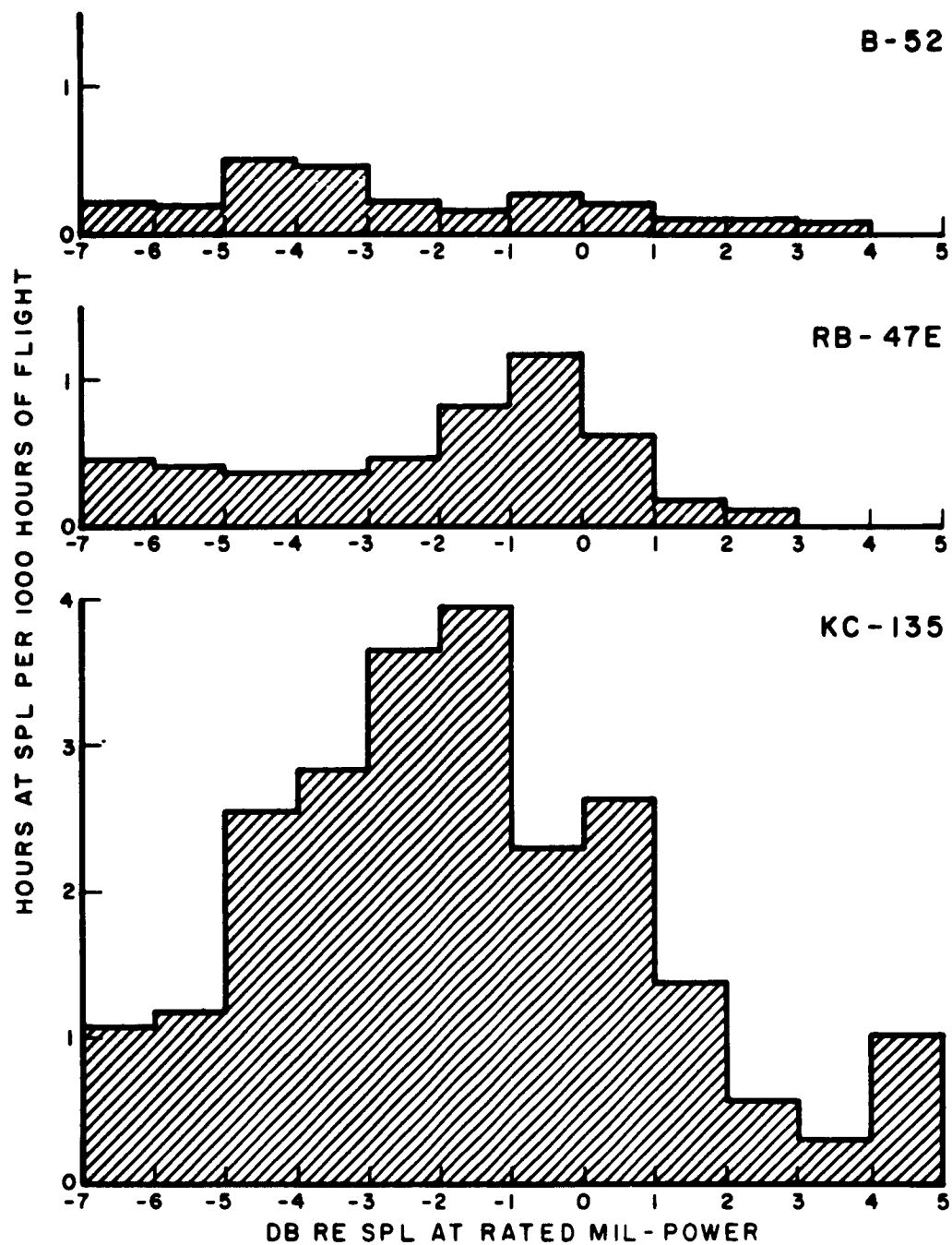


FIG. D-1 RMS DISTRIBUTIONS FOR GROUND
OPERATIONS FOR 600-1200 CPS BAND

APPENDIX E

OPERATIONAL RECOMMENDATIONS FOR THE RESPONSE RECORDER

A. SET UP PROCEDURE

The following steps are recommended in applying the response recorder to the measurement of the signal from a strain gage.

- 1) Establish by measurement the frequencies of the dominant modes of the structure. Obtain filters to cover these modes.
- 2) Install recorder and strain gage.
- 3) Perform voltage calibration as outlined in Section B below.
- 4) Set engines of aircraft 100% rpm without thrust augmentation. Adjust recorder sensitivity so that the strain level received at 100% rpm coincides with 7 db of the total 14 db range, i.e., detector output voltage is 2.07 volts.
- 5) Read ambient temperature and compensate the strain level to standard day by using the engine SPL variation with temperature. If it is expected that the aircraft will operate primarily at a radically different temperature than the standard day, set the strain level accordingly.
- 6) Apply engine thrust augmentation and check the resulting strain level. The signal should not be in the highest window (12-14 db). If it is, reduce the recorder sensitivity until it is in the 10-12 db window.

B. CHECKOUT AND CALIBRATION

1. Calibration Equipment Required

Oscillator in range 50 to 1000 cps, driving 1:1 transformer isolated from ground, capable of supplying 20 volts rms.

Decade Attenuator (600 Ω) with 10 db, 1 db, and 0.1 db steps.

Electronic Counter capable of counting frequencies up to 100,000 cps at ± 1 count.

DC Voltmeter with input impedance of 1 megohm minimum, range up to 30 volts with intermediate scales and accurate to within $\pm 2\%$.

2. Controls and Adjustments

The controls and adjustments built into the response recorder are itemized below:

Pre-Amplifier Gain: A continuous potentiometer on the input circuit. Should be set for maximum gain.

Gain Attenuator: A 30 db precision attenuator in 1 db steps which controls the effective gain of the Data Acquisition.

Frequency Band Attenuator (3 each): A 20 db precision attenuator with 2 db steps which is used to effect precise differences in gain between the narrow band channels and to extend the range of the Gain Attenuator.

Vernier Gain Control (3 each): A continuous potentiometer with a 9 db range which is used to adjust the gain to match the incremental 1 db levels and provide for gain matching between the four channels.

Bias Control: A continuous potentiometer which is used to adjust the Bias Supply output to yield a net 1.66 volt bias into the voltage-controlled oscillator.

Center Frequency Adjust: A control on the commercial voltage-controlled oscillator to set the frequency output.

Deviation Adjust: A control on the commercial VCO to adjust the sensitivity of the VCO.

Trigger Level Control (7 each): A continuous potentiometer which is used to set the trigger levels to correspond to a given peak detector output.

Clock Frequency Adjust: A continuous potentiometer which is used to set the clock output frequency.

Run-Cal Switch: A three position switch which is used to step between octave band channels during "Calibration" or to continuous sampling during "Run."

NOTE: The balance control of the quasi rms detector is adjusted to give temperature drift compensation over the range -50°C to 70°C . This control should not be changed during checkout or calibration.

3. Initial Checkout Procedures

This checkout is to be part of the final tests of a unit before being used in the field. In addition, this procedure would be useful after the instrument has been in use for a long period.

a) Step 1*

Check all chassis interconnections and power connections for correct polarity and value. Turn on power and measure and adjust power supplies to correct voltage.

b) Step 2

Set the initial position of the following controls to:

<u>Gain Attenuator:</u>	-30 db
<u>Frequency Band Attenuators:</u>	0 db for each band
<u>Vernier Gain:</u>	About middle for each band
<u>Run-Cal Switch:</u>	To Cal on one channel

Disconnect the Impulse Counter Package and plug in the Calibration Lamp Package.

c) Step 3

Apply an input of approximately 0.1 volt rms of the required frequency for the narrow band at the terminal marked "Insert Voltage." Monitor the voltage at the input of the VCO with the DC

* For a field calibration, disconnect the Elapsed Time Indicator before turning power on.

ASD-TDR-62-165
Volume II

voltmeter. Increase the insert voltage until the monitor reads approximately 6 volts. With linear graph paper plot the monitor voltage at 6, 4, and 2 volts versus the insert voltage in volts. Draw a straight line through these points and note accurately the value at which this straight line intercepts the insert voltage axis. This value should be -1.66 volts.

d) Step 4

If the intercept value is different than -1.66 volts proceed as follows. Note the actual intercept value obtained in Step 3. It is necessary to adjust the bias control of Fig. A-6 so that the intercept coincides with -1.66 volts. If, for example, the intercept were at -1.55 volts, it is apparent that the bias control needs to be more negative by 0.11 volts. This is done by setting the insert voltage to zero and noting the voltage output at the monitor. The bias adjust is then set so the monitor changes by the amount required. For example, if the monitor indicated -0.60 volts and the change desired is 0.11 volts, the bias is adjusted so the monitor output is -0.71 volts.

e) Step 5

Repeat Step 3 to check adjustment.

f) Step 6

Repeat Steps 3, 4, and 5 for the other channels.

g) Step 7

Compute the rms strain voltage from the gage at the full scale strain desired. Apply an insert voltage signal to the recorder which is 100 times the full scale strain voltage expected. Monitor the VCO input with the DC voltmeter. Adjust the Gain Attenuator until the monitor voltage is as close to 6.79 volts as possible. Use the Vernier Gain adjust to set at 6.79 volts.

h) Step 8

Using the Run-Cal Switch, advance the recorder to the next channel. Place in "Cal" position. Apply an insert voltage at the correct frequency with an rms level as determined in Step 7.

i) Step 9

Adjust the Vernier Gain for this octave band to yield 6.79 volts at the monitor of Step 7.

ASD-TDR-62-165
Volume II

j) Step 10

Repeat Steps 8 and 9 by applying for the remaining channel.

k) Step 11

The Frequency Band Attenuators are then set for the various maximum amplitudes in the other bands, i.e., spectrum compensation.

l) Step 12

With 5.00 volts at the VCO input, read the VCO output frequency on an electronic counter. Check that the frequency is 25,300 cps. If not, apply zero volts to the VCO by decreasing the insert voltage by 14 db. Adjust the output frequency to be 18,700 cps with the Center Frequency control on the VCO. Apply 5.00 volts again. Adjust the VCO Sensitivity until the output is 25,300 cps.

m) Step 13

Monitor TP-4 of Fig. A-8 of Volume I with a DC Voltmeter for the bandpass filter corresponding to the lowest band. Adjust the insert voltage from zero until the voltage at TP-4 is 6.00 volts. Observe the lamp corresponding to the amplitude level in the lamp package. Move the Trigger Level Control in a counter-clockwise direction until the lamp is off. Recheck and readjust the monitor to 6.00 volts. Carefully move the Trigger Level Control clockwise until the lamp just turns on.

n) Step 14

Repeat Step 13 for all six bandpass filters and the highpass filter.

o) Step 15

Place the Run-Cal Switch into "Run" position with one of the readout lamps on. Observe that the lamps cycle across the octave bands.

p) Step 16

Monitor the output "V" of Fig. A-14 of Volume I with the electronic counter examining the period of the output. Adjust the Clock Frequency Control for a period of 0.500 seconds.

ASD-TDR-62-165
Volume II

q) Step 17

Turn power off. Disconnect insert voltage. Reactivate the Elapsed Time Indicator and microphone. Replace the Lamp Readout Package with the Counter Readout Packages. Record the number of counts in each counter on the appropriate forms.

r) Step 18

Set Elapsed Time Indicator to zero.

4. Field Calibration Procedure

A field calibration would consist essentially of checking some of the steps listed for initial checkout. This would include Steps 1 to 3, 7 to 11, 15, 17, and 18.

The omitted steps include those required to determine the detector intercept point for the four detectors, the adjustment of the six trigger levels, and the adjustment of the clock frequency.

The first few calibrations of the first instrument constructed will want to be more extensive, enough to encompass all of the Initial Checkout Procedure. This will serve as a check to establish the critical Steps to be included in the Field Calibration Procedure.

C. DETAILED CIRCUIT

The following circuit changes are required to the sonic recorder of Appendix A, Volume I for the response recorder:

Fig. A-1

Replace the first stage with Fig. 14 of Volume II. The output of Fig. 14 would be connected to the top of the attenuator.

Fig. A-2

Delete.

Fig. A-3

Replace the four octave band filters with the three data filters described in Section IV of Volume II. Increase series resistors from $600\ \Omega$ to $10,000\ \Omega$ and the attenuators from $600\ \Omega$ to $10,000\ \Omega$.

ASD-TDR-62-165
Volume II

Fig. A-4

Increase the two 100 μ fd, 35 volt capacitors to 150 μ fd, 35 volts. Alter the 1.35 k Ω series resistor as discussed in Appendix B, Section E of Volume I.

Fig. A-8

Tabulation of components are altered in accordance with Table III of Volume II. A highpass constant-k filter is added.

Fig. A-9

Seven row drivers are required instead of six.

Fig. A-11 and Fig. A-12

Matrix is 7 x 3 rather than 6 x 4.

Fig. A-18

Three each of Fig. A-4 required. Seven each of Fig. A-8 required. Fig. A-3 deleted.

All other figures remain the same. The power supplies required are the same as for the sonic recorder with the exception that Supply 1 will be expected to supply currents as high as 180 ma. No filament supply is required.

Aeronautical Systems Division, Dir/
Aeromechanics, Flight Dynamics Lab, Wright-
Patterson AFB, Ohio.
Rpt Nr ASD-TDR-62-165, Pt II. STUDY OF A
RESPONSE LOAD RECORDER. Final report, War
63, 105p. incl illus., tables, 28 refs.

Unclassified

A compact instrument to measure the strain
history of a point on a resonant structure
of a flight vehicle is considered. The out-
put data from the instrument is designed to
aid in the estimation of acoustic fatigue
damage. The ability of a strain gage to
perform under fatigue conditions is exam-
ined. The design of circuitry to modify
the sonic recorder discussed in Volume I
to a response recorder are discussed. Per-
formance data of the breadboarded response

(over)

recorder, tested with a resonant structure,
are given.

1. Acoustics
2. Recording Systems
3. Noise Analyzers
4. Fatigue
- I. AFSC Project 1370,
task 137005
- II. AF 33(616)-7789
- III. Bolt Beranek and
Newman, Inc.,
50 Moulton Street,
Cambridge, Mass.
- IV. Edward A. Starr,
et al.
- V. EBN Report No. 947
- VI. Aval fr OTS
- VII. In ASTIA collec-
tion

Aeronautical Systems Division, Dir/
Aeromechanics, Flight Dynamics Lab, Wright-
Patterson AFB, Ohio.
Rpt Nr ASD-TDR-62-165, Pt II. STUDY OF A
RESPONSE LOAD RECORDER. Final report, War
63, 105p. incl illus., tables, 28 refs.

Unclassified

A compact instrument to measure the strain
history of a point on a resonant structure
of a flight vehicle is considered. The out-
put data from the instrument is designed to
aid in the estimation of acoustic fatigue
damage. The ability of a strain gage to
perform under fatigue conditions is exam-
ined. The design of circuitry to modify
the sonic recorder discussed in Volume I
to a response recorder are discussed. Per-
formance data of the breadboarded response

(over)

recorder, tested with a resonant structure,
are given.

1. Acoustics
2. Recording Systems
3. Noise Analyzers
4. Fatigue
- I. AFSC Project 1370,
task 137005
- II. AF 33(616)-7789
- III. Bolt Beranek and
Newman, Inc.,
50 Moulton Street,
Cambridge, Mass.
- IV. Edward A. Starr,
et al.
- V. EBN Report No. 947
- VI. Aval fr OTS
- VII. In ASTIA collec-
tion